

# **Modelling Corneal Transparency with reference to Stromal architecture**

James John Douth, B.Sc.

Thesis submitted to Cardiff University for the  
degree of Doctor of Philosophy in the Discipline of  
Biophysics

2009

UMI Number: U585184

All rights reserved

INFORMATION TO ALL USERS

The quality of this reproduction is dependent upon the quality of the copy submitted.

In the unlikely event that the author did not send a complete manuscript and there are missing pages, these will be noted. Also, if material had to be removed, a note will indicate the deletion.



UMI U585184

Published by ProQuest LLC 2013. Copyright in the Dissertation held by the Author.  
Microform Edition © ProQuest LLC.

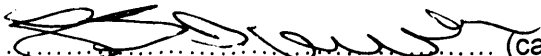
All rights reserved. This work is protected against  
unauthorized copying under Title 17, United States Code.



ProQuest LLC  
789 East Eisenhower Parkway  
P.O. Box 1346  
Ann Arbor, MI 48106-1346


**DECLARATION**

This work has not previously been accepted in substance for any degree and is not concurrently submitted in candidature for any degree.

Signed  (candidate) Date 30/03/09


**STATEMENT 1**

This thesis is being submitted in partial fulfillment of the requirements for the degree of PhD

Signed  (candidate) Date 30/03/09

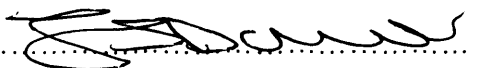
**STATEMENT 2**

This thesis is the result of my own independent work/investigation, except where otherwise stated. Other sources are acknowledged by explicit references.

Signed  (candidate) Date 30/03/09

**STATEMENT 3**

I hereby give consent for my thesis, if accepted, to be available for photocopying and for inter-library loan, and for the title and summary to be made available to outside organisations.

Signed  (candidate) Date 30/03/09

## **Thesis summary**

The arrangement of corneal collagen fibrils within lamellae was investigated by comparing fibril positions obtained from electron microscopy with distorted hexagonal, quasi-random and aperiodic arrays. By calculating the wavelength dependence and Fourier transforms of these various arrays it was determined that an aperiodic array based on the sunflower seed head is the most compatible with corneal ultrastructure.

An investigation of corneal light scattering away from the central axis was undertaken for the first time. Experimentally it was shown that corneal transmission decreases peripherally, particularly in the far periphery near the limbus. This was shown to be theoretically compatible with calculated positional changes in refractive index and fibril radius, by calculating transmission using the direct summation of scattered fields method. In swollen human corneas, it was determined that there was a notable change in wavelength dependence in the peripheral regions, possibly suggesting an increase in the size and relative number fibril free voids. .

Corneal infrared transmission is poorly studied. In this part of the spectrum, the cornea acts as an absorber of incident radiation. It was hypothesised that there should be a systematic variation between corneal hydration and infrared light transmission. Experimentally, by Fourier transform infrared spectroscopy a convenient linear relationship between hydration and transmission was found.

Riboflavin-UVA crosslinking is used to treat keratoconus, a degenerative corneal disorder. A swelling experiment was performed on porcine corneas in order to elucidate whether the crosslinking mechanism is intra- or inter-fibrillar. Swelling rates for the treated and untreated tissue were not statistically significant, excluding interfibrillar crosslinking. The penetration depth of the riboflavin molecule into corneal stroma was also examined by visible spectroscopy of thin segments of tissue. It was demonstrated that when riboflavin infiltrates a full thickness cornea, the highest concentration of riboflavin is present in the anterior tissue segment.



## **Acknowledgements**

Throughout my three years in the Structural Biophysics group at Cardiff University, I have considered myself most fortunate to have been surrounded by skilled and dedicated supervisors, mentors and colleagues. Firstly, of course, I offer sincere thanks to Professor Keith Meek for allowing me the opportunity to pursue my interest in Biophysics and being continuously enthusiastic and helpful as the research led us down unexpected pathways. At this point I also offer my gratitude to Dr. Andrew Quantock, my co-supervisor, not least for being a constant source of new ideas, and helping to ensure the group maintained a sociable outlook with his near-continuous cheer. Dr. Carlo Knupp, my adviser, proved to be an invaluable asset in the development of the more theoretical aspects of my work, and at this juncture I thank him for the time spent assisting me. In a similar fashion I also wish to thank Dr. Justyn Regini for fruitful discussion of much of my work.

I also take this opportunity to thank Dr. Carole Tucker and Professor Peter Ade at the School of Physics and Astronomy, under whose guidance during my undergraduate studies I developed an interest in Biophysics, and, during my PhD studies allowed me to develop a highly successful collaboration between our respective groups.

I would also like to thank Dr. Rob D. Young for seemingly limitless advice on electron microscopy and things biological, Dr. Sally Hayes for instruction and help with tissue handling and Dr. Craig Boote for help with computing and X-ray scattering. All of the above have helped to create an enjoyable working environment within the Biophysics group, and in this regard I also thank all colleagues past and present, in particular, Barbara Palka, Dr. Melody Liles, Dr. Christian Pinali, Dr. Clark Maxwell, Dr. Kirsten Hamilton and Leona Ho.

Last and not least, I offer my thanks to various outside partners who have helped with the development of this thesis, in particular, Dr. Valerie A. Smith of the UK Transplant Service and Professor Russ L. McCally of the Applied Physics Laboratory, Johns Hopkins University.

## Contents

<b>1. Introduction</b>	<i>Page</i>
1.1 Corneal structure and ultrastructure	1
1.1.1 Stromal collagens	4
1.1.2 Corneal extrafibrillar matrix	6
1.1.3 Influence of the extrafibrillar matrix on stromal hydration	8
1.2 Corneal transparency	9
1.2.1 Periodic arrangement of collagen fibrils	13
1.2.2 Short range ordering of fibrils	14
1.2.3 Long range order	18
1.2.4 Alternate formulations and corrections	20
1.3 Order and disorder	21
1.4 Light transmission through normal and swollen corneas	25
1.5 Aims	30
<b>2. General Methods</b>	
2.1 Preparation of tissue samples: Human and Animal	32
2.2 Preparation of dialysis tubing	33
2.3 Dialysis of human and bovine corneas for hydration control	33
2.4 Image processing of electron micrographs	34
2.5 Theoretical modelling of corneal transmission: Direct summation of scattered fields	36
<b>3. Spatial ordering of collagen fibrils within the corneal stroma</b>	
3.1 Introduction	39
3.2 Methods	44
3.2.1 Generation of theoretical lattices	44
3.2.2 Lattice analysis	46
3.3 Results	47
3.3.1 Radial distribution functions	48
3.3.2 Fourier transform (power spectrum) analysis	51
3.3.3 Wavelength dependencies	54
3.4 Discussion	57
<b>4. Light transmission through cornea as a function of position</b>	
4.1 Introduction	67
4.2 Methods	70

4.2.1	Sample preparation	70
4.2.2	Transparency measurement	70
4.2.3	Theoretical deduction of refractive indices and transmission	71
4.2.4	Theoretical measurements	76
4.3	Results	77
4.3.1	Measurement of corneal transmission	77
4.3.2	Modelling transmission in the human cornea	79
4.4	Discussion	80
<b>5. Light transmission and thickness of oedematous corneas: A comparison of central and peripheral zones</b>		
5.1	Introduction	88
5.2	Methods	91
5.3	Results	92
5.3.1	Ultrasound pachymetry of central and peripheral zones	92
5.3.2	Light transmission as a function of position	93
5.4	Discussion	96
<b>6. Infrared absorption in the cornea</b>		
6.1	Introduction	102
6.2	Methods	104
6.2.1	Tissue preparation and swelling experiment	104
6.2.2	Fourier Transform Infrared Spectroscopy	105
6.2.3	Analysis of experimental measurements	105
6.3	Results	105
6.3.1	Theoretical considerations	105
6.3.2	Corneal transmittance	108
6.4	Discussion	112
<b>7. Spectroscopic and swelling studies of corneas cross-linked with Riboflavin-Ultraviolet A (UVA)</b>		
7.1	Introduction	118
7.1.2	Clinical effects of Riboflavin/UV-A cross-linking on corneal stroma	121
7.2	Methods	124
7.2.1	Preparation of corneas	124
7.2.2	Cross-linking of corneas	124
7.2.3	Swelling studies of cross-linked corneas	125
7.2.4	Spectrophotometric studies of riboflavin penetration	125

7.3	Results	
7.3.1	Swelling studies on cross-linked corneas	126
7.3.2	Analysis of cross-linking agent penetration by means of spectrophotometry	130
7.4	Discussion and analysis	135
<b>8. Conclusions and future work</b>		
8.1	Results summary	
8.1.1	Spatial ordering of collagen fibrils within the corneal stroma	144
8.1.2	Light transmission through cornea as a function of position	145
8.1.3	Light transmission and thickness of oedematous corneas: A comparison between central and peripheral zones	146
8.1.4	Infrared absorption in the cornea	147
8.1.5	Spectroscopic and swelling studies of corneas cross linked with Riboflavin-Ultraviolet-A (UVA)	148
8.3	Future work	149
<b>References</b>		151

Appendix 1: List of published papers and abstracts

## List of figures

### 1. Introduction

1.1	Anatomy of cornea showing major layers	2
1.2	Transmission electron micrograph of bovine corneal stroma	4
1.3	Axial structure of D-periodic collagen fibrils	6
1.4	Radial distribution function for a human cornea	16
1.5	Periodic and distorted periodic lattices in real and reciprocal space	19
1.6	Penrose tiling represented as a point set and its Fourier transform	24
1.7	Generalised pinwheel tiling and its Fourier transform	24
1.8	Light transmission of ovine cornea	27

### 2. Methods

2.1	A, B, C represent steps outlined in the process of extracting fibril co-ordinates from electron micrographs	35
-----	---	----

### 3. Spatial ordering of collagen fibrils within the corneal stroma

3.1	Representations of human corneal electron micrographs	47
3.2	Perturbed hexagonal lattice	47
3.3	Quasicrystal in pure and perturbed form	48
3.4	Purely random arrangement	48
3.5	Generalised pinwheel lattice	48
3.6	Radial distribution function $g(r)$ for corneal stroma from electron microscopy	49
3.7	Radial distribution function $g(r)$ of a random point set of fibrils	50
3.8	$g(r)$ of sunflower quasicrystal point sets, from unperturbed through to a medium level of disorder	50
3.9	$(r)$ of generalised pinwheel quasicrystal point set	51
3.10	Power spectra of corneal electron micrographs (human), anterior to posterior (l-r)	51
3.11	Power spectrum produced by distorted hexagonal point set	52
3.12	Power spectrum of a generalised pinwheel set	53
3.13	Power spectrum produced by sunflower quasicrystal point set	53
3.14	Power spectrum produced by random point set	54
3.15	One dimensional plot of interference function for stromal micrographs l-r anterior to posterior	59
3.16	One dimensional plot of interference function for random array	59
3.17	One dimensional plot of interference function for quasicrystal array, and quasicrystal array with randomised disorder added	59
3.18	One dimensional plot of hexagonal lattice Fourier transform taken through 30 degree transept	60
3.19	Additional micrograph used for analysis (Giraud et al., 1975) b. One dimensional plot of Fourier transform from (a)	62
3.20	Voronoi tessellation of sunflower type quasicrystal	63
3.21	Voronoi tessellation of posterior tissue segment	64

#### **4. Light transmission through cornea as a function of position**

4.1	Transmission electron micrograph of human cornea	68
4.2	Diagram of spectrophotometer cell	70
4.3	Cross-sectional model of cornea	72
4.4	Translational transparency for human corneas near physiological hydration at 500nm	77
4.5	Representative three-dimensional plot of translational transparency versus wavelength for a human cornea at physiological hydration	78
4.6	Transparency at 500nm as a function of radial distance from the optical centre of the cornea	79
4.7	Theoretical versus experimental deductions of corneal transparency across the surface at 500nm	82
4.8	Transmission as a function of position for bovine cornea	86

#### **5. Light transmission and thickness of oedematous corneas: A comparison between central and peripheral zones**

5.1	Central and peripheral corneal thickness as a function of central corneal hydration	93
5.2	Corneal transmission as a function of position in swollen human corneas; taken at 500nm	94
5.3	Average of transmission at 500nm of both meridians	94
5.4	Three dimensional plot of corneal transmission as a function of position for a single cornea	95

#### **6. Infrared absorption in the cornea**

6.1	Infrared transmission of the cornea versus that of an equivalent path length of liquid water	106
6.2	Theoretical decreases in transmission (at $4500\text{ cm}^{-1}$ ) with increase in corneal hydration values	107
6.3	Transmitted Intensity in the Mid Infrared with increasing hydration (H) for one cornea	110
6.4	Transmitted intensity at $4500\text{ cm}^{-1}$ ( $2.22\mu\text{m}$ ) against hydration	110
6.5	Change in absorption coefficient with hydration	111
6.6	Relation between wet weight and infrared transmission (at $4500\text{ cm}^{-1}$ )	115
6.7	Normalised hydration values	116

#### **7. Spectroscopic and swelling studies of corneas cross-linked with Riboflavin-Ultraviolet A (UVA)**

7.1	Human eye affected by keratoconus	119
7.2	Experimental set up for riboflavin-UVA cross-linking of porcine cornea, showing whole porcine eye in Petri dish with UVA diode source placed above	125

7.3	Graph of hydration versus time spent in saline solution for untreated (control) corneas and treated (UVA-riboflavin) treatment	130
7.4	Light transmission for segments of untreated human cornea	131
7.5	Light transmission for treated and sectioned human corneas	132
7.6	Light transmission for layers treated after tissue sectioning	133
7.7	Transmission spectra for porcine corneas subjected to various methods of epithelial debridement	134
7.8	Transformed transmission data from anterior segment of untreated cornea	137
7.9	Normalised extinction coefficient for untreated human stromal sections	139
7.10	Normalised extinction coefficients for riboflavin-UVA treated corneal sections	140
7.11	Normalised extinction coefficients for corneal sections with riboflavin-UVA treated	141

## List of tables

3.1	Wavelength dependence ( $n$ ) for tested lattices (for 450-650nm)	56
4.1	Ultrastructural parameters used for modelling stromal transmission	76
4.2	Theoretical and experimental transmission values compared at 500nm	79
5.1	Wavelength dependence factor $n$ calculated for wavelength range 400-700nm	96
5.2	Wavelength dependence of developing chick cornea	100
5.3	Experimental dry/wet weights and intensities	109
7.1	Wet weights of control and riboflavin-UVA treated corneas as a function of time in swelling solution	127
7.2	Hydration values of control and riboflavin-UVA treated corneas as a function of time	128
7.3	Average hydration of treated and untreated corneas	129



## Nomenclature

E	Electric field
$\lambda$	Wavelength
$n_s$	Stromal index of refraction
$n_f$	Collagen fibril refractive index
$n_g$	Extrafibrillar (or ground) substance refractive index
$n_p$	Refractive index of dry extrafibrillar matter
$n_w$	Refractive index of water 1.333
m	Refractive index contrast ( $n_f / n_g$ )
a	Radius of collagen fibril
$\rho$	Fibril number density
$\sigma$	Scattering cross sections
c	Speed of light (in vacuum)
l	Length of fibril
S( <b>q</b> )	Interfibrillar structure factor (or interference function)
$\chi(\mathbf{q})$	Structure factor of individual fibril
i,j	Indicates ith and jth fibril
r	Displacement vector (real space)
q	Scattering vector (reciprocal space)
k	Wavevector
g(r)	Radial distribution function
$\theta$	Angle
I	Intensity
$\Delta$	Optical thickness
a	Extinction coefficient (includes absorption and scattering)
n	Wavelength dependence factor
i	Interfibrillar spacing
$d_b$	Bragg plane spacing
$\beta$	disorder parameter
$\kappa$	Constant of proportionality
$V_s$	Stromal Volume
$f_f$	Volume fraction of hydrated fibrils
$f_m$	Volume fraction of collagen molecules in a fibril

$f_c$	Volume fraction of dry fibrillar matter in the stroma
$f_p$	Volume fraction of dry non-fibrillar matter in the stroma
$f_{ew}$	Volume fraction of extrafibrillar water in the stroma
H	Corneal hydration

### **Common abbreviations**

FTIR	Fourier transform infrared spectroscopy
UVA	Ultraviolet-A
PEG	Polyethylene glycol

## **Chapter 1. Introduction**

### **1.1 Corneal structure and ultrastructure**

The cornea is the clear, transparent structure at the very front of the eye. It is the eye's most powerful refractive component, supplying some two thirds of the total refractive power for the terrestrial animal (approximately 43D of optical power). The crystalline lens supplies the remainder, which acts mainly as accommodative focussing. This optical system acts to focus light onto the retina, from where it interacts with a system of rod and cone receptors.

The cornea also acts as a protective barrier of great tensile strength, shielding the internal components of the eye. It is also noteworthy for being avascular, in that it has no blood supply. This means that, in general, the cornea has an immune privilege, and it is not normally necessary to perform tissue typing during keratoplasty (corneal transplant). The cornea is bathed on the posterior surface in aqueous humor which supplies the necessary components for metabolic action.

Water occupies 78% of the corneal structure and this is generally invariant between different species (Scott and Bosworth, 1990). In the human, the refractive index of the central cornea is 1.375, with slight variations between different species (Maurice, 1957), and this is known to vary through the depth of the tissue. The adult human cornea has a thickness which varies from 550 $\mu$ m in the centre to around 750 $\mu$ m in the peripheral regions. This thickness varies with the degree of corneal hydration and there is a well known linear relationship between the two (Hedbys and Mishima, 1966). It is generally assumed that swelling occurs almost exclusively in the thickness plane.

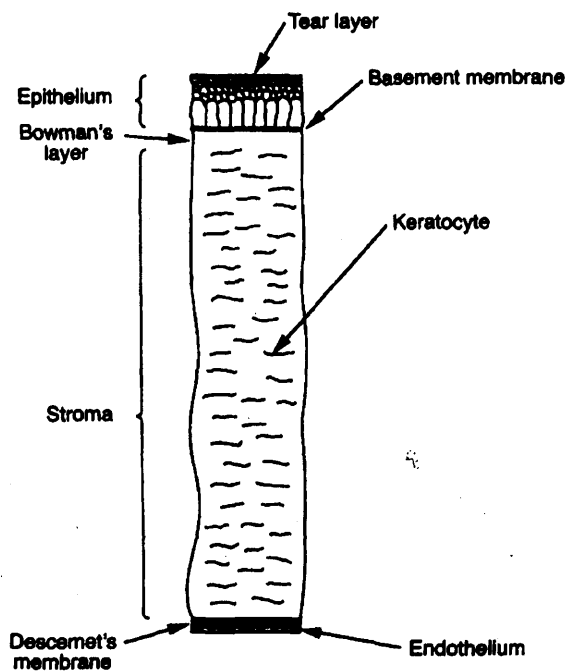


Figure 1.1 Anatomy of the cornea showing various major layers (Reproduced from Farrell and McCally, 2000)

The human cornea can be divided into several histologically distinct layers, as shown in figure 1.1, in the following scheme:

**Epithelium:** The first layer of the cornea, consisting of squamous cells arranged in several layers. These cells regenerate easily, and are maintained in a stable state with the aid of the tear film. This layer has an important role in helping to maintain the cornea in a constant hydration state.

**Basal lamina:** composed mainly of collagen types IV and VII, fibronectin and heparin sulphate. This layer acts to anchor the epithelium to the stroma.

**Bowman's layer:** A very thin layer of irregularly arrayed collagen fibrils, notably absent in certain species.

**Stroma:** Consists in the main of modified type I collagen fibrils, with smaller amounts of different collagen types. These collagen fibrils have fairly constant spacing and diameter and are packed into layers known as lamellae – in a lamella all collagen fibrils lie parallel to the surface and parallel to their neighbours. The ends of collagen

## **Chapter 1**

fibrils are not seen in electron micrographs and it is often assumed that they run the full width of the cornea. The human cornea contains some 200 lamellae (Naylor, 1953; Maurice, 1956) which occur in all possible angular rotations in relation to the surface of the cornea, ensuring strength in all possible directions. Also present are keratocytes, modified fibroblast cells which become activated in wound healing situations, and are found mainly between lamellae. These occupy some 4% of the stromal volume. The fibrils are embedded in an extrafibrillar matrix, sometimes referred to as the 'ground substance', which contains glycoproteins, mainly in the form of proteoglycans such as lumican, mimecan, keratocan and decorin, as well as inorganic ions and water. Other glycoproteins (mainly serum proteins), enzymes and inorganic salts are present. The hydration of the cornea must be controlled within fine limits to maintain transparency.

**Descemet's membrane:** Similar in composition to the basal lamina, this layer anchors the endothelial layer to the stroma.

**Endothelial layer:** A single layer of squamous cells bathed in the aqueous humor which has the most important role in controlling the flow of water and solute flow into the cornea. The endothelial cells do not regenerate and any defect in this layer will often require keratoplasty.

The stroma is the dominant layer of the cornea; it is this layer which, in general, most affects the propagation of electromagnetic radiation through the stroma. In order to understand this property it is necessary to obtain high magnification images of stroma. This is readily obtained by electron microscopy and is shown in figure 1.2.

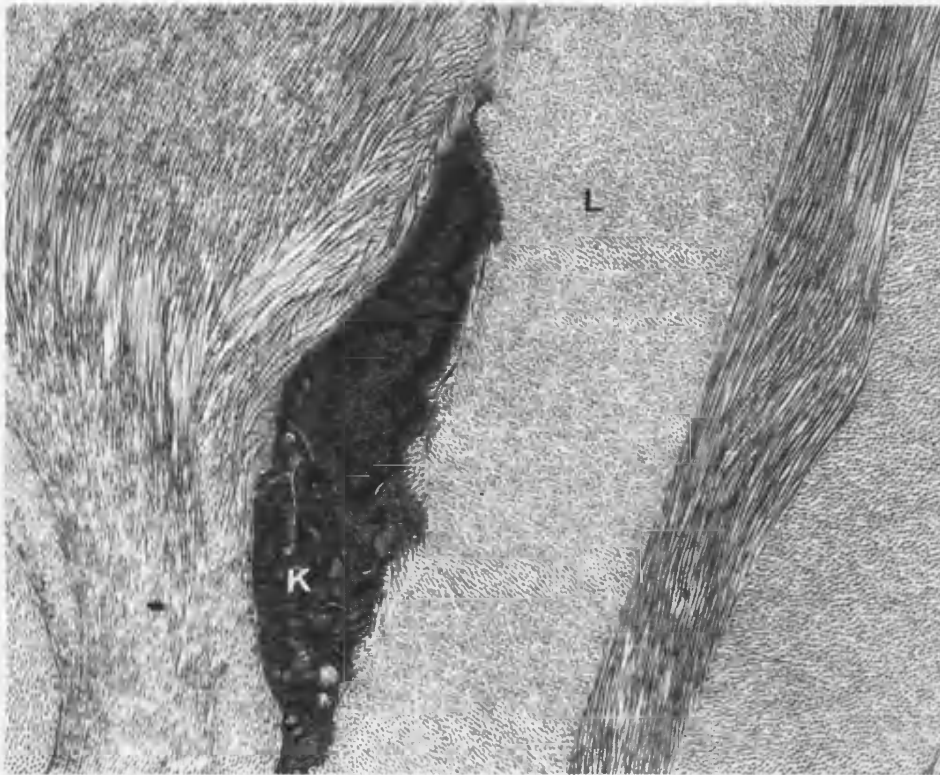


Figure 1.2. Transmission electron micrograph of bovine corneal stroma. A keratocyte (K), and lamella (L), containing fibrils in transverse section are labelled

### 1.1.1 Stromal Collagens

Aside from the hydrated fraction of the cornea, the structural protein collagen dominates the dry mass of the stroma. Collagen is a common component of many connective tissues, occurring in skin, tendon and cornea, and there are some 28 types. It is an insoluble protein composed structurally of three left hand polypeptide chains (alpha chains) which wrap around each other to form a triple helix. It contains large quantities of proline and hydroxyproline. The end of each chain consists of hydroxylysine residues which cross-link to stabilise the structure. Collagen also contains large amounts of glycine which occurs as every third residue in the polypeptide chain.

It is possible to generalise collagen types into three basic classes:

Class 1: Possess a D-periodicity (e.g. types I, III, V) and possess long uninterrupted domains, forming into fibrils.

Class 2: Do not form fibrils but do interact with other collagen types (Fibril associated collagens with interrupted triple helices or FACIT collagens)

Class 3: Form fibrous structures different to those formed by class 1. (E.g. type VI which has a beaded appearance in the electron microscope – it consists of large domains interrupted by globular regions).

Collagen type is defined by the alpha chains; different types of collagen have different amino acid sequences in these chains. Stromal collagens are mainly composed of modified type I collagen fibrils although other types are known to be present in small amounts and at certain intervals during development. For example, type III collagen has been reported in the bovine cornea in the normal state (Schmut, 1977) and also in neonatal or wounded corneas (Cintron et al., 1988). There is, however, a degree of controversy in relation to type III collagen in the cornea (Meek and Fullwood, 2001). It has been suggested that type V collagen may have a role in regulating collagen fibril diameter (Birk, 2001). Type VI collagen is also present in large amounts in the stroma (Zimmermann et al., 1986; Michelacci, 2003). This type of collagen may have a role in ensuring that the correct arrangement of collagen fibrils is maintained; experimental results suggest type VI is bound to fibrils via a proteoglycan intermediary (Nakamura et al., 1997). Various other collagen types are found in other parts of the cornea.

When electron microscopy of collagen fibrils is performed, there are regions of stain penetration and stain exclusion and this gives rise to the characteristic D-periodicity (67nm in rat tail tendon), i.e. each period contains a penetration (gap) and exclusion (overlap) region (Petruska and Hodge, 1964), as shown in figure 1.3 (Kadler et al., 1996). Each molecule is 290nm long, staggered axially between neighbouring molecules by distance D, with a gap of 0.6D between molecule ends. These D-periods were also seen in early meridional reflections in low angle x-ray diffraction patterns of rat tail tendon (Miller, 1976). The hydroxylysine unit at the end of each chain cross-links to stabilise the structure (Ramachandran, Bansal and Bhatnagar, 1973). The type I collagen fibrils in cornea are considered modified as they do not possess the 67nm D-periodicity present in rat tail tendon. The D-periodicity of corneal collagens is known to be 65nm (Meek et al., 1987) and it has been suggested

that this is due to collagen molecules forming into an intermediary layer of microfibrils orientated at an angle (Baldock et al., 2002).

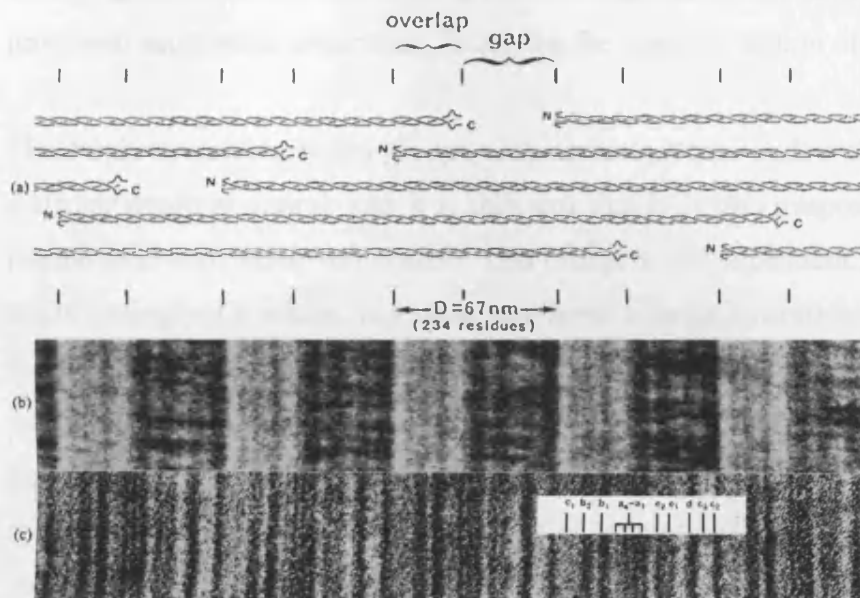


Figure 1.3 Axial structure of D-periodic collagen fibrils (reproduced from Kadler et al, 1996)

### 1.1.2 Corneal extrafibrillar matrix

The extrafibrillar matrix is composed of several components, the most important of which are the various glycoproteins, and in particular proteoglycans. Glycoproteins are carbohydrate molecules covalently linked to a protein. A subclass of these molecules is known as proteoglycans; here protein molecules are bound to long chain polysaccharide molecules – this part of the molecule is known as a glycosaminoglycan, which is a repetitive disaccharide unit. This disaccharide unit generally consists of hexosamine and an isomer of uronic acid.

Proteoglycans are an important class of molecules, as they form a key element of the extrafibrillar matrix. They have an important role to play in cornea and are thought to be involved in both stromal hydration (Hedbys, 1961) and fibril ordering. Corneal proteoglycans in general differ markedly from those present in other types of connective tissue, and are of the type referred to as small leucine-rich proteoglycans. The major glycosaminoglycan (GAG) species present is keratan sulphate (Robert and Dische, 1963), making up some 50% of stromal GAG content (Funderburgh et al.,



1988). Dermatan and chondroitin sulphate are also present, and make up 30% and 20% of stromal GAG content respectively (Scott and Bosworth, 1990). Proteoglycans were originally named after their glycosaminoglycan side chains. However, this has now been superseded somewhat, following the characterisation of the core proteins.

The sulphated and carboxyl groups of the proteoglycans endow these molecules with a strong negative charge and it is this part that is largely responsible for the strong interactions with water molecules. This charge is pH dependent. Dermatan sulphate binds strongly to water, but does not have a large hydration capacity. Keratan sulphate on the other hand binds only relatively weakly to water molecules, but has a far larger hydration capacity (Bettelheim and Plessy, 1975). In the normal cornea keratan sulphate is underhydrated and therefore has the capacity to dynamically alter hydration in response to local conditions or temporal changes. The hydration,  $H$ , of the cornea is defined as  $(\text{wet tissue weight} - \text{dry tissue weight})/\text{dry tissue weight}$  and must be controlled within fine limits to maintain transparency. In the normal cornea  $H \sim 3.2$  implying that water occupies some 78% of the total mass.

Proteoglycan molecules are synthesised within the stromal keratocytes and then secreted into the extrafibrillar space; decorin contains chondroitin/dermatan sulphate GAG chains whereas lumican, keratocan and mimecan contain keratan sulphate GAGs (Funderburgh and Conrad, 1990; Funderburgh et al., 1991). Keratocan, as the name suggests, occurs in a proteoglycan form only in the cornea (Corpuz et al., 1996). In other tissues these proteoglycans have minimal or no sulphation.

The proteoglycans are thought to affect fibril ordering. In order to maintain corneal transparency the fibrils must be of uniform diameter and spacing. Specifically, the proteoglycans appear to be present at certain binding sites on the fibrils (Meek, Elliott and Nave, 1986; Scott and Haigh, 1988); indeed one of the key models of stromal fibril arrangement suggests that proteoglycans radiate outwards from each fibril to connect it with its nearest neighbours (Maurice, 1956; Maurice, 1962; Muller et al., 2004), approximated to the form of a hexagonal crystal; therefore it has been suggested they are responsible for the maintenance of a constant interfibrillar spacing (Borcherding et al., 1975).

Mouse corneas in which lumican is not expressed are found to be opaque and have ultrastructural defects (Chakravarti et al., 2000) such as larger fibril diameter and a greater range of interfibril spacings. Mimecan is thought to have less of a role in controlling stromal architecture (Beecher et al., 2005). Mutations in the genes which encode keratocan have been implicated in the development of corneal plana (Pellegata et al., 2000).

### 1.1.3 Influence of the extrafibrillar matrix on corneal hydration

With the limiting cellular layers of the cornea removed (i.e. epithelium and endothelium debrided) the cornea will tend to swell rapidly, particularly if it is the endothelial layer which is damaged (Maurice and Giardini, 1951). The components of the extrafibrillar matrix are responsible for this process.

There are essentially two molecular influences on this process; one electrical and the other osmotic. The keratan sulphate GAGs, as outlined above, possess strong negative charge and it is these that are the source of the electrical imbalance that would tend to draw water into the stroma (Hodson, 1971). The other influence on the swelling process is essentially due to chloride anion binding to the extracellular matrix and indeed it is this process which is dominant (Hodson et al., 1992; Guggenheim et al., 1995) contributing over half the fixed negative charge in the stroma.

In-vivo, the water content of the stroma is regulated by active transport processes of sodium and bicarbonate ions due to the endothelial pump mechanism, and this regulation would tend to defeat much of the swelling potential of the stroma (Hodson and Miller, 1976).

Chloride anions are additionally thought to play a role in fibril ordering. X-ray and neutron scattering studies have suggested that disorder in the collagen fibril matrix increases when the concentration of chloride ions in the matrix is varied away from the physiological (Regini, Elliott and Hodson, 2004).

## **1.2 Corneal Transparency**

The cornea, sometimes described as ‘the window of the eye’, is required to be highly transparent. Even in aquatic animals, where the cornea supplies little effective refractive power, corneal structure must be such that the maximal flux of visible wavelengths reaches the retina.

The way in which this transparency is achieved has fascinated a diverse array of researchers crossing many disciplines, from theoretical physics through to structural biology, particularly since the advent of the electron microscope allowed detailed ultrastructure to be visualised. It is necessary at this point to come to define more precisely the somewhat vague term ‘corneal transparency’, as being the condition in which a high fraction of the incident light at visible wavelengths which the retina is sensitive to (in humans ~400-800nm) is transmitted through the cornea with a minimum of scattering or absorption. Experimentally it has long been known that this high fraction is generally above 80% across much of the visible spectrum (Pitts, 1959). Specifically the cornea’s interaction with visible light can be characterised biophysically by three factors (Lerman, 1984):

1. Refractive power, which is due to the radius of curvature maintained by the outward pressure exerted from within the eye
2. Refractive index, defined by the chemical composition
3. Tissue transparency, which is regulated by morphology and composition

The theoretical models of transparency all require one of two initial assumptions to be made:

1. That the extrafibrillar substance and the collagen fibrils have equal refractive index (Smith, 1970), or,
2. There is a differential between the refractive index of the extrafibrillar matrix ( $n_g$ ) and the collagen fibrils ( $n_f$ ) (Maurice, 1956)

The uniform refractive index model is generally dismissed on a number of counts. It can be shown that in order for the collagen fibril refractive index to be equal to that of

## Chapter 1

the ground (extrafibrillar) substance the fibrils would have to be at a higher hydration state than is evident from the fibril diameters shown in electron microscopy (Maurice, 1956; Maurice, 1970). It could be contended that the appearance in electron microscopy is a processing artefact due to shrinkage effects. However, readings obtained by X-ray scattering methods on unfixed tissue (Leonard and Meek, 1997) show a fibril diameter consistent with that of electron microscopy, with only very minor shrinkage. The diffusion of large molecules such as haemoglobin through the stroma (Maurice, 1956) would also seem to point away from the hypothesis of Smith (1970) that fibrils may subdivide into smaller units to increase their hydration state. The observed wavelength dependence and angular scattering from cornea also do not match what would be expected from a system with uniform refractive index (Maurice, 1970). Of course, the observation that the cornea becomes reversibly opaque under mechanical strain is also incompatible with a uniform index of refraction.

With the uniform refractive index model seemingly dismissed, it is necessary to consider the second initial assumption; that the interfibrillar substance (i.e. the matrix of proteoglycan, ions and water) and hydrated collagen fibrils have different indices of refraction.

This difference in refractive index does of course cause the collagen fibrils to scatter incident light away from the incident direction. In the simplifying assumption that the collagen fibril can be regarded as an infinitely long dielectric needle or cylinder (Maurice, 1956) embedded in medium of different refractive index, the scattering of electric fields by such an object can be computed from first principles of electromagnetism (van de Hulst, 1981; Bohren and Huffman, 1983). It is of course assumed that an incident beam strikes the cylinder, or fibril, purely perpendicular to its axis. The fibril diameter is much smaller than that of visible light. Simplifying the fibril diameter to 30nm, we find that this is much smaller than  $\lambda/2$  for visible wavelengths and therefore fulfils the criteria for Rayleigh scattering mechanisms (Maurice, 1956; van de Hulst, 1981). At this juncture, it should be stated that the molecules in the interfibrillar matrix are considered to have dimensions too small to induce any scattering at visible wavelengths (Hart and Farrell, 1969).

## Chapter 1

The cornea is of course composed of a great many collagen fibrils, lying in all possible orientations through the stromal depth; therefore a wave train encounters many such scatterers as it moves through any given optical path through the cornea. When a given electric field is incident on a fibril it induces a dipole moment which is dependent not only on the incident field but on the fibril polarizability, which varies according to geometric size and index of refraction. This dipole then radiates in all possible directions. The electric field scattered from each fibril has two main distinguishing properties, magnitude and phase, and these dictate, through the principle of superposition, how the scattered waves interfere with each other. In order to formulate the electric field scattered from each fibril it is necessary to recognise two polarization cases: the first where the incident field is polarized parallel to the fibril axis and the other when it is polarized perpendicular to the fibril, as shown below (Maurice, 1956).

Eq 1.1

$$E_{\parallel} = \frac{1}{2} E \left( \frac{\lambda}{4r} \right)^{1/2} \left( \frac{2\pi a}{\lambda} \right)^2 (n_f^2 - n_g^2)$$
$$E_{\perp} = E \left( \frac{\lambda}{4r} \right)^{1/2} \left( \frac{2\pi a}{\lambda} \right)^2 \left( \frac{n_f^2 - n_g^2}{n_f^2 + n_g^2} \right) \cos \phi$$

Here,  $\lambda$  is the incident wavelength,  $a$  is the fibril radius,  $r$  is the displacement to some distant viewing point,  $n_f$  and  $n_g$  represent the refractive indices of the fibril and ground (extrafibrillar) substance respectively and  $\phi$  represents the angle through which the scattered field is deviated from the incident. The factor  $E$  represents the incident field.

Whether the interference effect between scattered fields is constructive or destructive depends on the path length between the objects acting as scattering centres. The total transmitted intensity is the square of the sum of the electric fields scattered from each fibril. In cornea therefore, it is necessary to define the spatial ordering of the fibrils (i.e. define positions for the fibril axes within a given lamella) to compute the

transmitted light fraction. A number of techniques for achieving this have been applied to cornea.

At this stage it will be convenient to define the scattering cross section. The scattering cross section is the area in which the total intensity of all scattered light from an object is concentrated – in the case of an infinitely long cylinder it is conventionally referred to as the scattering cross section per unit length. Furthermore, the efficiency factor for scattering can be defined as the scattering cross section divided by the geometric cross section of the object (van de Hulst, 1981). In the case of individual collagen fibrils it is found that they are somewhat inefficient at scattering.

Starting with equation 1.1 Maurice (1957) gave the following expression for the scattering cross section per unit length of a fibril:

Eq 1.2

$$\sigma = \int_{-\pi}^{\pi} \frac{n_s c (E_{\perp}^2 + E_{\parallel}^2)}{4\pi} l r d\phi$$

Here,  $n_s$  is the overall corneal refractive index and  $l$  is the length of the fibril. This is readily integrated. The term  $c$  represents the speed of light and  $r$  the fibril radius, and  $E$  represents the perpendicular and parallel electric field, as outlined in equation 1.1. Under the assumption that each fibril scatters independently it can be shown, using equation 1.2, that the cornea would scatter appreciably, i.e. it would not transmit the majority of light in the forward direction (Maurice calculated the total transmitted fraction of light would be 6% (Maurice, 1957). However, such a low fraction is disputed (Worthington, 1984)). Of course, this case would correspond to collagen fibrils having completely random relative spatial ordering. Since a completely random arrangement would lead to a high degree of light scattering, it is accepted that there must be some degree of interference between fields scattered from different fibrils. This must of course be reconcilable with the structural appearance as shown in electron micrographs, as well as the parameters which can be derived by X-ray scattering methods. The following sections are therefore a short survey of each model

of ‘correlation’; a general mathematical review for transmission through various different lattice types with reference to cornea may be found in Worthington (1984).

### 1.2.1 Periodic arrangement of collagen fibrils

Maurice (1957) proposed in his seminal paper that corneal collagen fibrils were arranged in a periodic lattice; specifically, a hexagonal lattice was proposed as an efficient form of crystalline packing. In this instance the cornea would act as a simple diffraction grating. The structure factor of such an arrangement would consist of Dirac delta function singularities, or spikes. Since the wavelength of visible light is much larger than the spacing between fibrils, the ‘grating’ would transmit light exclusively in the forward direction as a ‘zeroth order’. The cornea would therefore be perfectly transparent. It was suggested that ‘mucoïd proteins’ now known as proteoglycans helped to order the structure.

Maurice therefore proposed a number of conditions for a tissue to be transparent based on comparison between stroma and sclera:

1. Fibrils must be parallel to the surface
2. Fibrils must be equal in diameter
3. Fibrils must have their axis disposed in a lattice

The electron micrographs did not, however, show the hexagonal lattice seemingly required by this theory. Indeed point three was debatable as the thick Bowman’s layer of certain shark species with its disordered distribution of fibrils did not seem to be a barrier to light transmission (Goldman and Benedek, 1967). Future workers therefore diverted attention to proving that the appearance of stroma in the electron microscope was consistent with efficient light transmission. If the corneal collagen fibrils were not to be modelled as a periodic lattice then an alternative device was required to compute the light scattering; there are two principal methods by which this has been formulated.

### 1.2.2 Short range ordering of fibrils

Although the electron micrographs did not show what might be termed periodic order, the cornea was obviously not completely random in the sense that a classical ideal gas would be. One of two possibilities put forward was a distribution of collagen fibrils based on the supposed short range order thought to be present in simple liquids and glasses.

In X-ray scattering from liquids and gases, a common method of analysing the degree of short range positional correlation is to utilise the radial distribution function  $g(r)$ , which is the real space equivalent of the structure factor  $S(\mathbf{q})$ . The structure factor is obtained by deconvolving the diffraction spectrum  $J(\mathbf{q})$  with the structure factor due to a single scattering object  $\chi(\mathbf{q})$ . The radial distribution function essentially shows the probability of any two scattering objects having spacing  $r$  (or the ratio of density at any given radial displacement to the bulk density).

The derivation of the radial distribution function is a relatively straightforward procedure (Ziman, 1979) outlined succinctly below. Firstly it is necessary to define the structure factor.

Eq. 1.3

$$S(\mathbf{q}) = N^{-1} \sum_{i,j} \exp(-i\mathbf{q} \cdot (\mathbf{r}_i - \mathbf{r}_j))$$

The term  $N$  denotes the number of scattering objects and the subscripts  $i$  and  $j$  represent the  $i$ th and  $j$ th scattering elements (here, fibrils). Equation 1.3 can be further simplified by recognising that terms for which  $i=j$  produce a constant factor of unity, and that if the sample has homogeneous density ( $\rho$ ) the summation can be replaced with an ensemble average thus:



Eq. 1.4

$$S(\mathbf{q}) = 1 + \langle \exp(-\mathbf{q} \cdot (\mathbf{r}_i - \mathbf{r}_j)) \rangle$$

The structure factor is defined by eq. 1.4 as being dependent on the scattering vector  $\mathbf{q}$ , which is the angle between the initial and final wave vectors, and  $\mathbf{r}_i$  and  $\mathbf{r}_j$  are the positions of two given scattering elements  $i$  and  $j$ . If the array of scattering objects were a classical perfect gas and all positions were completely independent then  $S(\mathbf{q})$  would become unity. In Maurice's perfect lattice model,  $S(\mathbf{q})$  would, as outlined above, consist of Dirac  $\delta$  functions, and be purely discrete. The structure factor therefore varies with the amount of classical order and disorder present.

This ensemble average can be transformed to:

Eq. 1.5

$$S(\mathbf{q}) = 1 + \rho \int g(\mathbf{r}) \exp(-i\mathbf{q} \cdot \mathbf{r}) d^3\mathbf{r}$$

Where  $g(\mathbf{r})$  is, the pair distribution function, and  $\mathbf{r}$  is the vector to some arbitrary point in relation to the origin. To convert this into the radial distribution function it is necessary to assume that the sample is rotationally symmetrical and isotropic; in this case we only need concern ourselves with the modulus of  $\mathbf{q}$ , as the diffraction spectra should also be rotationally isotropic.

A Fourier inversion can then be applied to eq. 1.5 in order to obtain  $g(r)$ , the radial distribution function; it is necessary to account for the fact that the radial distribution function approaches unity at large displacements  $r$ , therefore a factor of unity is subtracted from it giving the total correlation function  $h(r) = g(r) - 1$ . A full derivation and discussion may be found in Ziman (1979).

In the case of corneal stroma, fibril positions can be obtained from segments of electron micrographs which show transverse fibrils; Hart and Farrell were the first to convert these into radial distribution functions (Hart and Farrell, 1969) and suggest

that the form of  $g(r)$  was consistent with that of a simple liquid or amorphous system. Local order was found to extend some 200nm (see figure 1.4), with latent scatter in the sample masking any details beyond that. The first peak is, of course, the average interfibrillar spacing. The remaining peaks shown the positional correlation in terms of shells radiating out from the nearest neighbour; the second peak is thus the second nearest neighbour and so forth.

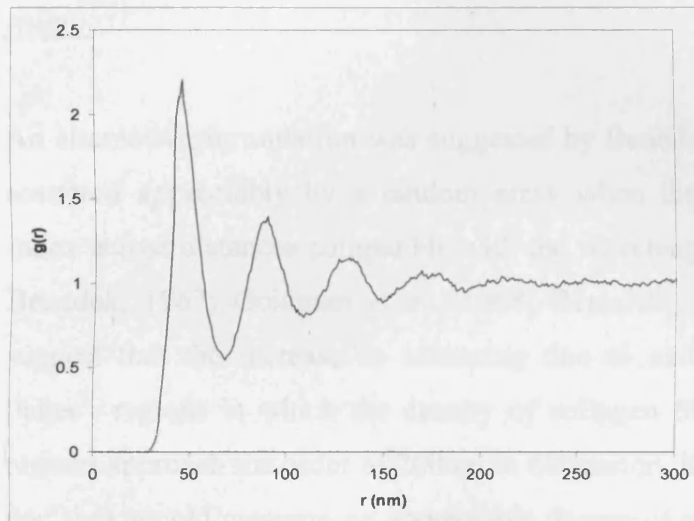


Figure 1.4 Radial distribution function for a normal human cornea (posterior section) showing order extending approximately 200nm.

It was therefore possible to apply a straightforward transformation to obtain the scattering cross section from the radial distribution function. Using the precedent set by Maurice (1957) the scattering cross section of an individual fibril is a Bessel function.

The derivation of the average scattering cross section per fibril for a distribution of cylinders may be found in the original paper (Hart and Farrell, 1969). Here, the final result only is stated:

Eq. 1.6

$$\frac{\sigma_s}{\sigma_0} = \frac{\sigma_{//} + \sigma_{\perp}}{2} - \frac{4\pi\rho}{k_0} \int_0^r r(1 - g(r))(G_1(r) + G_2(r))dr$$

## Chapter 1

Here,  $\sigma_s$  is the average scattering cross section per fibril,  $\rho$  is the fibril number density,  $G_1(r)$  and  $G_2(r)$  contain the integrals of a Bessel function of the first kind. The term  $k_0$  is the wavevector. The factors  $\sigma_{//}$  and  $\sigma_{\perp}$  are the scattering cross section of a single cylinder with incident electric field in the parallel and perpendicular directions. This approximation is valid provided that the incident beam is unpolarized. Hart and Farrell were able to obtain satisfactory agreement between theory and experiment using this methodology, using the positions of 700-1400 fibrils.

An alternative formulation was suggested by Benedek by observing that light is only scattered appreciably by a random array when there are fluctuations in refractive index across distances compatible with the wavelength of visible light (Goldman and Benedek, 1967; Goldman et al., 1968; Benedek, 1971). They were also able to suggest that the increase in scattering due to oedema was caused principally by 'lakes', regions in which the density of collagen fibrils decreases rapidly. If these regions approach the order of 200nm in dimension, it is theoretically possible to show that they would generate an appreciable degree of scattering (Goldman et al., 1968; Benedek, 1971). This has been further investigated by analysis of Fourier components calculated from electron micrographs, demonstrating that in cornea the spatial fluctuations in fibril number density occur across intervals of 80nm, compared with 300nm in the opaque sclera, leading to the concept of a 'scattering range' (Vaezy and Clark, 1991). It was determined that a quarter of the Fourier components in a power spectrum of corneal ultrastructure occur in the scattering range, which corresponds to wavelengths of 200-1100nm, compared to over half in the sclera.

In the short range ordering models the scattering cross section is found to have an inverse cubic relationship to wavelength and it is thought that this is an excellent match to the wavelength dependence of corneal transmission as measured by spectrophotometry (Hart and Farrell, 1969; Farrell, McCally and Tatham, 1973; Farrell and McCally, 2000).

The radial distribution function is, however, somewhat limited in computing the light scattering from corneas in which the fibrils have their axis disposed in such a manner

that they lack radial symmetry; such as the case in corneas at a high level of oedema, for example. In this case, an alternative statistical device is required to determine the structure factor, using the so called 'direct summation of scattered fields approach' which will be discussed in a subsequent chapter. Succinctly, a given distribution of fibrils is divided into a grid to produce 'boxes'; the scattering cross section of each box is then determined; a summation is then performed across all grid elements and then canonical distribution methods used to extrapolate this throughout a whole cornea.

### 1.2.3 Long range order

An alternative hypothesis to classical short range order would suggest that the fibrils are arranged in a perfect periodic lattice with small, isotropically random displacements (Feuk, 1970). Feuk additionally proposed that this small level of disorder was the source of the low level of light scatter that does occur in the cornea. This can be understood by referring back to eqn's 1.3 and 1.4; if the generating set of points is periodic in real space with some random displacement, a diffuse background component will be added to the discrete structure factor  $S(\mathbf{q})$ , that will increase as the amount of displacement from the periodic lattice positions becomes higher. An example is illustrated in figure 1.5.

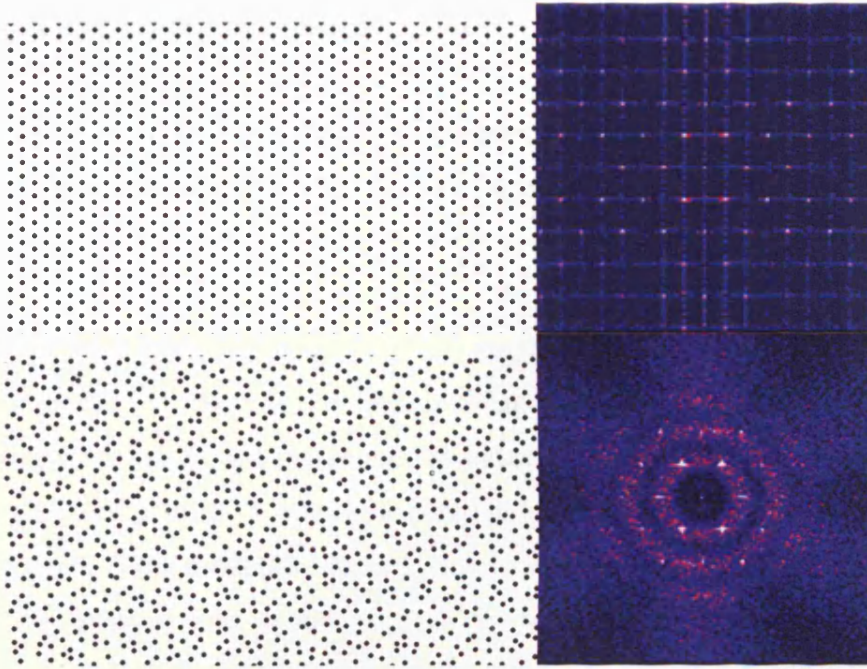


Figure 1.5 Periodic (top) and distorted periodic (lower) lattices in real and reciprocal space (left to right). Distorted lattice generated after the method of Feuk (1970)

It can be seen however from figure 1.5 that even at quite high levels of disorder one can still observe a discrete component of the structure factor, revealing the presence of a hexagonal lattice even when it may not be obvious from visual inspection of the generating set.

Feuk determined that the wavelength dependence of a perturbed hexagonal lattice would be an inverse fifth power, although it was also determined that a purely random system would produce inverse cubic dependence (Feuk, 1970). He conducted experimental measurements of this for rabbit cornea which appeared to give inverse fifth power dependence of scattering (Feuk, 1971). Unfortunately there is disagreement in the literature on this matter and an inverse cubic relation for normal corneas has been found in subsequent literature (Farrell et al., 1973; Farrell and McCally, 2000). This apparent contradiction will be discussed in the following chapters.

#### 1.2.4 Alternate formulations and corrections

There are a small number of alternative formulations of corneal transparency which require some degree of coherence between the fields scattered from each fibril in order to enable efficient transmission.

One such formulation is that of Twersky, in which the stroma is modelled as being composed of fibrils which have a collagen based core and a surrounding outer core of a material to match the refractive index with the interstitial media (Twersky, 1975). The formulation is otherwise similar to that of Farrell's (1969) radial distribution model. This model produces good correlation with experimental readings of corneal transmission and would appear to have good agreement with the two stage dehydration theory of Fratzl. However this hypothesis would rely on the majority of water below  $H=1$  being removed from the fibrils rather than the extrafibrillar substance (Fratzl and Daxer, 1993). This does not fit well with the results of Huang and Meek which appear to show both inter- and intra-fibrillar spacing showing variation below  $H=1$  (Huang and Meek, 1999). In a swelling scenario, this model would rely on the loss of transparency being solely due to an increase in interfibrillar spacing (and subsequent change in fibril volume fraction) and would ignore the influence of lakes on the process, which is certainly far greater.

One of the most interesting models of corneal transparency relies on a relatively recent development; photonic band theory (Pendry, 1996), and has only thus far been applied to cornea by Ameen (1998). This theory is analogous to the band theory for electrons well known from solid state physics. When electrons propagate through an atomic system, the atomic lattice potentials have the effect of creating band gaps; regions in which electron wavevectors  $k$  with certain energy are forbidden from propagating. These band gaps can be approximately calculated by making the observation that it is possible to divide  $k$  (or frequency) space into regions known as Brillouin zones, which can be defined as the unit cell of the reciprocal lattice – this is of course intimately dependent on the structure factor of the system in question. An identical effect can be achieved using electromagnetic radiation by creating periodic variations in refractive index; for example air holes can be periodically etched into a layer of material – normally semiconductor materials with high index of refraction –

the resultant construction may be called a photonic crystal. Although normally used to produce rather exotic optical effects, there is an obvious analogy with the structure of the cornea as presented above, a concept which has received attention in the literature (Maksimova, 2001).

The photonic band theory analysis of Ameen and co-workers was slightly limited as it required the use of purely periodic arrays to solve the necessary equations exactly. In their work, a hexagonal lattice was used (Ameen, 1998), thus the formulation of a Brillouin zone is elementary. Using this methodology, it was found that structural parameters comparable with sclera produced band gaps in the visible region whereas parameters which could be associated with cornea did not. This methodology predicted an almost perfectly transparent cornea, with no decrease in transmission observed at shorter wavelengths; it was further shown that this was identical to what may be found from a uniform refractive index model; although Ameen attributed this in the main to the low contrast between the refractive index of the fibril and that of the ground substance, it would seem likely that the hexagonal structure factor they were limited to using could also cause this effect.

None of the methodologies described previously (bar that of Ameen) account for multiple scattering. Using the Born approximation it is generally assumed that each fibril experiences a driving electric field equal to the incident one, i.e. the incident field is not affected by that scattered from another fibril. A correction to the work of Hart and Farrell (1969) has been developed to account for this, although it leads only to a very modest change in final corneal light transmission (Smith, 1988). Calculations have suggested that there is almost no discernable effect on corneal transmission; a very slight increase in transmission was observed when the correction was applied to scattering from a bovine corneal stroma (Leonard, 1996).

### **1.3 Order and disorder**

Thus far, in previous sections, various methods for describing and modelling the fibril distributions in order to compute the structure factor have been outlined. Until 1984 it had been thought that there were essentially two methods of packing finite objects into a given volume at the nanometer scale. The first, deterministic, method used the

## Chapter 1

Bravais lattices to produce purely periodic arrangements, in the sense that the unit cell possessed only two, three, four and six fold rotation axes. This allowed crystallographers to define space groups, a group of isometries which is invariant under transformation. This leads to arrays which possess the fundamental property of translational invariance. The crystallographic restriction theorem prevents purely periodic, translationally invariant arrays from being formed of any unit cell with rotational symmetry that is either pentagonal or greater than six in a given two or three-dimensional plane. The principle of the crystallographic restriction can be extended to higher dimensions, however (Senechal, 1996).

The alternative is a rather broad range of disordered systems said to be liquid/glass-like or amorphous. These systems are often wholly formulated by recourse to pair and radial distribution functions; for example the random close packed structure or the random walk on a lattice. A full theoretical exposition of these systems may be found in the literature (Ziman, 1979). If a perfect crystal lattice is in some way distorted, as for example in the work of Feuk, it is referred to as substitutional disorder. Alternatively, a system in which no crystal order is present but is still densely packed, in the sense that it has similar average density to a perfect crystal, can be referred to as topographical disorder and is the type of fibril packing envisaged by Hart and Farrell. A system with topological disorder should be statistically homogeneous across small distances; in a very crude fashion therefore these systems may have, in a sense, translational invariance across very short 'coherence' lengths. Of course the models must account for the volume fraction occupied by the objects in order to ensure that the arrangement is not so random that they overlap, which is essentially the computational problem with modelling this form of packing. Realistically only in an ideal gas at very low densities does a given model become truly random. However, the distribution of impurities in the lattice of a semiconductor material approaches this gas like disorder at low concentrations and with no chemical reactions (Ziman, 1979).

As might be expected, both of these main groups have interesting subgroups. Examples include microcrystalline powders in which conglomerates of unit cells are arranged with random rotation with respect to each other and nematic order found in liquid crystals in which ellipsoidal molecules may be arranged amorphously but their axes are regularly aligned.



In 1984, X-ray diffraction experiments yielded evidence for the first time of atomic assemblies which possessed rotational symmetry clearly forbidden by the crystallographic restriction theorem – in this instance a crystal with ten-fold symmetry order. This presented a conundrum as it was clear that ‘order’ need not be synonymous with perfect, classical periodicity – and thus these materials were dubbed ‘quasicrystals’ (see Senechal (1996) for a full historical overview of the experimental work).

Mathematicians had been aware for some time that it was possible to generate deterministic and ordered arrays with ‘forbidden’ symmetries, generally known as non-periodic tilings – arrays which have long range order but no average unit cell and which are not translationally invariant (Senechal, 1996). It was found that one class of non-periodic sets, the famous Penrose tilings and their generalisations could be used to produce models of these quasicrystals and their ten-fold symmetry order. A tiling is the act of mathematically tessellating given building blocks (i.e. prototiles) in the given space with no gaps or overlaps. The Penrose tilings are referred to as aperiodic as the prototiles can only tessellate the plane without periodicity; where a set of prototiles also allows construction of periodic sets, the term non-periodic tiling should be used – spiral tiling is one example (although these definitions are not always strictly adhered to).

It will also be useful to clarify at this stage that strictly, a crystal has a purely discrete diffraction spectrum i.e. all or most of the energy in the object’s diffraction pattern should be concentrated in Bragg singularities. Therefore, to qualify as a true quasicrystal, the generating non-periodic tiling should have a diffraction spectrum composed primarily of Dirac delta functions. However, the term quasicrystal is used to loosely describe a broader range of systems than this definition would allow, see for example (Radin, 1999; Macia, 2006; Parker et al., 2006). In this work the terms nonperiodic/quasacrystalline are used. A Penrose tiling, with its Fourier transform, is shown below in figure 1.5. The Penrose tiling can be constructed with the aid of two rhombs of fixed internal angle, which occur in the ratio  $1:\tau$ , where  $\tau$  is the golden mean. Particular attention is drawn to the Bragg peaks arranged with a symmetry forbidden in classical periodic systems, shown in figure 1.6.

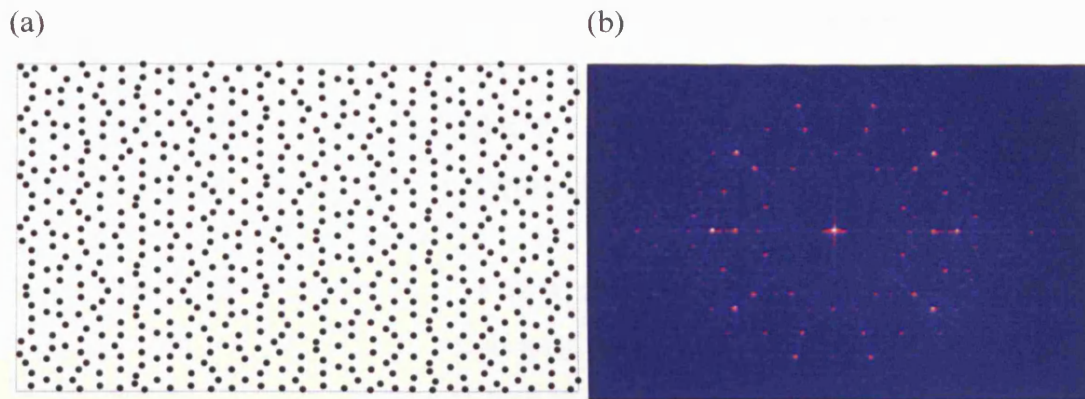


Figure 1.6 Penrose tiling (a) represented as a point set and its Fourier transform (b)

Some of the most intriguing non-periodic sets that have been generated are those which possess effectively infinite symmetry, i.e. the constituent prototiles are tessellated in the plane in every possible orientation. In this case, the Fourier transform spectrum will consist of rings, rather than discrete delta functions. These are referred to as ‘round quasicrystals’ (Radin, 1999). They may be of great interest in modelling certain natural materials since they are deterministic but have structure factors which resemble that of amorphous, short-range ordered systems. This suggests the possibility that natural structures may, in fact, possess a high degree of order which has previously been overlooked. An example is found below in figure 1.7, which is a generalised pinwheel tiling (Sadun, 1998).

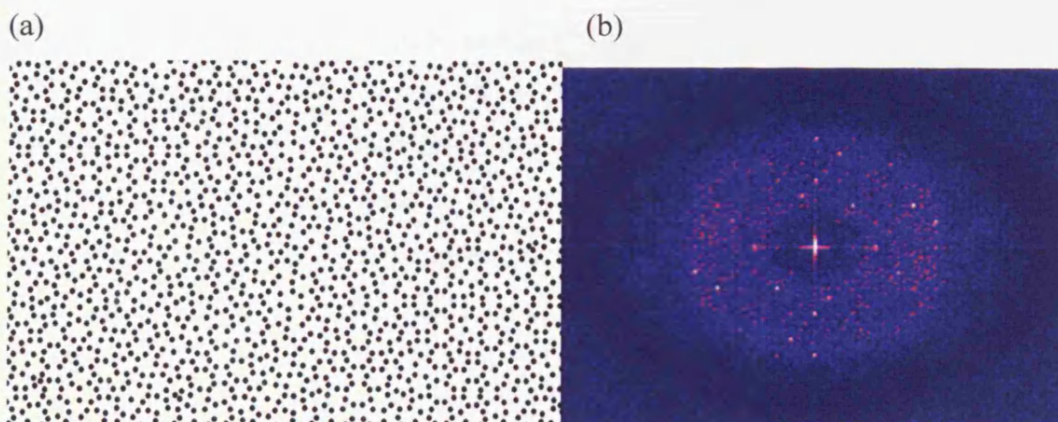


Figure 1.7 Generalised pinwheel tiling (a) and its Fourier transform (b) (represented by point sets)

It can be seen from figure 1.7 that the generalised pinwheel has as its Fourier transform a weak, broad ring. There are some singularities present. However these

are caused by a truncating effect – in any given direction in the real space array there will be a finite number of unit cell directions. This type of structure factor is thought to be absolutely continuous (Godreche, 1992; Radin, 1999), i.e. it is the same as that which may be encountered from an assembly of amorphous matter.

The pinwheel lattice shown above is a good example of how even crystalline behaviour is not essential to establish long range order, since the diffraction pattern shown does not meet the criteria to be a true crystal, despite its deterministic nature. It can be shown that, in fact, there are strict mathematical conditions which need to be imposed on a tiling for the structure factor to be discrete; for example, the binary tiling is a type of Penrose tiling with a singular continuous structure factor (in this type of structure factor, the expected Bragg peaks would be diffuse and the diffraction spectrum hazy) (Godreche, 1992; Senechal, 1996).

One other example of an array family which possesses a liquid-like structure factor are the spiral tilings; these can be constructed from logarithmic spirals and one particular example can be used to model the packing of seeds in the sunflower head. This will be discussed in detail in chapter 3.

### **1.4 Light transmission through normal and swollen corneas**

The cornea efficiently transmits incident electromagnetic radiation in the visible spectrum between 400-700nm. It is found, however, from experimental and theoretical considerations that the cornea does, in fact, transmit wavelengths slightly outside this range, and is found to transmit radiation in the range 295 – 1400nm, i.e. from the near ultraviolet to the near infrared (Kenshalo, 1960; Boettner, 1962; Hart and Farrell, 1969; Lerman, 1984; Fregard, 1997; Douth, Quantock and Meek, 2007).

The attenuation in the ultraviolet region is due to a combination of increased Rayleigh scattering at these wavelengths and absorption due to electronic transitions between different energy levels – near ultraviolet absorptions in cornea are due to proteoglycan and collagen molecules, with liquid water and other simpler molecules having excitations at much shorter wavelengths. This is related to the types of bond present

in complex protein molecules; it is found that absorptions in the visible and near ultraviolet are due to electron transitions between non-bonding states and  $\pi^*$  states (Banwell, 1983). A transition which causes absorption in the UV/Visible range is referred to in spectroscopic terms as a chromophore. These types of transition occur principally in systems which have alternating double and single bonds, i.e. are conjugated; this occurs particularly frequently in molecules such as amino acids. The splitting of d-orbitals in transition metal ion complexes also gives rise to visible absorptions. Neither corneal proteoglycans nor corneal collagens are known to have chromophores in the visible part of the spectrum.

Infrared attenuation is caused predominantly by molecular vibrational absorptions, with their origin not just in the collagenous matrix and the extracellular substance, but also in the large quantities of liquid water present in the cornea. Absorptions in the far infrared, or terahertz region (1000-30 $\mu$ m) are predominantly caused by energy transitions between torsional vibrational modes of a molecule; energy transitions of fundamental vibrations cause mid-infrared absorptions (30-1.4 $\mu$ m). It is also possible for overtones of fundamental modes to cause absorption bands in the near infrared (1400-700nm). Of course, in order for a vibrational mode to be 'infrared active' (ie to interact with infrared radiation) it must induce a change in the molecular dipole moment.

Early visible transmission spectra of the cornea often gave curious results (see Pitts, 1959 for a review of earlier attempts). This is probably due to minimal hydration control on the part of these authors. It is thought that absorptions in the infrared region in the cornea are caused exclusively by the high water content, and indeed this is thought to be a good model for the near infrared region in which the major absorption feature is the free, weak OH line at 1400nm. Whether this can be applied to the mid and far infrared (terahertz range) has not been thoroughly investigated (see review by (van den Berg and Spekrijse, 1997). An analysis of the published infrared spectra of cornea has shown that, although water absorption is a good model for the whole ocular tissue, in isolation there may be contributions from other molecules (van den Berg and Spekrijse, 1997). The far infrared properties do not seem to have been studied in depth up to this point, although this region of the spectrum is considered to

be damaging to the cornea (Zuclich et al., 1984). It is likely that water absorption lines will again be the principal attenuating agent.

Several small absorptions in the visible range have been observed in experimental results from certain species (mainly bovine specimens). These have been attributed to the cytochrome c respiratory enzymes, and are thought to account for only 1% of corneal structure (Lerman, 1984; Leonard, 1996; Kostyuk et al., 2002). The absorption peaks were found to occur in the 400-420nm range, with a smaller bimodal peak at 520-600nm. The effect of these absorption features is not sufficient to cause significant transmissive loss at those frequencies. Certain fish corneas are known to possess absorption pigments which can be regulated (Siebeck et al., 2003). In addition there appear to be varying types and amount of pigment in different parts of the cornea. An example spectrum of visible corneal light transmission is shown in figure 1.8, from sheep cornea.

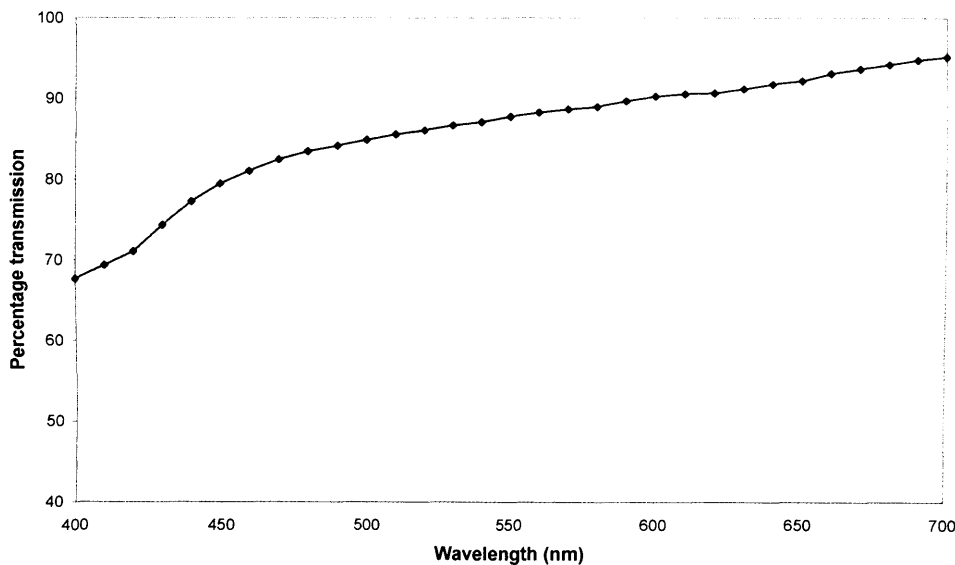


Figure 1.8 Light transmission of ovine stroma (adapted from Dutch, Quantock and Meek, 2007)

Since the cornea is transparent to visible wavelengths, presumably the reduction in transmission through the cornea will be a result of scattering away from the incident direction although it will be quite small and will become more significant in the violet end of the spectrum. Light scattering can therefore be analysed quantitatively by

measuring transmission in the spectrophotometer. If the incident beam is paraxial the light is scattered primarily within a relatively small solid angle (Feuk and McQueen, 1971).

In the ultraviolet region, the cornea possesses low transmission, caused by scattering effects and also, at shorter wavelengths, chromophores in the polysaccharide and amino acid molecules contained within the ground substance of the stroma (Lerman, 1984). Collagen itself has a weak absorption at 280nm which is thought to be due to the presence of aromatic amino acids. Lerman (1984) was able to show that the cornea was opaque to wavelengths greater than 295nm and offer a theoretical explanation. This is certainly not a bar to ultraviolet vision utilised by some species. For example, certain fish species are known to possess ocular media that transmit UVA wavelengths relatively efficiently (Siebeck and Marshall, 2001) and similar findings have been reported on pigeon ocular media (Emmerton et al., 1980).

It was initially found that UV transmission of the cornea decreased slightly with age. This was thought to be due to photochemical action in the ageing cornea. The lens also displays this effect to a higher degree, with visible light transmission decreasing with age (Lerman, 1984). However, later researchers noted no correlation between increasing age and corneal transmission using a blue-green argon laser (Best, 1988; Beems and Best, 1990). Best et al (1988) believed the apparent contradiction occurred because they used whole eyes with photodiodes attached to the surfaces, rather than extracted corneal sections as been the case in the past. One problem with this study, acknowledged by the authors, is that since the photodiode was mounted on the surfaces under study, some scattered light from the cornea will hit the detector. Another survey published only a few years later seems to confirm that age-related correlations are insignificant (van den Berg and Tan, 1994).

Corneal transmission is also dependent on the hydrostatic pressure exerted on the stroma (Maurice, 1957). Light transmission is known to decrease by about 30% for a sudden increase in pressure from 4.5 mm Hg to 18 mm Hg, in the rabbit. There is an element of time dependence (Farrell and McCally, 2000) and is quite reversible. Kostyuk et al (2002) found that corneal transmission showed a decrease of around 5% when the cornea was not pressurized. This study utilised 10nm sampling and showed

## Chapter 1

95% transmission in the long wavelength region, decreasing to 80% in the short wavelength limit, at a physiological hydration and concentration of chloride anion, in the bovine cornea. These results correspond closely with those of Farrell who used a very similar experimental set-up (Farrell et al., 1973).

A full quantitative study of light scattering from corneal wounds (scarring) has only been recently performed. Electron microscopy shows regions of voids or lakes and the wavelength dependence of light transmission in scarred regions is similar to that of swollen corneas, with populations of enlarged fibrils. Light scattering was still quite a prominent feature of these regions even four years after the wounding event (McCally et al., 2007).

Amniotic membrane, which is sometimes used to repair irreversibly damaged corneas, is also known to be translucent (Ijiri et al., 2007), presumably due to its broadly similar structure to cornea, with long thin collagen fibrils organised into defined layers (Connon et al., 2007).

The influence of keratocytes on corneal transparency is not entirely clear. Keratocytes possess cross sectional size of 80-200 $\mu\text{m}$  (Prydal et al., 1998), and are thus not small enough that their scattering cross section can be modelled by reference to Rayleigh theory. They must be treated by the more general case of Mie scattering. If the keratocytes were simple spheres it would be a relatively simple matter to approximately compute a scattering cross section for a single cell. However, keratocytes are not simple spheres and have quite a complex shape. The refractive index of keratocytes does not appear, to the author's knowledge, in the extant literature. An additional complication is the influence of organelles and cell nuclei which almost certainly induce some scattering. Integration into present models of corneal transparency would be somewhat difficult and it will further be necessary to determine whether there are any positional correlations in keratocyte position or whether they can be regarded as randomly distributed; it is known that their distribution is fairly homogeneous throughout the thickness of the central cornea (Muller, Pels and Vrensen, 1995).

Keratocytes can have a detrimental effect on efficient light transmission. They are often found, or thought, to be associated with corneal haze in various clinical settings (Moller-Pedersen et al., 1998; Connon et al., 2003; Moller-Pedersen, 2004), particularly where the cells have become activated during wound healing. From biochemical studies, it was determined that keratocytes in clear corneas express two water soluble proteins at a far higher level than that found in wounded corneas. These proteins are similar to the crystallin proteins found in lens tissue and would appear to have a role in regulating the optical properties of keratocytes, perhaps by modifying the refractive index to match that of the stroma and thus minimise scattering losses (Jester et al., 1999; Jester, 2008).

It is well known that the cornea loses transparency when it undergoes oedema. A theoretical basis for this has been discussed in section 1.2. There are few controlled studies which have sought to actually measure the decrease in light transmission; generally, transmission is found to decrease by some 40% when the cornea swells to twice its physiological thickness (Farrell et al., 1973). However, the cornea can swell up to 1.25 times its physiological thickness before transmission decreases considerably.

### **1.5 Aims**

This thesis describes corneal light transmission at visible and infrared wavelengths and aims to investigate this from both theoretical and experimental standpoints. The work aims to improve basic understanding of corneal transmission and pave the way for new potential uses of light-based techniques in basic research and clinical settings. The first results section will detail a new approach to deterministically model the array of collagen fibrils within a lamella. This is achieved by using novel non-periodic arrays, upon which models of so called quasicrystal materials are based, different to the pseudo-hexagonal and amorphous-type arrays used previously.

The second results section deals with the visible (400-700nm) transmission of human corneas, with particular attention paid to the transmission away from the central axis, where variations in ultrastructural parameters are known to occur. This is



investigated using spectrophotometry and light scattering theory (Direct summation of scattered fields).

The third section deals with the swelling properties of human corneas; specifically, the relative amount in which the central and peripheral portions of human cornea swell when placed in free solution, and how transmission varies away from the central axis under these conditions. It is known clinically that central and peripheral portions swell at differing rates; this work will seek to place this observation on a more quantitative basis.

The fourth section investigates transmission of infrared wavelengths, a somewhat ignored portion of the spectrum in so far as the cornea is concerned. In this portion of the spectrum, scattering becomes quite negligible as an attenuation mechanism; light loss occurs primarily through absorption by liquid water (and of course the protein matrix). With this in mind, it is probable that there will be a correlation between tissue hydration state and infrared transmission.

The final section investigates Ultraviolet A / riboflavin induced cross-linking of corneal collagens. This is used in the treatment of keratoconus, an ectatic condition which affects the optical properties of the cornea due to changes in corneal shape. Cross-linking the corneal collagen is thought to stabilise this condition. The effects of cross-linking treatment on transparency have not been examined previously; specifically I will attempt to use spectrophotometry to track the presence of riboflavin within the tissue, utilising this molecule's spectral properties. Using this method the effects of varying levels of epithelial on riboflavin penetration will be extensively tested. Furthermore, free swelling studies will be used on thin segments of corneas in order to attempt to detect signatures of cross-linking.

## **Chapter 2. General methods**

This chapter will describe methods which have been used throughout the work; particularly tissue handling procedures. More specific procedures are referenced in the appropriate chapter.

### **2.1 Preparation of tissue samples: Human and Animal**

All experiments involving human tissue were approved by the institutional ethics committee and were conducted in accordance with the tenets of the declaration of Helsinki, and with reference to the Human Tissue Act 2004.

Fresh bovine globes were obtained from the abattoir at Cinderford, Gloucestershire within hours of death. The corneas were excised from the eye with a small ring of sclera to enable clamping within the sampling chambers with an appropriate scalpel.

Human corneas were obtained from the Bristol Eye Bank, run by the United Kingdom Transplantation Service. The corneas were delivered with a rim of sclera attached, and stored in HEPES buffer with MEM culture medium. All were rejected for transplant due to low endothelial cell count.

The epithelial and endothelial layers were removed from human and bovine corneas, by the use of a surgical blade and by the use of laboratory blotting paper. Any remaining ciliary body or staining was removed. Corneas were rejected for use if they were found to possess obvious deformity such as blood staining or thermal damage.

Following dissection, the corneas were then transferred to dialysis tubing and dialysed overnight against a de-swelling solution, using the procedure outlined in section 2.3, or stored in the refrigerator for 1 day wrapped in clingfilm or mylar.

### 2.2 Preparation of dialysis tubing

Dialysis tubing with a molecular weight cut-off of 12000-14000Da was used. Following the method of Khan (2003), the tubing was cut to appropriate lengths, and then placed in ethanoic acid at 1% for 60 minutes, and then rinsed in distilled water for approximately 30 minutes. The tubing was then transferred to a solution of 1% sodium carbonate and 10mM diethylaminetetraacetic acid (EDTA), for 30 minutes and heated to 75°C. They were again heated to 75°C in distilled water and allowed to cool. The tubing could then be stored in this solution for as long as needed.

### 2.3 Dialysis of human and bovine corneas for hydration control

Corneas are invariably swollen when they are removed from culture medium. This also occurs in abattoir tissue as there is a time delay between the enucleation of the eye in the abattoir and arrival in the laboratory, during which time a modest amount of swelling can occur. Light scattering is dependent on the hydration level of the cornea and for the purposes of this work it was necessary to adjust the stromal water content to produce a physiological value of hydration (generally taken as 3.2). The dialysis method is one way of achieving this and can be used to produce other hydration levels if needed. This works by creating an osmotic gradient between the stroma and the solution it is being dialysed in, in this case, polyethylene glycol. The dialysis method minimises leaching of interstitial material from the collagenous matrix. Human and bovine corneas were placed in dialysis tubing prepared using the method outlined above. The ends of the tubing were sealed with dialysis clips. To produce a hydration of 3.2 in a bovine cornea the following solution was used:

0.154M sodium chloride

4.45% polyethylene glycol (PEG) of molecular weight 20kDa.

From previous work (Meek et al., 1991; Khan, 2003) it was noted that a solution of 2.4% PEG produces this hydration in the human cornea. An increase in concentration of PEG will dehydrate the tissue further. The difference in concentration of PEG required is due to the differing relative masses of the corneas, with bovine cornea for example being much thicker than human

### 2.4 Image processing of electron micrographs

The following steps were performed to extract relative fibril positions from micrographs, based on the method of Connon (2003), as shown graphically in figure 2.1:

#### Step A. *Acquisition*

Micrographs were scanned in from film or from literature. This was done using a *HP ScanjetADF*. The files were saved as 8-bit TIFF files at high resolution.

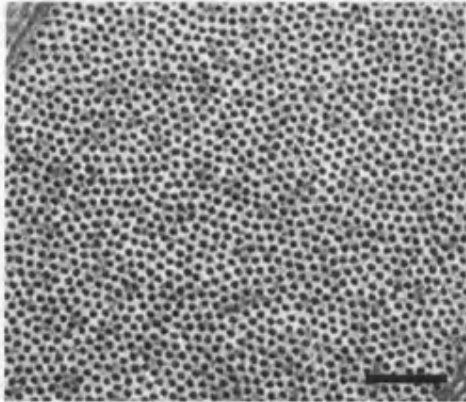
#### Step B. *Area selection and Contrast Enhancement*

ImageJ software (NIH freeware) was used to select an appropriate area of the micrographs for analysis. The rest of the image was then cropped. Contrast was enhanced as required.

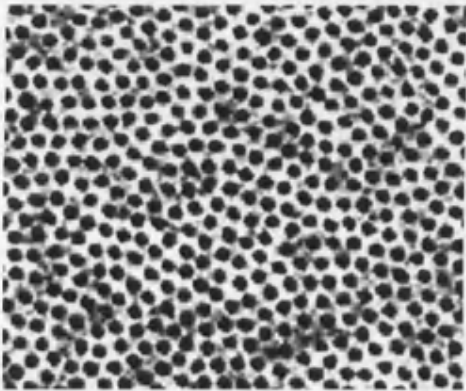
#### Step C. *Filtration and thresholding*

- i. The scale was set according to that in the original micrographs. A band pass filter can then be used to remove objects within a certain pixel size range if required, although this was found to be unnecessary for images processed in this thesis.
- ii. Once this was done, the threshold feature of the software was used to select an upper and lower pixel intensity limit. An appropriate range was selected to separate the fibrils from any surrounding media or contamination. True fibrils tend to have a density value which reaches a maximum at the centre of the fibril, presumably due to stain penetration. Pixels which lay outside this range were then given a value of 0. Pixels within this range were assigned a value of 255 and these were taken to be representative of fibrils.

A.



B.



C.

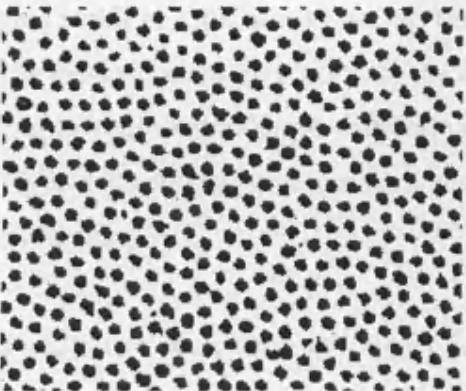


Figure 2.1: A, B, C represent steps outlined above in the process of extracting fibril co-ordinates from electron micrographs. Scale bar shown in A ( $1 \mu\text{m}$ ). A. Image acquisition B. Area selection and contrast adjustment C. Image in B after filtration and thresholding.

### Step D. *Fibril position determination*

ImageJ is supplied with an in-built function to determine spatial positioning from the 'centre of mass' of a given distribution of pixels with intensity value 255 (i.e. black). These were output as a \*.txt file and ported into Excel. It is possible to derive a diameter by having the analysis algorithm determine the area of each fibril. This feature is not used in this work, as diameter parameters are used from X-ray scattering work. Diameters derived from X-ray scattering are

### **2.5 Theoretical modelling of corneal transmission: Direct summation of fields**

Transmission of corneal electron micrographs and theoretical fibril arrangements was calculated using Freund's (1987) direct summation of scattered fields methodology, with the aid of extant computer programs written in C used for a previous study (Leonard, 1996; Meek et al., 2003b).

In order to understand the essence of the direct sum methodology it is necessary to appreciate that electron micrographs of cornea only show the fibril distribution within a comparatively small area. Attempting to calculate the scattering cross section of this small portion would lead to undesired truncation effects. This can be seen from the mathematical derivation of the direct sum model, in which it is necessary to factor out a whole term due to diffraction effects (Freund, McCally and Farrell, 1986) The direct sum model therefore uses statistical techniques in an attempt to circumvent this problem.

Firstly, two basic assumptions are required:

1. All lamella have the same bulk fibril number density
2. Fibrils have their axes disposed in a similar, but not identical manner within different lamella.

For practical calculation of light transmission it is of course necessary to know the refractive indices of the fibrils and extrafibrillar matrix and the gross fibril number density. The full derivation is available in the literature (Freund, McCally and Farrell,

1986; Freund et al., 1995) and it is furthermore provable that we need not overly concern ourselves with the effects of fibril orientations if the incident beam has no average polarization.

As outlined in the introduction, the actual method by which the computation of the scattering cross section is obtained involves dividing a given 'lamella' (in the practical case an appropriate micrograph segment of transverse section fibrils) into a grid of boxes. Thus each fibril belongs to a particular grid element. The electric fields within a box can then be superposed and summed; this allows calculation of the differential scattering cross section per fibril (i.e. the scattering cross section at any given angle); if this is performed for every box, an ensemble average can be calculated for the whole stroma. It can be shown that it is statistically equivalent to compute the scattering cross section using this method as it would be to compare an ensemble of corneas having the same fibril number density and the same interfibrillar forces (Freund et al., 1986).

The differential scattering cross section, which is the cross section at any given angle, can be defined in this case as:

Eq 1.7

$$\sigma_s(\lambda, \theta) = \frac{K}{(K-1)N} \left( \overline{|\Omega(\mathbf{q})|^2} - \left| \overline{\Omega(\mathbf{q})} \right|^2 \right)$$

Where K is the number of boxes in a grid and N is the average number of centres (of fibrils) per box. The factor  $\Omega(\mathbf{q})$  is the average sum of scattered fields within each box. The two terms encompassing  $\Omega(\mathbf{q})$  must cancel to a high degree to render the cornea transparent. This can be transformed into the total scattering cross section by integration:

Eq 1.8

$$\sigma_t = \int_0^{2\pi} \sigma(\lambda, \theta) d\theta$$

## **Chapter 2**

In the implementation of the algorithm used in this work, 200 equally spaced angles in the integration limits were used for calculation of the total scattering cross section. The dimensions of each grid element were set to be 600x500nm. This is fixed regardless of the number of fibrils in the sample. The dimensions are therefore much larger than the fibril correlations found in the cornea, which are of the order of 200nm. It is of course relatively straightforward, within this model, to compute scattering in arrangements with varying fibril diameters. A generalised methodology for the calculation of refractive indices will be presented in chapter 4, based on that of Leonard and Meek (1997) and Meek et al (2003).

The algorithm used in this work also includes a scaling procedure. This procedure allows the interfibril spacing and fibril diameter to be rescaled. This allows data from X-ray diffraction, unaffected by shrinkage effects, to be used. This can be useful for determining the effects of increases in interfibril spacing and fibril diameter on light scattering, whilst preserving overall spatial ordering.



## Chapter 3. Spatial ordering of collagen fibrils within the corneal stroma

### 3.1 Introduction

As outlined in chapter 1, the cornea is the primary refractive component of the terrestrial eye and is responsible for over two-thirds of the optical power. To achieve these properties, the cornea contains uniform diameter collagen fibrils laid down in a series of lamellae with each lamella running at a specific orientation from one side of the tissue to the other and remaining approximately parallel to the surface. The collagen fibrils are embedded in an extrafibrillar matrix composed of highly charged proteoglycans and glycoproteins. This extrafibrillar matrix possesses a different refractive index to the collagen fibrils (Maurice, 1956; Freund et al., 1995; Leonard and Meek, 1997). Unlike other collagenous tissues, however, the cornea is required to be highly transparent. The way in which this transparency is achieved has produced a small but steady flow of literature from theoretical and experimental standpoints. Theoretical deductions of scattering in the cornea usually follow the precedent, set by Maurice, of modelling the cornea as a matrix of dielectric needles or cylinders (the fibrils) embedded in some substance, possessing a distinct refractive index (Maurice, 1956), with light travelling perpendicular to the cylinder axis. The form of the scattered field from a dielectric cylinder of length much greater than the incident wavelength is known (van de Hulst, 1981; Bohren and Huffman, 1983), and it is therefore possible to determine the interference function or structure factor which modulates these scattered fields. Here, this is expressed with the following equation, conventionally used in X-ray scattering theory:

Eq. 3.1

$$J(\mathbf{q}) = |\chi(\mathbf{q})|^2 S(\mathbf{q})$$

Where  $J(\mathbf{q})$  is the intensity distribution of scattered light,  $\chi(\mathbf{q})$  is the Fourier transform due to a single cylinder or fibril and  $S(\mathbf{q})$  is the interference function.. The vector  $\mathbf{q}$  is the scattering vector.  $\chi(\mathbf{q})$  takes the form of a Bessel function, the behaviour of which

is well documented elsewhere (Hart and Farrell, 1969; Freund et al., 1986; Farrell and McCally, 2000; Meek et al., 2003b).

The interference function  $S(\mathbf{q})$  is the square of the spatial frequency spectrum (the Fourier transform of the point set) and it will be useful to briefly recap its main properties at this juncture. If the scattering sample were a perfect crystal,  $S(\mathbf{q})$  would be purely discrete, in the form of weighted Dirac delta functions. If, on the other hand, the sample were completely random and had no positional correlation (like a gas) then  $S(\mathbf{q})$  would be unity and scattering would thus be incoherent (this can be referred to as absolutely continuous scattering). Clearly the  $S(\mathbf{q})$  of many real systems will contain both coherent and incoherent elements; even many perfect crystals will possess a degree of thermal broadening of the delta functions. There is one further case of interest which occurs when  $S(\mathbf{q})$  is said to be singular continuous, a situation which could occur for example in a material possessing order, but in which the Bragg peaks are diffused by some local apparently random structure. Certain sequences and binary tilings are known to produce these types of peaks in their diffraction spectra (Godreche, 1992; Senechal, 1996; Wolny, Wnel and Verger-Gaugry, 2000).

Although the lamellar structure of the cornea had long been known, detailed ultrastructural information was not available until the advent of the electron microscope. On the basis of the structure elucidated under transmission electron microscopy, Maurice proposed that the collagen fibrils were arranged in a perfect hexagonal lattice; although the micrographs did not show a perfect array, the effects of chemical fixation were unclear at the time (Maurice, 1956). It was proposed that the interfibrillar proteoglycans were acting to position the fibril axes in this manner; thus each fibril would be linked to its six nearest neighbours in the hexagon. In this case  $S(\mathbf{q})$  would have a form such that the scattered fields from each fibril would cancel exactly. In that case, the cornea would effectively be acting like a simple diffraction grating, and all scattered waves would cancel exactly. This would give transmission in the incident direction only.

Later workers on transparency have assumed that the structure represented in the micrographs is a satisfactory representation of the in-vivo tissue, and therefore

developed methodologies in which the necessary destructive interference effects would occur without perfect crystalline lattices.

By utilising the radial distribution function (frequently used in analysing the X-ray and neutron diffraction spectra of liquids and powders) to evaluate positional coherence of the fibrils, Farrell and colleagues (Hart and Farrell, 1969) were able to demonstrate that the apparent fibrillar arrangement shown was indeed consistent with transparency. Furthermore, they showed that the cornea appeared to possess some form of short range order extending from a given reference fibril to about 200nm; this was thought to be representative of the fibrils being arrayed in a liquid-like manner. Benedek and colleagues also showed that, as long as spatial variations in refractive index did not exceed half the wavelength of light, the cornea should be transparent and further postulated that the loss of transparency in oedema occurred due to the formation of substantial voids, or lakes of fibril-free zones that act as scattering centres (Benedek, 1971). An alternate formulation of transparency was achieved by assuming that the fibrils are disposed in a hexagonal lattice with random, thermal perturbations from the perfect lattice positions (Feuk, 1970). Analysis of X-ray scattering data to obtain the fibril volume fraction suggested that the volume fractions of corneal collagen fibrils are best modelled by assuming they are arranged as in a planar liquid (Worthington, 1984; Worthington and Inouye, 1985).

Leaving the vague notions of liquid-like and random networks aside, there is one, as yet, unexplored, possibility for modelling fibril arrangement, which is ordered and deterministic but would not require the fibrils to have their axes disposed in a classical crystallographic unit cell or anything resembling it. These are structures with aperiodic (or non-periodic) order such as quasicrystals, a quasicrystal being an atomic assembly which produces ordered diffraction patterns but which does not possess the fundamental crystallographic property of translational invariance and has a classically forbidden symmetry, as introduced in section 1.3. Thus, these materials possess long-range order but no average unit cell (Senechal, 1996).

The quasicrystal diffraction spectrum will contain discrete Dirac delta functions (the discrete element of  $S(\mathbf{q})$  mentioned above), set at the points of the dual or reciprocal lattice of the arrangement, i.e. the power spectrum is the Fourier transform of the

auto-correlation of the real space distribution, as in a conventional crystal. The dual lattice will however show symmetry forbidden to a classical crystal.

Restricting ourselves to the two-dimensional plane, crystals or quasicrystals can be regarded as materials whose internal space is tessellated efficiently and deterministically with one or more basic building blocks, for example triangles of internal angle  $60^\circ$  (hexagonal lattice) or the famous Penrose rhombs. If one constructed an array in which a basic unit repeats in every rotational configuration, there would be an infinite array of delta functions set at certain radii in the dual lattice leading to the formation of rings rather than discrete delta 'singularities' in the Fourier transform. It is known that the distribution of fibrils in the stroma is radially isotropic (Hart and Farrell, 1969) and therefore if we are to attempt a model of fibril distributions we must replicate this unique type of order. Of course powders of microcrystal clusters clearly fulfil this requirement as the unit cell of a homogeneous sample of these clusters will occur randomly in all possible orientations; however this is not deterministic and may not tile space efficiently.

The diffraction spectra of these structures would be consistent with diffraction patterns obtained when X-ray or neutron scattering is performed on liquids or glasses, the primary difference being that our array would be a fully deterministic form of aperiodic order, which has been termed a 'round quasicrystal' (Radin, 1999). It is thought that there are means by which these structures can be distinguished from the random amorphous networks. Two examples of structures which may produce this infinite symmetry are the pinwheel tiling (Radin, 1999) and its generalisations (Sadun, 1998) and the sunflower seed head pattern (Vogel, 1979; Parker et al., 2006), a form of spiral or similarity tiling. These structures have generally been obtained by hierarchical inflation methods (Radin, 1999).

The radial distribution function is the real-space equivalent of the interference function  $S(\mathbf{q})$ , under the limiting assumption that the objects under test are distributed in a radially symmetric manner (clearly the round quasicrystal fulfils this requirement, as do simple liquids and random networks). It is linked to the interference function by

the use of equation 3.2, and allows us to investigate the interplay between real space statistical correlations and the form of the interference function (Ziman, 1979):

Eq 3.2

$$S(q) = 1 + 4\pi \int_0^{\infty} r^2 (g(r) - 1) \frac{\sin qr}{qr} dr$$

where  $r$  is the real space displacement and  $g(r)$  is the radial distribution function. It can be shown then that when objects are packed into coordination shells (for example a simple liquid with its short range order caused by intermolecular interactions) rings will be observed in the diffraction spectrum. This behaviour will also occur when the sample is a powder consisting of randomly orientated microcrystal clusters. These rings essentially result from the rotation of the unit cell clusters (and thus their dual lattice) into all possible orientations, again leading to correlation shells in  $g(r)$ . However, in this instance, since the ‘cluster’ undergoing rotation is constant,  $g(r)$  contains a repetitive element not found in a random network. Although round quasicrystals are deterministic, their lack of an average unit cell causes  $g(r)$  to consist of coordination rings (of gradually decreasing intensity) resembling those of an amorphous or liquid-like system.

The novel diffraction properties of quasicrystals have made them a popular choice for the fabrication of a new class of materials, the photonic quasicrystal, devices which seek to control light in a similar way to the way semiconductor devices control the flow of electrons. This is achieved by creating a periodic potential such that there are band gaps in which electron wavefunctions cannot propagate. There is an analogous treatment for the propagation of electromagnetic waves known as photonic band theory (Pendry, 1996) where the atomic lattice potentials are replaced by periodic refractive index variations. In practice this often involves the placement of air holes by electron lithography in blocks of high refractive index dielectric in a periodic array. The quasicrystalline arrangements possess interference functions in the diffraction pattern which become more isotropic and circular the higher the symmetry in the design – a circular Brillouin zone is more suitable for producing complete band gaps (see Parker et al., 2006 for review). Although actual photonic crystals are in

general designed to produce optically exotic effects, there would seem to be some parallels to the cornea in terms of structural design, an idea which has already been suggested (Maksimova, 2001). It is of interest that an attempt has been made to link corneal transparency with the theory of photonic bands (Ameen, 1998) which did predict a transparent cornea but not the correct wavelength dependence, probably due to the type of lattice used. Many of these quasicrystal designs, however, do not remotely resemble the arrangement of corneal collagen fibrils; the pinwheel arrangement for example can be ruled out on these grounds (Radin, 1999; Parker et al., 2006), as can its generalisations (Sadun, 1998). The so-called sunflower seed head arrangement however is worthy of investigation (Vogel, 1979). Arrays based on this design are known to produce circularly symmetric diffraction spectra (Parker et al., 2006) and thus could be a promising candidate to assign a more deterministic structure to stroma. This arrangement is also widely regarded as a particularly efficient form of packing. Its structural properties are therefore investigated here in comparison with those of the cornea. It is shown that a distorted hexagonal lattice is not an adequate model of the interference function. It is necessary, however, to apply the caveat that models of fibril distributions are unlikely to ever completely and unambiguously describe the fibril positions, as a biological system will invariably possess a certain disordering influence. With this in mind, this chapter will be, in the main, observational.

### 3.2 Methods

Micrographs were digitised in Excel based representations according to the procedure outlined in section 2.4.

#### 3.2.1 Generation of theoretical lattices

Three classes of lattice were generated as comma separated variable files with the aid of Excel 2003 (Microsoft corp.), with points or 'TS fibrils' disposed in the following ways:

1. An hexagonal unit cell
2. With the high symmetry quasiperiodic 'sunflower' arrangement of Vogel (1979)

3. A random arrangement of fibrils generated on condition that the fibrils must not approach closer than the fibril diameter (Freund 2006)
4. For comparison, an generalised pinwheel lattice obtained from Tilings encyclopedia (Frettlöh, 2006) based on the methods of Sadun (1998)

Each arrangement that was generated contained at least 1500 lattice points. The hexagonal lattice can be generated quite readily. The quasiperiodic arrangement is generated by assuming that fibrils radiate outwards from some point of origin at an angle of 137.5 degrees with respect to each other, based on models of the sunflower seed head (Vogel, 1979). This is most simply expressed via the use of polar coordinates. In order to ensure that fibrils are equally spaced, the following equation (eq. 3.3) must be used

Eq 3.3

$$r(\theta) = a\theta^{1/2}$$

Where  $r$  is the radial coordinate from the centre, and  $a$  is the total area to be covered by the distribution and thus controls the relative spacing between fibrils and  $\theta$  is the angle. All distributions were assigned an interfibril centre-to-centre spacing of 53nm and a fibril diameter of 33nm (Boote, 2003). The pattern was generated by quantising the continuous function of equation 3.3 at 2.3998 radian rotations (Vogel, 1979) and then converting the resultant angle versus radial displacement into Cartesian x-y coordinates.

The effects of introducing a certain amount of disorder to the generated fibril distributions were also examined. This was achieved relatively simply with the aid of the RAND() function supplied by Excel. The randomisation or thermal shifting was applied only to the Cartesian coordinates. Succinctly, four random numbers were generated for each lattice point; two to affect the x-position and two for the y-position. One random array, with output values ranging from 0-0.999 acted as a decision array to determine whether or not displacement from the lattice point should be positive or negative, and the other to determine the absolute value of the displacement. The absolute displacement value was generated between 0-0.999 but

could be scaled to be on the same magnitude scale as fibril separations. Here, it was not considered necessary to modify the disordering algorithm to impose the condition that fibrils cannot overlap as the level of disorder that is the subject of this work was not sufficient to cause overlapping.

### 3.2.2 Lattice analysis

We adopted a number of interrelated approaches to analyse micrographs and the theoretically generated lattices.

1. The radial distribution function was calculated using in-house software for arrays which possess radial symmetry, i.e. are rotationally invariant; the mathematical method and examples of its application to the normal cornea are in the literature (Hart and Farrell, 1969; Connon et al., 2004; Cooper et al., 2006)
2. Using ImageJ freeware (NIH) the Fourier transform (power spectrum) was calculated at the centre of an exported excel image. This was done using the FFTJ plugin rather than the default FFT module. The fibrils were modelled as circles of small font size in the scatterplot feature of Excel 2003 (Microsoft). The transforms produced by the program were checked by performing Fourier transforms on hexagonal and square lattices and comparing these against what would be expected from simple crystallographic considerations. It must also be noted that in Fourier transforms produced this way, the interfibrillar interference function is convolved with the transform of the fibrils, represented in our case by small circles. The circle size was chosen to produce a satisfactory signal to noise ratio; since the 'fibril' interference function occurs at high frequencies in the reciprocal lattice, it need not concern us; computed transforms were checked by using diffracting apertures of varying shape; the low frequency interfibrillar interference function remains unaffected.
3. The wavelength dependency of each of the theoretical point sets was calculated with the aid of the Direct summation of fields model (Freund et al., 1986) and compared with computation from actual electron micrographs according to the procedure described in section 2.5. Experimental



transmission data for human corneas was also used. This method does require certain assumptions to be made; the interfibrillar spacing was fixed at 55nm for comparison. The refractive index ratio was assumed to be 1.044 with a ground substance refractive index of 1.365; fibril radius was fixed at 33nm for all fibrils (Boote et al., 2003). It should be noted, however, that refractive index and fibril diameter variations only affect the intensity magnitude and not the wavelength dependence of the Direct Sum calculations.

### 3.3 Results

Prior to analysis it will be descriptive to show here the experimental and theoretical fibril arrangements used throughout this work, as represented in Excel. A large number of perturbed lattices were generated; here a representative sample is shown.

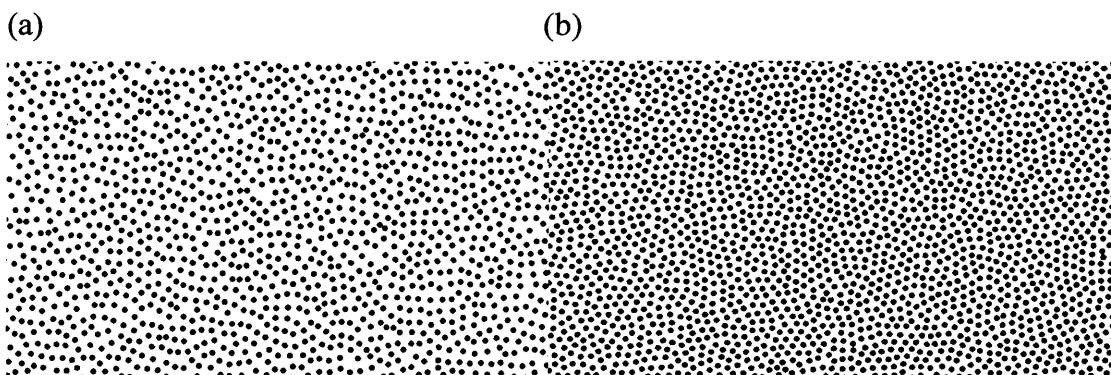


Figure 3.1: Representations of human corneal electron micrographs (a) Anterior (b) posterior

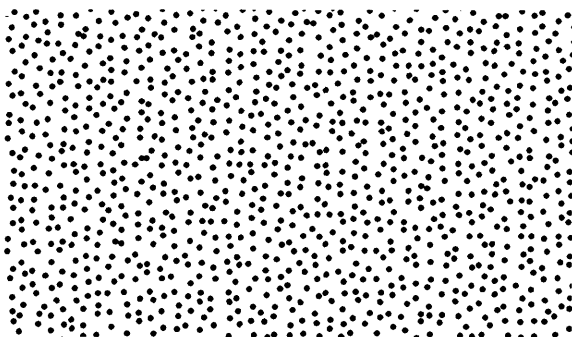


Figure 3.2 Perturbed hexagonal lattice

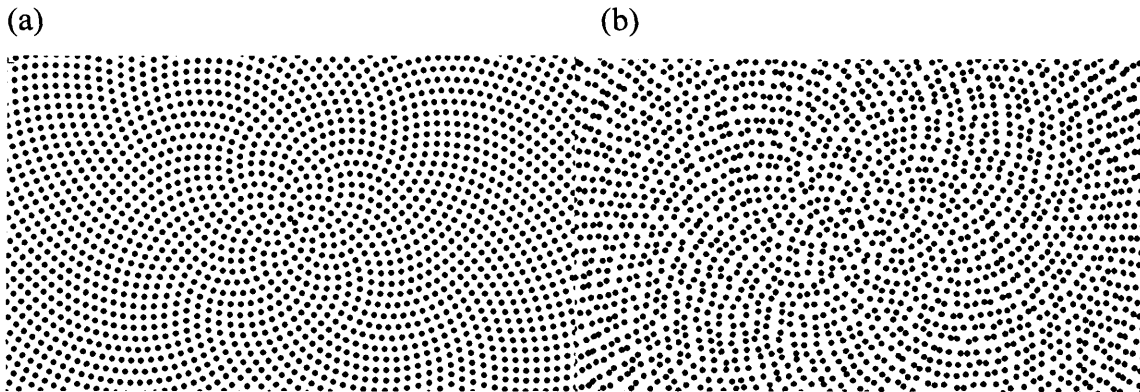


Figure 3.3 Sunflower seed head quasicrystal model. (a) In perfectly ordered form (b) With thermal disorder added

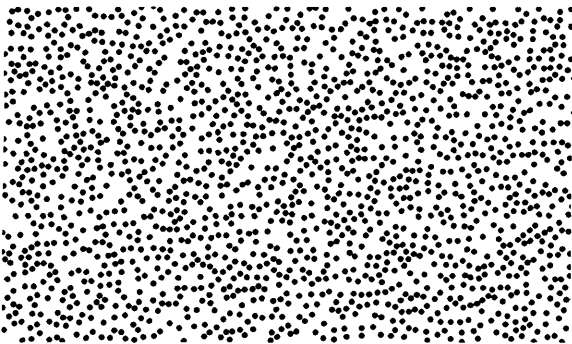


Figure 3.4 Purely random arrangement

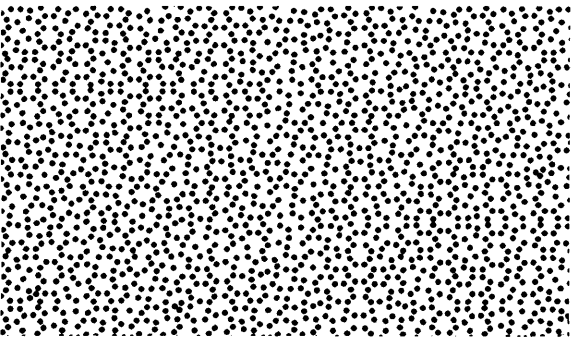


Figure 3.5 Generalised pinwheel lattice

### 3.3.1 Radial distribution functions

Since the hexagonal lattices lack the prerequisite circular rotational symmetry they were not subjected to this test. Figure 3.6 shows the radial distribution function  $g(r)$  obtained from corneal micrographs, assuming circular symmetry. The normalised radial distribution functions for the corneal stromas used here are in the literature (Freund et al., 1995).

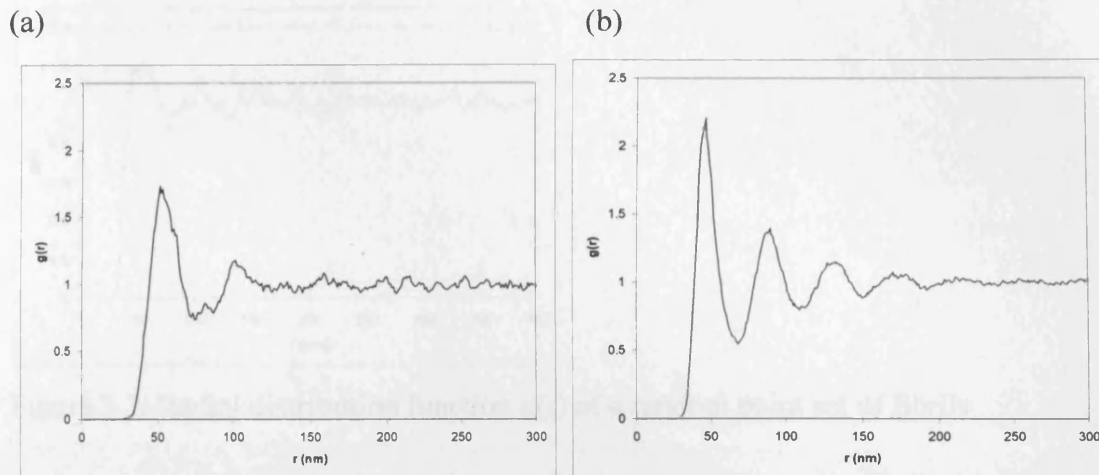


Figure 3.6. Radial distribution function  $g(r)$  for two different tissue depths of corneal stroma, from electron microscopy. (a) Anterior segment (b) Posterior segment

The radial distribution function of corneal stroma possesses several peaks of decreasing magnitude; eventually coalescing after a distance of some 200nm (the radial distribution functions are therefore somewhat similar to that obtained by x-ray diffraction for simple liquids, (albeit on different scales). The first peak represents the interfibrillar spacing. The other peaks therefore represent the spatial coherence extending out from the nearest neighbours. The area beneath the first peak gives the co-ordination number of the structure i.e. the number of nearest neighbours (Ziman, 1979).

The random arrangement of fibrils produces only one or two weak coherence peaks, as might be expected; this means that although there is an average interfibril spacing, there is no spatial coordination beyond the nearest neighbour 'shell', as shown in figure 3.7.

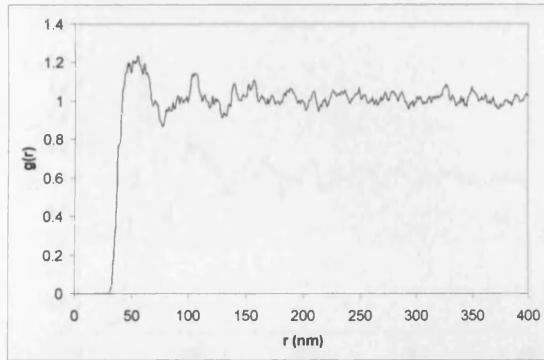
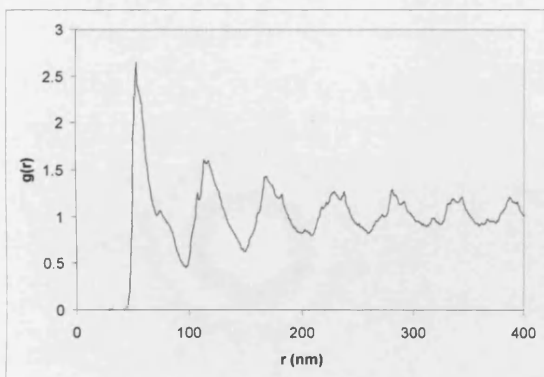


Figure 3.7. Radial distribution function  $g(r)$  of a random point set of fibrils

The quasicrystal point set produces radial distribution functions of interest. The perfect, unperturbed point set produces, as expected, many quite sharp (but *not* discrete) peaks (see figure 3.8). However, these peaks quickly decrease in intensity. As a greater amount of perturbation is applied to the perfect point set, the peaks broaden and decrease in number, starting to resemble closely those observed from the electron micrograph of posterior stroma (Figure 3.6).

(a)



(b)

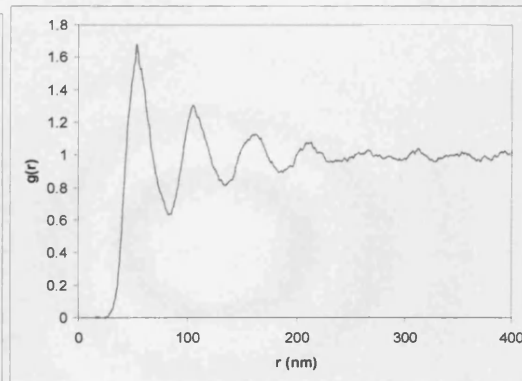


Figure 3.8. Radial distribution function  $g(r)$  of sunflower quasicrystal point sets. (a) Unperturbed and ordered arrangement (b) Perturbed arrangement with medium level of disorder ( $n=6$  generations of disorder averaged). Note differing scales.

Figure 3.9 shows the radial distribution function for a generalised pinwheel system. A first, very sharp interfibrillar peak is observed followed by a series of subsidiary maxima. The peaks within the function do appear to contain a great deal of noise.

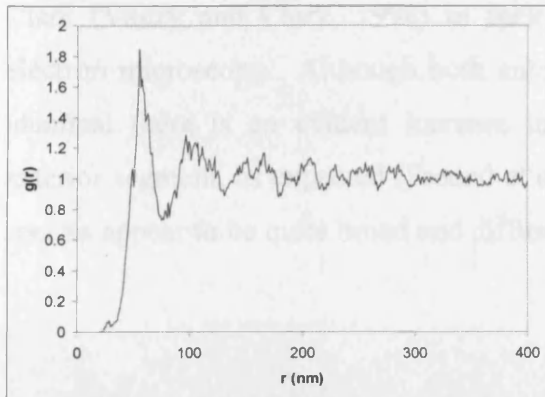


Figure 3.9  $g(r)$  of generalised pinwheel quasicrystal point set

Since the radial distribution function is probably obscuring details of the fine structure (see Ziman (1979) for a discussion of the uses and problems of radial and pair distribution functions in elucidating fine structure), a Fourier analysis of corneal ultrastructure to obtain and analyse the interference function directly was undertaken.

### 3.3.2 Fourier transform (Power spectrum) analysis

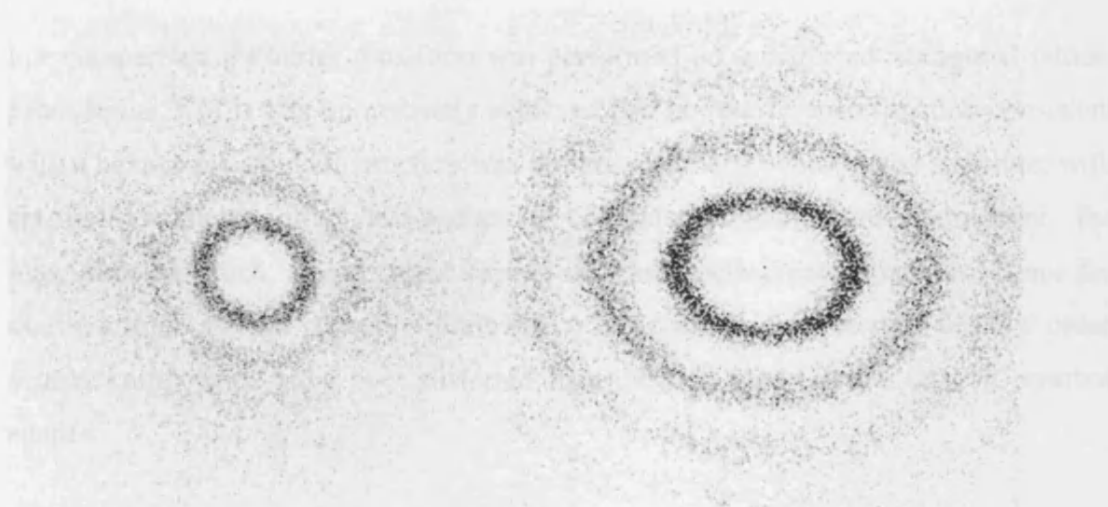


Figure 3.10. Power spectra of corneal electron micrographs (human), anterior to posterior (l-r). Images from 512 by 512 pixel area of stroma, central 256 x 256 pixel area of transform shown.

The power spectrum of fibril arrangements in the corneal stroma appears to produce isotropic diffraction rings in reciprocal space, against a background continuous spectrum (Figure 3.10). This is consistent with the determinations of Vaezy and

Clark (Vaezy and Clark, 1994) in their Fourier analysis of corneal stroma from electron microscopy. Although both anterior and posterior segments are essentially identical there is an evident increase in incoherent background scattering in the anterior segment, as expected (Freund et al., 1995). The rings observed in the power spectra appear to be quite broad and diffused.

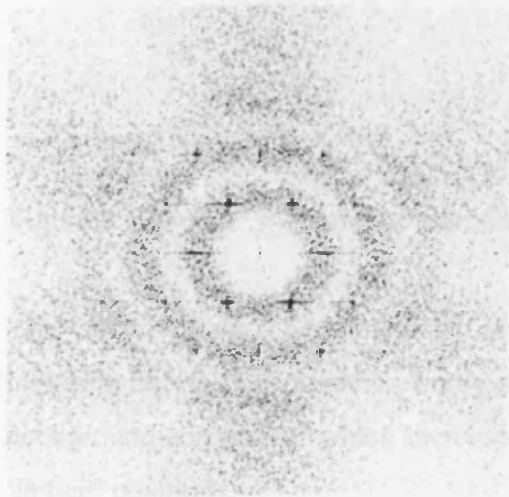


Figure 3.11. Power spectrum produced by distorted hexagonal point set

For comparison a Fourier transform was performed on a distorted hexagonal lattice. From figure 3.11 it was immediately observed that an interference function consistent with a hexagonal unit cell structure was present even in the disordered structure, with six-fold symmetry order set against a continuous background component, the magnitude of which, as one might expect, increases with greater disorder. Since for clarity a high contrast is used, a finite size effect can be seen whereby the first order fourier components have been distorted from normal Dirac deltas into '+' symbol shapes.

The dual lattice of the generalised pinwheel is shown in figure 3.12. The spectrum is found to be hazy and appears to consist of a diffuse ring. There are Dirac deltas apparent due to finite size effects. This spectrum is thought to be absolutely continuous (Radin, 1994; Senechal, 1996)

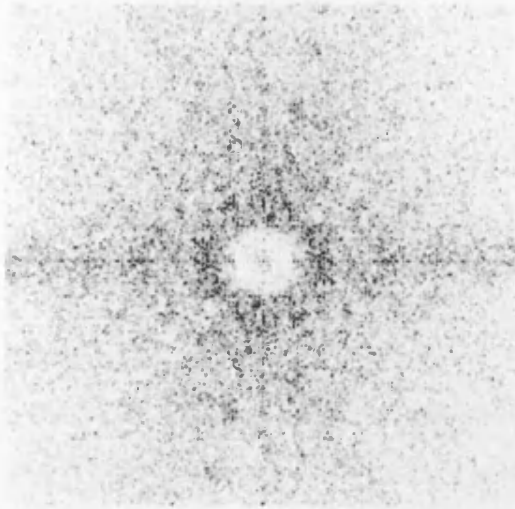


Figure 3.12 Power spectrum of a generalised pinwheel set

The ‘sunflower seed head’ point set produces as its dual lattice (Fig. 3.13) a circular, isotropic interference function, implying very high symmetry order with a continuous background component which increases with increasing perturbation from the perfect ‘lattice’ positions.

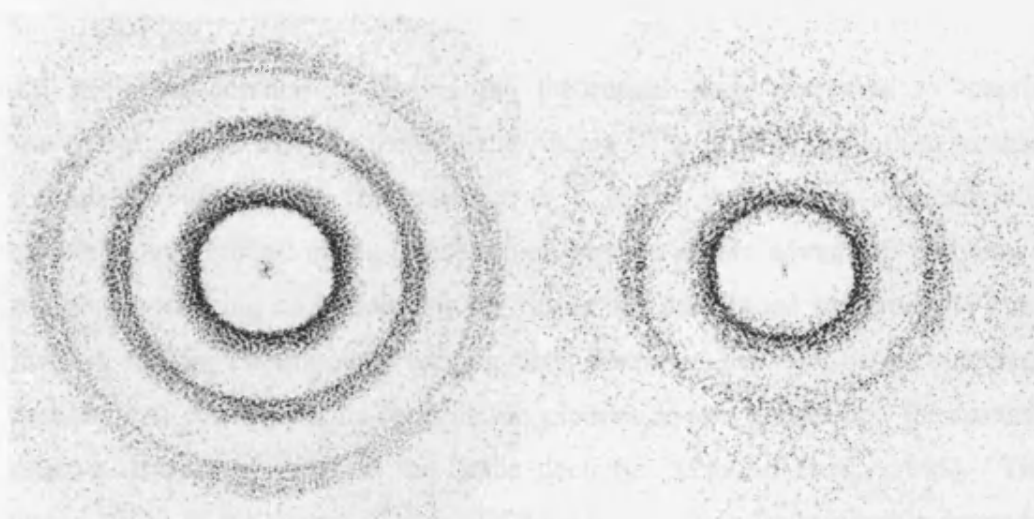


Figure 3.13. Power spectrum produced by sunflower quasicrystal point set (disordered set on right)





Figure 3.14. Power spectrum produced by random point set

The Fourier transform of a random array of fibrils (Fig. 3.14) produces broad, weak rings (essentially a continuous spectrum), as expected from the diffraction pattern of a set of randomly arranged apertures.

### 3.3.3 Wavelength dependencies

An additional method of testing the theoretical point sets was to examine the wavelength dependence of the structure factor. The present prevailing mathematical formulation of corneal transparency is a direct summation of scattered fields methodology (Freund et al., 1986) which has the major advantage of being able to calculate scattering cross sections for fibrils not distributed in a radially symmetric fashion, and for continuously varying fibril diameters (as may be encountered in the pathological cornea). This formulation predicts lower transmitted intensities as the relative amount of order in the tissue decreases (Freund et al., 1995). The light transmission of the cornea is generally found to have an inverse cubic dependence in relation to wavelength, which has been thought to be indicative of short range ordering in fibril position.



It is possible to formulate corneal transparency in the following manner:

Eq 3.4

$$T(\lambda) = \exp(-\sigma(\lambda)\rho\Delta)$$

Where  $T(\lambda)$  is the transmission as a function of incident wavelength,  $\sigma(\lambda)$  is the total scattering cross section as a function of wavelength,  $\rho$  is fibril number density and  $\Delta$  represents tissue thickness respectively. This equation may be rearranged as

Eq 3.5

$$\sigma(\lambda) = -\ln(T(\lambda))/\rho\Delta$$

For our present purposes, since the primary concern is with wavelength dependence, the terms  $\rho$  and  $\Delta$  are constant and will be suppressed; therefore  $-\ln T(\lambda) = \kappa \sigma(\lambda)$ , where  $\kappa$  is a constant of proportionality.

The total scattering cross section is formulated elsewhere (Hart and Farrell, 1969; Farrell and McCally, 2000) and is found to contain terms dependent on refractive indices of ground substance and fibril, fibril radius and relative fibril positions. For our purposes, it is sufficient to note that  $\sigma(\lambda)$  is inversely proportional to wavelength raised to some power,  $n$ . Therefore:

Eq 3.6

$$\sigma(\lambda) = k\lambda^{-n}$$

where  $k$  is a constant. This equation can be transformed further:

Eq 3.7

$$\ln \sigma(\lambda) = -n \ln \lambda + \ln k$$

As  $\sigma(\lambda)$  is known from Eq. 3.5, it is then straightforward to determine  $n$  graphically. This was done for the theoretical lattices and for actual transmission measurements obtained from human cornea at exactly physiological hydration ( $H=3.2$ ) using extant data (Doutch et al., 2007). The full graphical method is shown in chapter 7.

Table 3.1. Wavelength dependence ( $n$ ) for tested lattices (for 450-650nm)

Lattice	$n$
Generalised pinwheel	3.62
Sunflower lattice	2.99
Sunflower with disorder	3.02
Random array	3.00
Human posterior	3.07
Human anterior	2.90
Human experimental	2.99
Distorted hexagonal	5.20

The exact values for wavelength dependence  $n$  for each lattice tested are shown in table 3.1. The distorted hexagonal lattice was consistent with the known literature (Feuk, 1970; Farrell et al., 1973).

From table 3.1 it is noted that the lattices generally have wavelength dependence close to three. Anterior and posterior segments have slightly different dependencies. Possible explanations for this are discussed elsewhere (Freund et al., 1995) and may be related to a difference in hydration state. The average of the two values is 2.99, which is consistent with the experimental transmission spectrum through the whole tissue thickness. As expected from short range order, the random array gives a dependence of exactly 3. It is of interest that the sunflower lattice, despite being deterministic, gives dependence close to 3. Adding disorder to the sunflower array would appear to increase the value of  $n$ . The generalised pinwheel has the highest wavelength dependence, considerably displaced from that of the corneal array.

### 3.4 Discussion

It will be useful at the beginning of this discussion to refer back to the concept of liquid-like order. Unfortunately it is difficult to quantify this type of order as it does include a somewhat broad range of systems. For example, molten sodium chloride gives a similar radial distribution function in the distribution of its ions to that of the collagen fibrils observed in the cornea (Ziman, 1979). In some respects fibril arrangement is much simpler than these molecular systems and we are fortunate to have to contend only with a two dimensional plane, since the fibrils could be regarded as traversing large distances across the cornea. If one were to attempt to generate a point set with liquid-like short-range order, one would have to ensure that the generation produced an average fibril surface separation and possessed efficient packing density- *without* invoking any kind of long range order. An easier and valid way of modelling fibril disposition therefore is to attempt to generate arrangements which correlate with the experimental evidence available (Ziman, 1979).

Based on the results presented here it would seem sensible to discard derivatives of the hexagonal lattice; even at high levels of disorder it would seem that a distinct hexagonal unit cell is identifiable by reference to the Fourier spectrum. This clearly does not reflect the results obtained from electron micrographs of corneal stroma, which should be radially symmetric in real and reciprocal space. By extension, a hypothesis which suggests that fibrils could be arrayed as a hexagonal or cubic crystal powder can be discarded; the pattern of rings obtained from the corneal arrangements does not appear to correspond to this possibility (Warren, 1990) when the diffraction patterns are compared.

The increase in the amount of continuous background component with an increasing amount of disorder is easily explained. In a completely random point set the structure factor  $S(\mathbf{q})$  is equal to unity. When a point set which produces a purely discrete Fourier transform undergoes random perturbation about the mean lattice position, an extra, incoherent term will be added to the observed Fourier intensity distribution, leading to diffuse background scatter (the absolutely continuous part referred to in the introduction). All corneal micrographs analysed produced at least a small amount of this diffuse scatter

With the hexagonally based arrangements seemingly eliminated as a viable model for the distribution of corneal fibrils, attention can be diverted to random and aperiodic arrays. A purely random arrangement, as outlined above, theoretically leads to a structure factor  $S(\mathbf{q})$  of unity. Since our random array was generated under the condition that fibrils do not touch, there is a small degree of vestigial ordering required and thus in this case  $S(\mathbf{q})$  is not unity, but presumably close, and takes the form of a highly diffuse ring. Inspection of the power spectrum produced indicates one low intensity peak of coherence, corresponding to a nearest neighbour orbit, which is also visible in the RDF; this is far less order than is generally seen in micrographs. This single peak can also be seen if the random array power spectrum is plotted in one dimension through a transept, as a point of maximum intensity. When analysed using the direct sum algorithm it would seem that this vestigial order is sufficient to allow the cornea to transmit light; the arrangement produced excellent agreement (as might be expected) with the cubic wavelength dependence 'benchmark'. However the absolute transmitted magnitude was lower than would generally be expected for the normal cornea. The golden pinwheel power spectrum is somewhat similar to the random array, and contains a great deal of diffuse scattering.

As outlined above, the power spectra will be more useful for analysis if they are reduced to one dimensional plots of intensity versus position, allowing detailed structure within the diffraction halo to be visualised. This can be achieved by plotting a rectangular transept of 10 pixels width across the whole image meridionally through the central maximum of the spectrum, and mapping intensities within that block in relation to pixel distance. This is shown in figure 3.15 for two of the stromal micrographs (the human anterior and posterior segment), the random network (fig. 3.16) and the round quasicrystal in its normal state and with thermal disorder added (fig. 3.17).

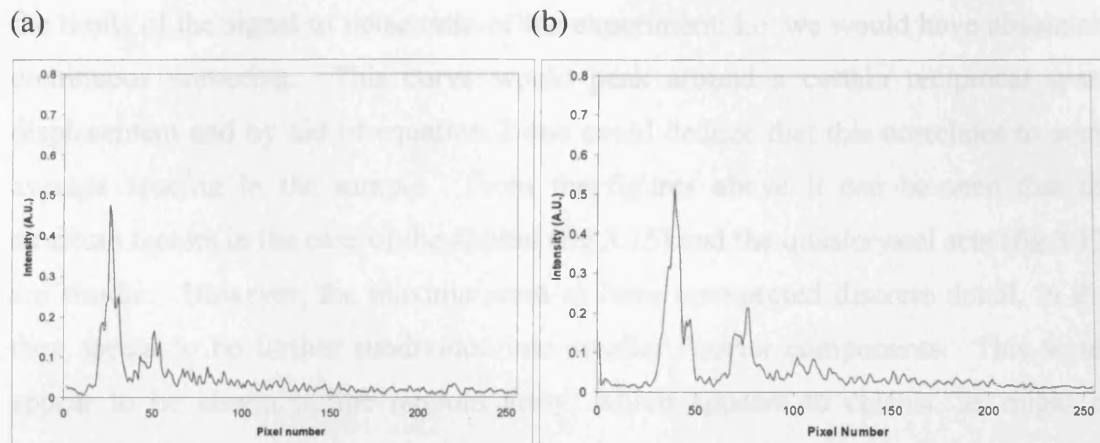


Figure 3.15. One dimensional plot of interference function for stromal micrographs (a) anterior (b) posterior (averaged around zeroth order, suppressed here)

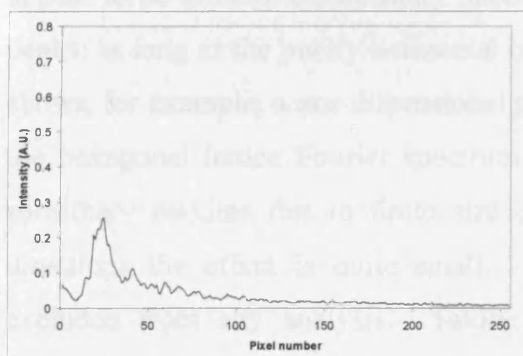


Figure 3.16. One dimensional plot of interference function for random array.

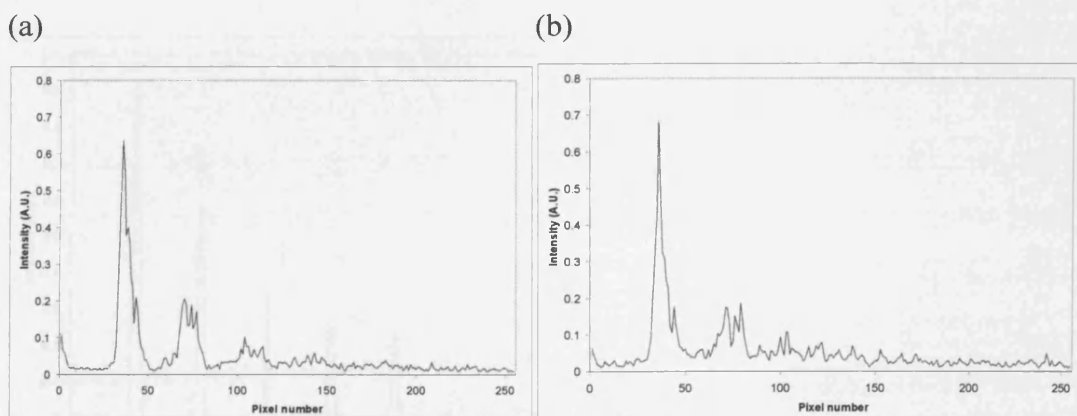


Figure 3.17 One dimensional plot of interference function for quasicrystal array (a), and quasicrystal array with randomised disorder added (b)

If this were performed on an X-ray or neutron diffraction spectrum from a liquid, one would expect that the diffraction halo would take the form of a smooth curve within

the limits of the signal to noise ratio of the experiment; i.e. we would have absolutely continuous scattering. This curve would peak around a certain reciprocal space displacement and by aid of equation 2 one could deduce that this correlates to some average spacing in the sample. From the figures above it can be seen that the structure factors in the case of the stroma (fig 3.15) and the quasicrystal sets (fig 3.17) are similar. However, the maxima seem to have unexpected discrete detail, in that they appear to be further subdivided into smaller Fourier components. This would appear to be absent in the random array, which appears to consist, as might be expected, of a large maximum of fairly low intensity with several subsidiary orders. At least some of this should be due to finite size effects, although a one-dimensional plot of the hexagonal lattice power spectrum suggests that finite size effects would appear to be limited to subsidiary maxima of very low intensity relative to the main peaks; as long as the purely horizontal or vertical directions are not used. Figure 3.18 shows, for example, a one dimensional plot through a 30 degree orientated transept of the hexagonal lattice Fourier spectrum. There appears to be little or no evidence subsidiary maxima due to finite size effects. Even in the horizontal and vertical directions the effect is quite small. However to remove uncertainty they were excluded from any analysis. Taking heed that plotting the 30 degree transept produced no appreciable finite size effect in the hexagonal lattice transform, all one dimensional representations were created using this convention.

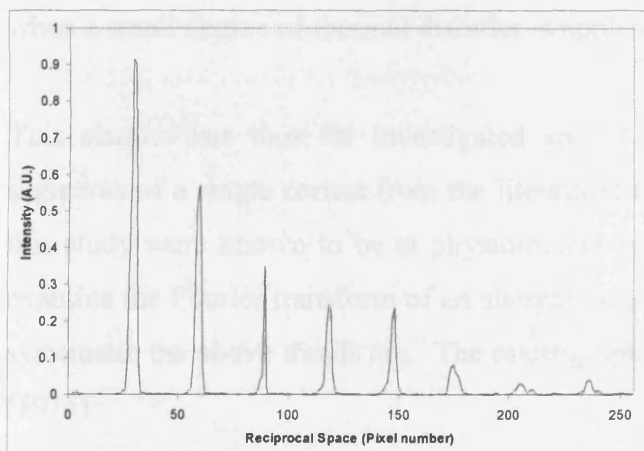


Figure 3.18 One dimensional plot of hexagonal lattice Fourier transform taken through 30 degree transept.

However, this does not exclude the possibility that these quasiperiodic arrays may generate unusual truncation effects due to their intrinsic nature, as can be observed from the pinwheel arrangement (see figure 3.12). This curious pattern is approximately radially isotropic; however, there is distortion in certain directions in the form of stretching and compressing which has made circular integration of the pattern of limited use. The most intense peak presumably corresponds to the interfibril spacing. This behaviour can also be observed, albeit more diffuse, in the corneal power spectrum. There would appear to be sharp peaks in both anterior and posterior segments. However, there does appear to be a change in the profiles going from anterior to posterior. Close comparison of these systems with various other arrays would seem to suggest that at least part of the origin of these singularities may lie in a truncation effect due to the finite sizes of the areas analysed, i.e. that there are a number of configurations which occur periodically in the relatively small areas analysed. This can vary in certain directions, especially in the case of the sunflower lattice due to the simplistic way in which it is generated. A certain configuration may occur more frequently in a certain direction and thus render itself at greater intensity at the appropriate frequency in the spatial spectrum. The information supplied, however, allows us to observe that the power spectrum intensity in cornea is quite comparable with the deterministic array – the random array is quite diffuse by comparison and the singularities register quite prominently against the background in the case of both sunflower array and cornea. There is particularly good agreement when a small degree of thermal disorder is applied to the corneal array (figure 3.17).

This chapter has thus far investigated spatial order in the anterior and posterior segments of a single cornea from the literature; this was done as the corneas used for this study were known to be at physiological hydration. It will be useful to briefly examine the Fourier transform of an alternative electron micrograph to determine how systematic the above trends are. The micrograph shown in figure 3.19 is from Giraud (1975).



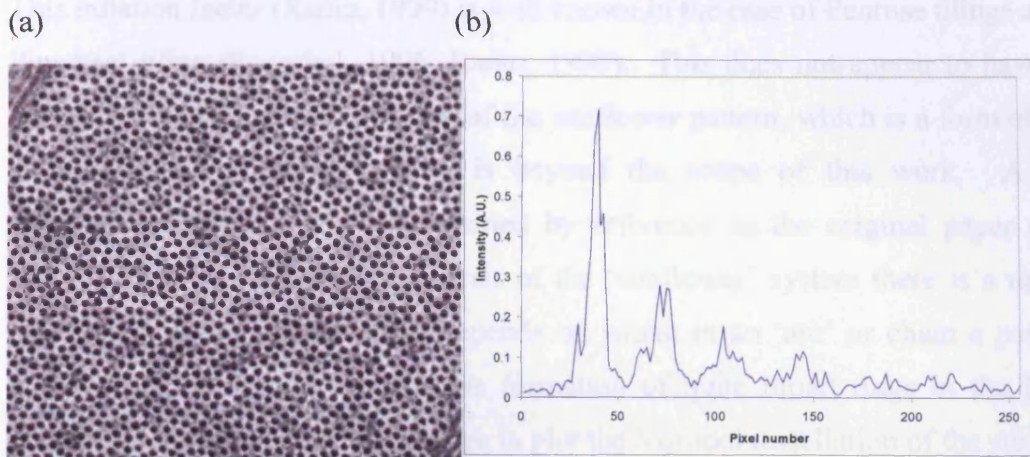


Figure 3.19 a. Additional micrograph (unknown tissue segment) used for analysis (Giraud et al., 1975) b. One dimensional plot of Fourier transform from (a).

Figure 3.19 shows the same trend as observed from micrographs above; each Fourier component seems to be subdivided into at least two components. It is likely they are in fact several components positioned very close together.

The Fourier transform of the spiral lattice, of which the sunflower seed array is part, is generally thought to be absolutely continuous (Macia, 2006). The peaks are not of the intensity exhibited by the Bragg peaks that might be observed in, say, a hexagonal lattice, but are more intense than any singularities present in the random lattice structure factor.

Here it has been shown that the form of  $S(\mathbf{q})$  for corneal stroma is at least consistent with a form of quasiperiodic order. Radin (1999) has suggested that differentiating liquids from round quasicrystals is elementary; as outlined in the Introduction a crystal sample, periodic or otherwise is composed of finite elements, for example triangles or penrose rhombs (see Senechal (1996) for discussion). It is possible to construct a tiling by using an inflationary method on these basic elements. This is achieved by inflating the prototiles around some constant factor, endowing the tiling with a hierarchical structure. Radin (1999) was able to show that although the rings in a round quasicrystal would be translation invariant, the radial displacement of rings would be self similar, i.e. the pattern of rings would repeat at an interval indexed by the inflation factor. A simple liquid (or glass) with short range order will not have this constant self similarity as it (generally) has no long range statistical correlation.



This inflation factor (Radin, 1999) is well known in the case of Penrose tilings and the Pinwheel tiling (Senechal, 1996; Radin, 1999). This does not appear to have been defined in the literature in the case of the sunflower pattern, which is a form of spiral tiling, and a rigorous derivation is beyond the scope of this work. A broad interference function can be explained by reference to the original paper on the pattern (Vogel 1979). In his analysis of the ‘sunflower’ system there is a range of nearest neighbour distances that depends on where in an ‘arc’ or chain a particular point lies; – this range leads to the formation of quite broad rings in the Fourier transform. It will be informative here to plot the Voronoi tessellation of the sunflower seed head quasicrystal. These can be obtained by using the real space coordinates of the array and using Statistica 7’s Voronoi scatterplot function. This is shown in figure 3.20. Here it can be seen that the array appears to consist primarily of hexagonal and cubic unit cells. This undoubtedly leads to the splitting effect observed in the structure factors above. It seems likely that some Fourier components arise due to the hexagonal unit cells and others due to the cubic portion.

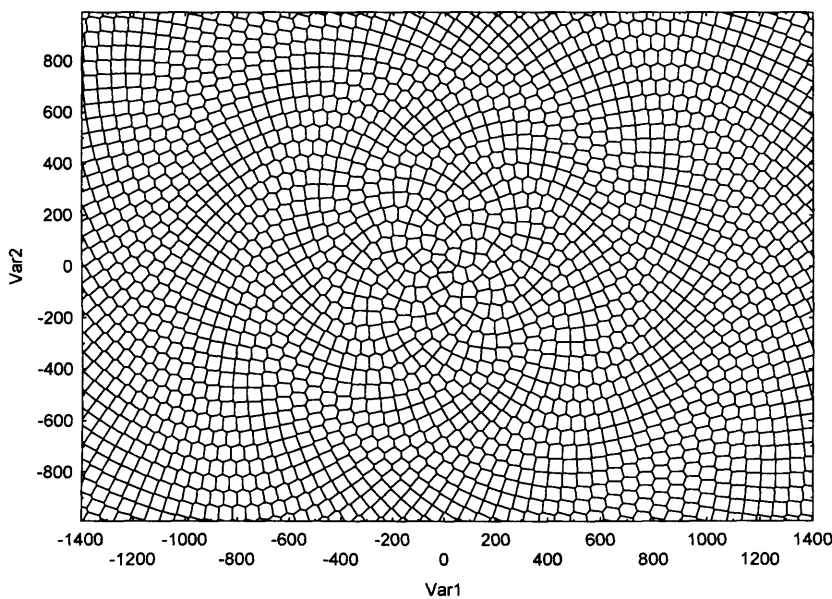


Figure 3.20 Voronoi tessellation of sunflower type quasicrystal

When this procedure is performed on, for example, the posterior corneal tissue segment, figure 3.21 is obtained. It appears to contain the same distorted hexagons as the sunflower type quasicrystal. However there appear to be pentagonal unit cells present within the tessellation. Further work is planned to investigate this particular

property, with a view to determining the relative statistical frequency in which the various unit cell shapes occur. In the sunflower type pattern the two shapes certainly appear to have approximately equal frequency. This may not be the case in the stromal patterns.

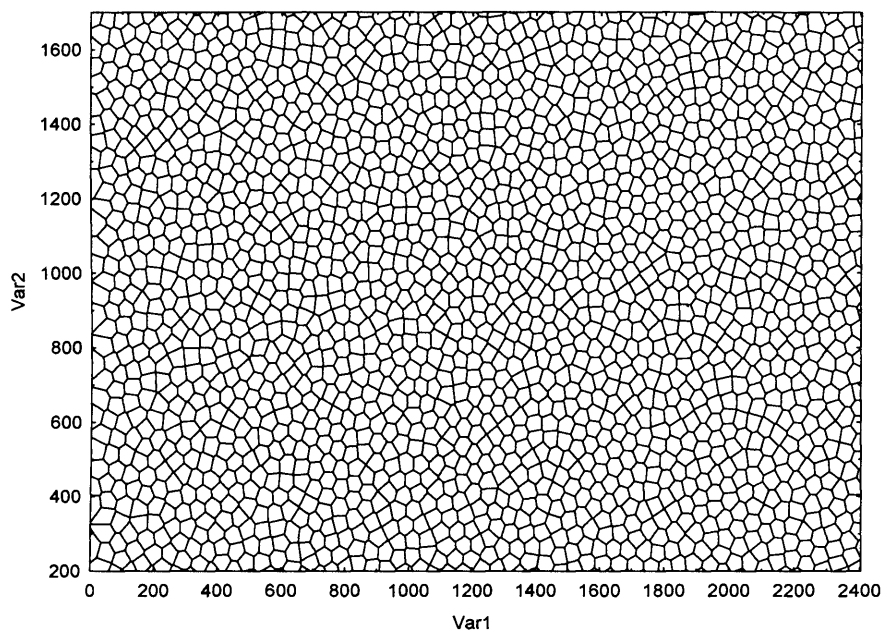


Figure 3.21 Voronoi tessellation of posterior tissue segment

It may also be of interest to investigate how the Fourier transforms vary with the size of the area analysed, i.e. the relationship between the global (or gross) and ‘local’ (regional) structure factors. With this in mind another interesting possibility suggested by close inspection of figure 3.21 is that the stroma could be arranged in regions in which the sunflower type quasicrystal occurs on an almost local length scale; therefore it would be a kind of quasicrystal powder.

As outlined in the section 3.1 the vast majority of quasiperiodic tilings bear little resemblance to anything found in nature (although it has been suggested that natural quasicrystals may have been confused for other structures (Radin, 1999; Lu et al., 2001)); some verge on the bizarre owing to the mathematical rules under which they are constructed. However, they do allow for the construction of sets which possess symmetry and periodicity without resorting to conventional crystallography. Of course, although the so-called ‘Sunflower seed’ pattern illustrated here is a

satisfactory model, nature is not in general so flawless, and it seems likely that preparation for electron microscopy increases the entropy in the fibril distributions; the present work has reflected this by attempting to model small amounts of disorder. This design may have optical implications for corneal transparency, in addition to being an efficient packing arrangement. The sunflower seed model would appear to be the best available at this time; in the course of this work we have analysed other space tilings in which the basic building blocks occur in every rotational configuration. Other arrays are found to tile space inefficiently or to induce Bragg peaks in their diffraction spectrum owing to the finite size of the areas analysed in this work (in order that they contain comparable numbers of fibrils to TEM images); for example the generalised pinwheel system (Sadun, 1998). The sunflower pattern would appear to generate circular rings in the interference function even with a relatively small number of points. A more precise model of fibril distributions will require definitive electron micrographs showing native tissue preservation, perhaps through cryoelectron microscopy or new developments in X-ray imaging technology. It will be of particular interest to settle questions relating to the role of proteoglycans, ions and other collagen types present in the matrix in ordering the fibrillar array. Perhaps the fibril distribution may be best modelled by reference to turbulent or chaotic crystals (Berend and Radin, 1993; Le Berre, Ressayre and Tallet, 2002). In this case, it could well be that although the underlying order is essentially compatible with that of stroma, the unit cells actually tessellate according to different mathematical rules, or in accordance with some quantifiable degree of thermal randomisation, perhaps a kind of 'rule for the disorder'. These type of structures have been referred to as quasi-quasi-crystals (see Senechal (1996))!

In terms of photonic band methods, the sunflower packing arrangement produces a more complete band gap or forbidden region in which waves would not be able to propagate. Corneal light transmission is known to decrease quite rapidly for short visible wavelengths; the sunflower lattice mimics this effect. This suggests the intriguing possibility that the apparent disorder or randomness in the fibril arrangement does in fact have a purpose in reducing potentially harmful wavelengths from reaching the other ocular components.

### **Chapter 3**

It is likely that increased mathematical understanding of aperiodic structures will lead to better models being developed in the future, along with advanced 3-D reconstructions of cornea showing in detail the relationship between proteoglycans and collagen fibrils, obtained from electron microscopy. With this in mind it is important to emphasise that this section does not conclude that the sunflower seed array is the exact method in which the stromal fibrils are arranged; rather, it seeks to show that the array is the only deterministic one presently available that has similar structural properties to the stroma, in terms of its structure factor and, by extension, its light scattering. This will provide a stable structure with well known light transmission and wavelength dependence in which the effects that pathologically induced fluctuations in fibril ordering, such as lakes, have on stromal light scattering can be explored.

## **Chapter 4. Light transmission through cornea as a function of position**

This chapter investigates how the cornea transmits light at visible wavelengths away from the central axis, in the peripheral regions. This does not appear to have been studied in the literature up to this point. This chapter also deals with reformulating the equations of Leonard and Meek (1997) for refractive index into ones valid in the peripheral regions.

### **4.1 Introduction**

The transparent cornea combines its interesting optical properties with great tensile strength and thus must have a structure that allows strength and transparency to be achieved simultaneously. As outlined in chapter 1, the thickest layer is the stroma, composed in the main of type I hybrid collagen fibrils. There are some 200 lamellae within the central human cornea (Naylor, 1953; Maurice, 1956). Although lamellae are arranged at all rotational angles throughout the depth of the cornea, there would seem to be preferential orientations (Meek et al., 1987; Aghamohammadzadeh, Newton and Meek, 2004) in which a larger proportion of fibrils lie in the inferior-superior and medial-lateral directions. The collagen fibrils are surrounded by an interstitial matrix of proteoglycans. The collagen fibrils in the central cornea possess a highly uniform diameter (~32nm in the human) (Meek and Leonard, 1993). An electron micrograph of a typical human cornea is shown in figure 4.1.

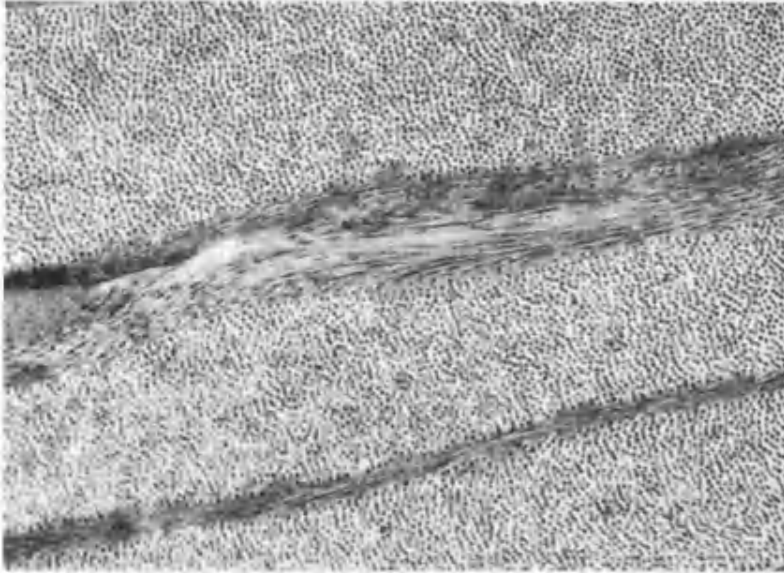


Figure 4.1. Transmission electron micrograph of human cornea (courtesy of R.D. Young)

As outlined in the introduction, Maurice (1956) was one of the first to attempt a solution of the problem of why a tissue containing light scattering collagen fibrils is transparent. He proposed that the corneal collagen fibrils were arranged in a hexagonal lattice, and that the scattered fields from the fibrils would interfere destructively in all directions except that of the incident beam. When oedematous, however, the fibrils would be perturbed from the perfect lattice and laterally scattered light would not be removed from the beam (Maurice, 1956; Maurice, 1962). Most theories of transparency use the work of Maurice as a starting point; theories about the physical basis of corneal transparency were outlined in section 1.2.

Despite the number of models proposed to explain corneal transparency, all the currently recognised paradigms accept that the crucial parameters affecting corneal transparency are:

1. Number density of collagen fibrils
2. Collagen fibril diameter
3. Refractive index differential between the interfibrillar or ground substance and the fibrils
4. Stromal thickness
5. Spatial ordering of the fibrillar array

The effects of these parameters on light scattering will be outlined in subsequent sections. However at this stage it should be noted that they must be controlled to within fine limits to ensure optimum transmission of visible wavelengths. It has been shown that none stay constant across the cornea in relation to translational position from the central cornea to the limbus, the region where the cornea adjoins the white sclera. Both interfibrillar spacing and fibril diameter are found to show variation approaching the limbus (Borcherding et al., 1975; Boote et al., 2003), and the cornea thickens in the same region. To date, light scattering from the peripheral cornea has been neglected, despite the contribution of this region to peripheral vision. The current study, therefore, is designed to model the observed change in corneal transparency from the centre to the limbus.

There are a small number of studies in the literature of the transmission spectrum of the cornea, whether it is being investigated as a tissue in isolation or in association with the other optically transparent tissues and fluids within the ocular sphere. Although adaptations of conventional spectrophotometry are most commonly used (see section 4.1), it is possible to make estimations of transparency based on backscattered light in the confocal microscope (Moller-Pedersen et al., 1998; Jalbert et al., 2003; Jester et al., 2007). Optical coherence tomography can also be used to calculate backscattered light, but these measurements may not be valid outside the central region (Hrynchak and Simpson, 2000). Care must be taken when dealing with backscattered light and its relationship to ultrastructure. For most particles, scattering in the forward direction (i.e.  $0^\circ$  relative to angle of incidence) predominates over backscattered ( $180^\circ$ ) light by several orders of magnitude (Bohren and Huffman, 1983). Thus although the signal obtained through backscattering methods may be sufficient to analyse increased light scatter from gross pathologies perhaps associated with cells and wounds, it may be not be sufficient to quantify accurately changes in light scatter caused by fibrillar or refractive index effects occurring on nanometer scale lengths.



## 4.2 Methods

### 4.2.1 Sample preparation

All corneas were debrided of their endothelium and epithelium using laboratory razor blades and blotting paper. They were then equilibrated to physiological hydration using 20kDa polyethylene glycol (PEG). See sections 2.1 – 2.3 for general methods pertaining to tissue preparation and dialysis.

### 4.2.2 Transparency measurement

A Pye Unicam SP8-100 double beam spectrophotometer with detector half angle acceptance of 3 degrees and beam size adjusted to 1x1mm was used to determine the transmitted light intensity through a corneal preparation clamped within custom built sample chambers, a cross-section of which is shown in figure 4.2.

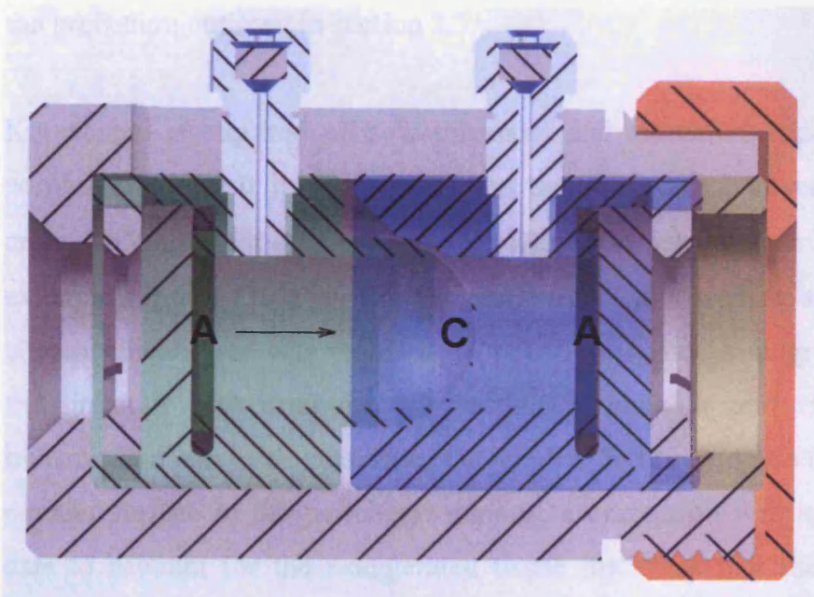


Figure 4.2 Diagram of spectrophotometer cell used to measure corneal light transmission. A indicates apertures, into which quartz or plastic windows can be inserted. C shows the position of the cornea. The half chambers are coloured green and blue; the grey outer covering secures both half chambers, with the aid of the screw cap (orange) on one half of the cell, holding the corneal preparation in place. Arrow shows direction of light propagation through cell.



The half chambers were filled with silicon oil (Dow Corning 200/5cS). Baseline readings were made from cells filled only with silicon oil. These were recorded prior to each corneal measurement, which was then expressed as a ratio to the baseline reading. The cell position in the beam path could be adjusted laterally by the aid of a vernier scale and intensity measurements were thus recorded at 1mm intervals radiating outwards from the apparent geometric centre of the sample cells. If the optical centre was found not to coincide with the geometric centre the results were laterally shifted. In this work, position 0 is the centre; negative displacements are to the left of the central point and positive to the right when viewed relative to the incident beam direction. The sample cell was placed within the spectrophotometer such that the beam was perpendicular to the cell window at all times.

### 4.2.3 Theoretical deduction of refractive indices and transmission

Corneal transmission was computed with the aid of a computer algorithm according to the procedure outlined in section 2.5.

Knowledge is required of how thickness and refractive indices change across the corneal surface. It is well understood that the cornea increases its thickness from around 550 $\mu\text{m}$  in the centre to some 700-800 $\mu\text{m}$  in the peripheral region (see, for example Li et al (2006)). For the purposes of this work more detailed mapping of corneal thicknesses was required. Optical coherence tomography (OCT) data from the literature was used for this work (Li, Shekhar and Huang, 2006). In our transmission measurements, since the incident light beam was not perpendicular to the corneal surface in the peripheral regions, a correction was applied to the thickness data to account for the exaggerated tissue thickness that the beam would traverse (here termed the optical thickness). This correction was achieved by a simple geometric model of two circles, with one of smaller radius enclosed within a larger one, thus supplying a basic model of the cornea (Meek, 2002). The equations of the circles were set such that a correct perpendicular thickness was achieved in the central and peripheral regions. It was then straightforward to determine a correction from perpendicular to optical thickness. The model is shown below in figure 4.3 This

model is sufficient for our purposes and the values appear to be consistent with measurements obtained from images of cornea and anterior segment obtained by OCT (Li et al., 2006).

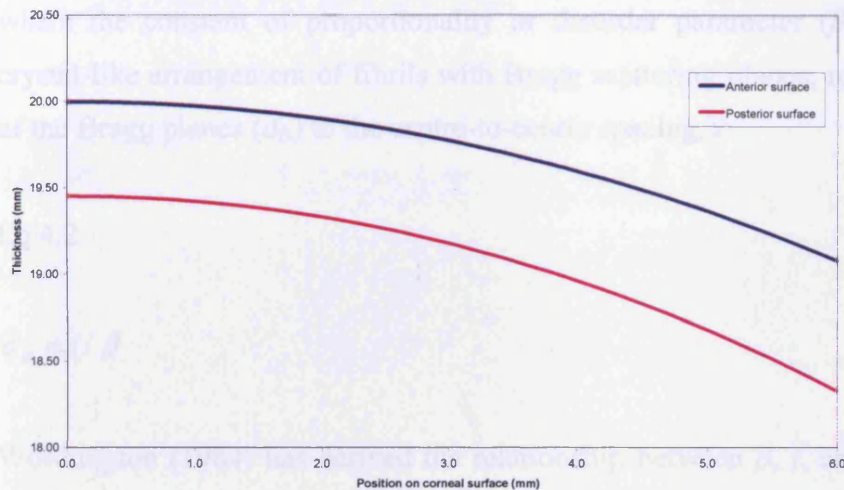


Figure 4.3. Cross-sectional model of cornea composed of two concentric circles with differing radii, adjusted to match true corneal perpendicular thickness in the central and peripheral region.

The change in ultrastructural parameters will lead to changes in the fibril volume fractions and therefore, changes in the refractive indices of the hydrated interfibrillar matrix. The refractive index of the interfibrillar matrix cannot be measured directly, but in principle, can be calculated from knowledge of the refractive index of the stroma as a whole (Leonard and Meek, 1997). Using an Abbe refractometer, an attempt was made to measure corneal refractive index as a function of position. However, this was unsuccessful because of the relatively small size of the human cornea compared to the illuminating beam in the refractometer. Therefore, with the data of Boote et al (Boote et al., 2003) and application of Gladstone and Dale's Law (Leonard and Meek, 1997), appropriate refractive indices from the central cornea to the limbus were calculated as follows.

The first step was to measure the disorder parameter for the packing of collagen fibrils in the stroma. The volume associated with each fibril ( $V_s$ ) is related to the centre-to-centre fibril spacing ( $i$ ) thus:

Eq 4.1

$$V_s = i^2 / \beta$$

where the constant of proportionality or disorder parameter ( $\beta$ ), in the case of a crystal-like arrangement of fibrils with Bragg scattering planes, relates the separation of the Bragg planes ( $d_B$ ) to the centre-to-centre spacing,  $i$ :

Eq 4.2

$$d_B = i / \beta$$

Worthington (1984) has derived the relationship between  $\beta$ ,  $i$ , and the fibril number density,  $\rho$ :

Eq 4.3

$$\beta = \rho i^2$$

Here, his notation is replaced, so  $\beta$  is  $1/\alpha$  and  $\rho$  is  $\sigma$  in his notation. The quantities  $i$  and  $\rho$  were determined from fibril radial distribution functions (Hart and Farrell, 1969; Cox et al., 1970) obtained from three electron micrographs, two taken from the literature (Komai and Ushiki, 1991; Muller et al., 2004) and the third from Figure 1 in the present paper. An average value of  $\beta$  was then calculated as 1.06, which is comparable with Worthington's factor of 1.12 for liquid-like fibril arrangements.

Equations 4.1 and 4.2 indicate that  $V_s = \beta d_B^2$  and this can be combined with our measured value of the disorder parameter to give the volume fraction of hydrated collagen fibrils  $f_f$ :

Eq 4.4

$$f_f = \pi a^2 / \beta d_B^2 = \frac{\pi a^2}{1.06 d_B^2}$$

Where  $a$  is the fibril radius. The volume fraction of hydrated fibrils in the stroma  $f_f$ , the volume fraction of dry collagen molecules in a fibril  $f_m$ , and the volume fraction of dry fibrillar matter in the stroma  $f_c$  are related thus:

Eq 4.5

$$f_m = f_c / f_f$$

Using  $f_c$  and  $f_f$  data in Leonard and Meek (1997) for the average of 40 species,  $f_m$  is calculated to be 0.39. If the hydration state of the fibril remains constant as a function of position in the cornea (Hayes et al., 2007), then  $f_m$  is constant as this is dependent on molecular spacing within the collagen fibril (Leonard and Meek, 1997).

With known values for  $f_f$  and  $f_m$  for the central cornea, we can now turn our attention to formulating how the refractive indices will change away from the central axis. This can be simplified somewhat by assuming that the dry volume of extrafibrillar component remains constant, as does the hydration state of the collagen fibril. Changes in the fibril diameter are taken into account by changes in the fibril volume fraction  $f_f$ , so will not need to be considered separately.

The total solvent or hydration fraction of the cornea ( $H$ ) is given by (Meek, Dennis and Khan, 2003a):

Eq 4.6

$$H = 1 - f_p - f_f f_m$$

Here,  $f_p$  is the volume fraction of dry non-fibrillar material in the stroma. By equation 5 the final term is  $f_c$ , the volume fraction of dry fibrillar material in the stroma. In the central cornea  $H=0.78$ , which corresponds to a physiological hydration of 3.2. The other parameters are then known and in the central cornea we can thus obtain  $f_p=0.11$ .

Applying Gladstone and Dale's Law (Meek et al., 2003b), the total stromal refractive index  $n_s$  is given by:

Eq 4.7

$$n_s = n_f f_f + n_p f_p + n_w f_{ew}$$

where  $n_s$  is the refractive index of the stroma (1.375),  $n_f$  is the refractive index of hydrated collagen (1.416),  $n_w$  is the refractive index of water (1.333),  $n_p$  is the refractive index of the dry ground substance and  $f_{ew}$  is the volume fraction of extrafibrillar water, which is given by  $1 - f_p - f_f$ . Using these formulae a value of 1.501 is obtained for  $n_p$ .

If the volume of extrafibrillar material remains constant but the volume associated with each fibril ( $V_s$ ) increases, then the volume fractions of the components change. This has no effect on the refractive index of the hydrated fibril but will affect the ground substance and total stromal refractive indices (see equations 5 and 8 of Leonard and Meek (35)). The value of  $f_p$  will decrease and  $f_{ew}$  will therefore increase. This can be represented mathematically by:

Eq 4.8

$$f'_p = f_p \frac{V_s}{V'_s}$$

where dashed quantities indicate states modified from that which exists in the central cornea. The value of  $V_s$  may be derived from the interfibrillar spacing using equation 4.1. The change in  $f_p$  is thus calculated as a function of position across the cornea. It

is therefore fairly straightforward to calculate how the refractive index of the hydrated ground substance,  $n_g$ , changes using equations 4.4 and 4.8 together with Leonard and Meek's (35) equation 4.3:

Eq 4.9

$$n_g = n_w + \frac{f_p(n_p - n_w)}{(1 - f_f)}$$

The other experimental and mathematically derived ultrastructural parameters are illustrated in table 4.1. The Bragg spacings and fibril diameters shown were used to calculate the various volume fractions using the equations derived above, and from these the refractive index value  $n_g$  was calculated. The quantity  $m$  is the ratio between the refractive index of the fibril and that of the extrafibrillar substance.

Table 4.1. Ultrastructural parameters used for modelling stromal transmission

Position (mm)	Bragg spacing, $d_b$ (nm)	Fibril diameter (nm)	$f_f$	$f_p$	$f_{ew}$	$n_g$	$m$
0	53.4	33.0	0.283	0.110	0.608	1.3585	1.042
1	54.1	33.0	0.276	0.107	0.618	1.3576	1.043
2	55.2	33.0	0.265	0.103	0.632	1.3563	1.044
3	57.0	33.0	0.249	0.096	0.655	1.3544	1.045
4	57.9	34.0	0.256	0.093	0.651	1.3539	1.046
5	62.7	35.5	0.238	0.080	0.683	1.3504	1.049

(Bragg spacing and fibril diameter data from Boote, 2003)

#### 4.2.4 Theoretical measurements

Three micrographs of central human cornea were digitised according to the method of section 2.4. Transmission was then determined through the sample according to the methods of section 2.5. This method allowed the interfibril spacing, fibril diameter and relative refractive index contrast between fibril and extrafibrillar substance to be



dynamically varied in accordance with the required ultrastructural parameters for each point across the corneal surface, whilst keeping spatial ordering constant.

### 4.3 Results

#### 4.3.1 Measurement of corneal transmission

Figure 4.4 shows the variation in transmission for 10 human corneas as a function of position on an arbitrary meridian across the surface. For ease of presentation only one wavelength is presented (500nm). This wavelength was chosen as it will give a sufficiently large range for analysis which would not occur in the long wavelength region, but will not be affected by absorptions which can occur at short wavelengths.

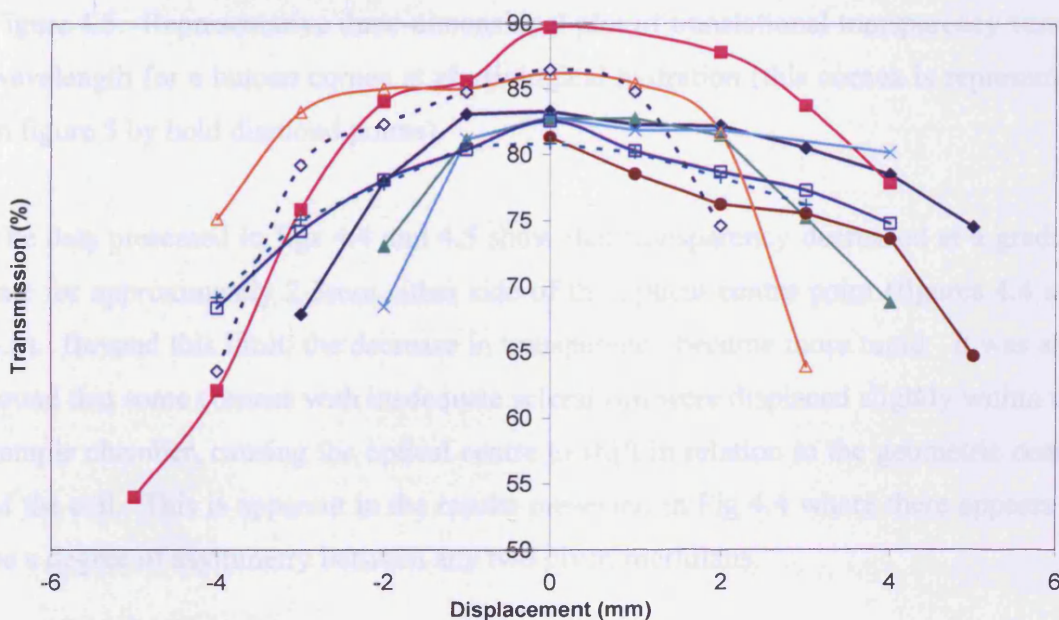


Figure 4.4: Translational transparency for human corneas ( $n=10$ ) near physiological hydration at 500nm

Figure 4.5 shows, for a given cornea, a three dimensional plot of position and wavelength versus intensity. It is quite noticeable that although the absolute transmitted magnitude decreases, the wavelength dependence remains constant even at the far periphery.

### Three dimensional plot of corneal transparency across the surface

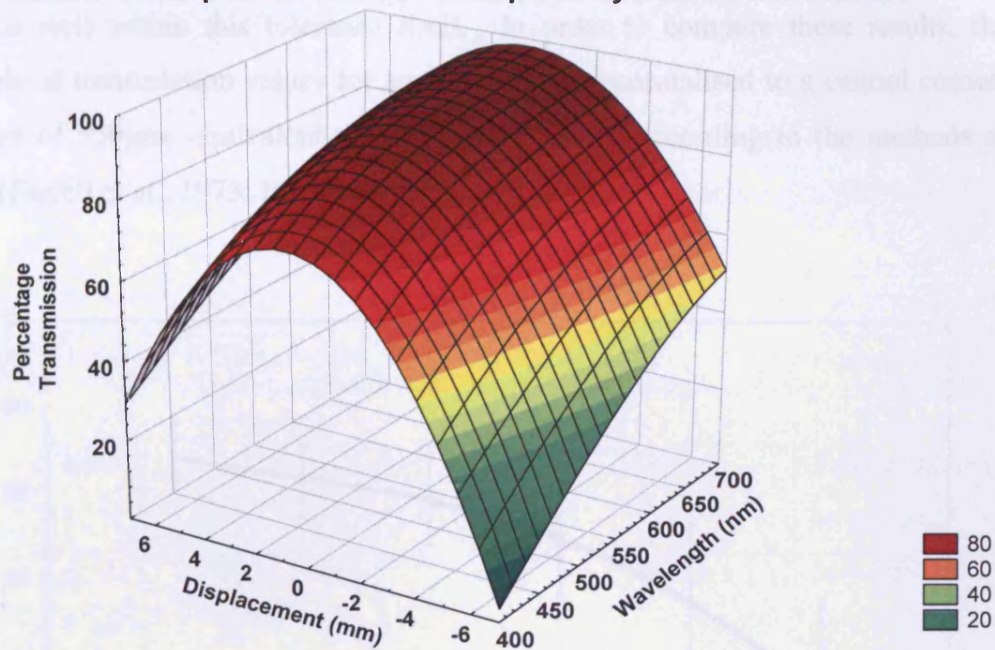


Figure 4.5. Representative three-dimensional plot of translational transparency versus wavelength for a human cornea at physiological hydration (this cornea is represented in figure 3 by bold diamond points).

The data presented in figs 4.4 and 4.5 show that transparency decreased at a gradual rate for approximately 2-3mm either side of the optical centre point (figures 4.4 and 4.5). Beyond this limit, the decrease in transparency became more rapid. It was also found that some corneas with inadequate scleral rim were displaced slightly within the sample chamber, causing the optical centre to shift in relation to the geometric centre of the cell. This is apparent in the results presented in Fig 4.4 where there appears to be a degree of asymmetry between any two given meridians.

Since the exact orientations in which corneas were placed in the holder were unknown, the average of the two displacements either side of the optical centre, shown below in figure 4.6, was compared. Due to small variances in collagenous mass between samples not all corneas achieved the same hydration end point. The average end hydration was  $3.3 \pm 0.2$ . The actual range of hydrations extended from 3.0 to 3.8. The transmission properties of the cornea are relatively insensitive to hydration changes until the thickness increases beyond about 25% of its normal value (Farrell et al., 1973). Since hydration has a linear relationship to corneal thickness



(Hedbys and Mishima, 1966) it is possible to calculate that the upper hydration of  $H=3.8$  is well within this tolerance limit. In order to compare these results, the ensemble of transmission values for each cornea was normalised to a central corneal thickness of  $550\mu\text{m}$ , equivalent to a hydration of 3.2 according to the methods of Farrell (Farrell et al., 1973; Farrell and McCally, 2000).

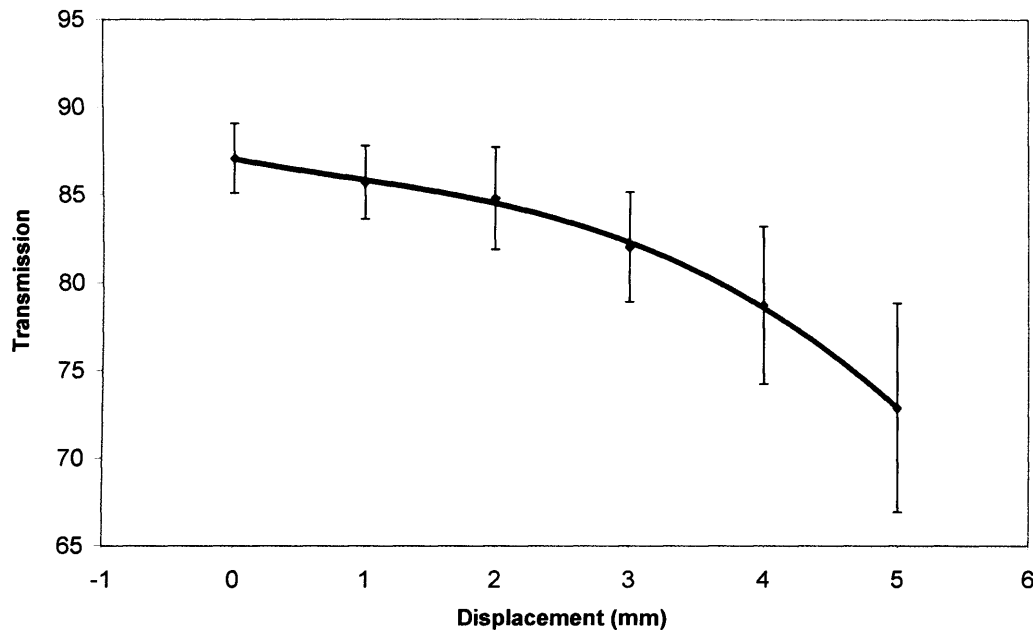


Figure 4.6 Transparency at 500nm as a function of radial distance from the optical centre of the cornea ( $n=10$  for positions 0-4mm,  $n=3$  for 5mm, error bars are standard deviation)

From figure 4.6, it can be observed that the transmission observed off the central axis decreases approximately linearly up to 3mm from the central axis, with an accelerated decrease after this point.

#### 4.3.2 Modelling transmission in the human cornea

Corneal transmission was computed using average ultrastructural parameters derived from the Boote et al. (2003) study, by further averaging both raster scan directions, from the centre to 5mm displacement. Stromal thicknesses were corrected to actual optical depth traversed by a beam incident on and parallel to the central optical axis, and the refractive indices calculated in table 4.1 were used. Relative fibril positions

were measured from several micrographs and the predictions made were based on an image from our laboratory (figure 4.1), and two published images (Komai and Ushiki, 1991; Muller et al., 2004) of a normal human cornea. The average fibril spacing (determined by the radial distribution function) and fibril radius in the micrographs were set to the parameters in table 4.1 with the aid of a simple scaling algorithm.

Table 4.2. Theoretical and experimental transmission values compared at 500nm

Position (mm)	Optical depth ( $\mu\text{m}$ )	Theoretical Transmission				Experimental Average Transmission (error s.d.)
		Fig. 1	Muller et al	Komai and Ushiki	Average (error s.d.)	
0	550	89.6	87.1	89.1	$88.6 \pm 1.3$	$87.1 \pm 2.0$
1	590	88.9	86.0	88.5	$87.8 \pm 1.6$	$85.7 \pm 2.1$
2	605	88.7	85.6	88.3	$87.5 \pm 1.7$	$84.8 \pm 2.9$
3	645	86.7	84.1	87.7	$86.1 \pm 1.9$	$82.0 \pm 3.1$
4	760	84.5	81.0	84.1	$83.2 \pm 1.9$	$78.7 \pm 4.5$
5	800	79.5	76.1	81.0	$78.9 \pm 2.5$	$72.9 \pm 5.9$

It is of note from table 4.2 that corneal transmission remains relatively constant across the central, prepupillary cornea, covering some 3mm from the optical centre. Beyond this point, as the fibril diameter starts to increase towards the limbal region, the scattering increases. It has been shown previously that changes in organisation between anterior and posterior collagen fibrils affect the transmission predicted by the direct sum method, and recognised that these may in themselves be artefacts of the hydration at which the samples were held prior to fixation (Freund et al., 1995). However, using the average of the three transparency predictions for physiologically hydrated corneas, the decrease in transmission from optical centre to limbal region was calculated to be  $9.7 \pm 1.2\%$ .

#### **4.4 Discussion**

From both experimental and theoretical standpoints these findings indicate that there is a reduction in absolute transmitted intensity through human corneas as a function of

distance from the optical centre. It was therefore of interest to determine the cause of this decrease and how it relates to ultrastructural observations. Corneal thickness is known to increase at the periphery, and although this will increase transmitted intensity losses, it has previously been shown that in bovine corneas this is incompatible with the observed data, even after correction for non-normal incidence (Doutch et al., 2007). Two main possibilities suggest themselves:

1. Increased specular scattering
2. Ultrastructural changes

Although it is known that the keratocyte density increases towards the peripheral and limbal zones (Moller-Pedersen and Ehlers, 1995), in the normal cornea the excess contribution that these cells would make to specular scattering is unknown, but considered to be small.

In analysing the relationship between ultrastructural changes and transmission, the transparency of the stroma can be explained by reference to the following equation, which is rewritten from eqn.3.4:

Eq 4.10

$$I_t = I_0 \exp(-\sigma\rho\Delta)$$

Where  $I_t$  and  $I_0$  are the transmitted and incident intensity, respectively,  $\sigma$  is the total scattering cross section per fibril,  $\rho$  is the number density of fibrils and  $\Delta$  is the optical path length, or the actual thickness of stroma traversed by an incident beam. It is easiest to investigate the effects of ultrastructural parameters by reference to the differential scattering cross section per unit length for an individual fibril formulated thus (Freund et al., 1986):

Eq 4.11

$$\sigma(\theta) = \frac{n_g^3 (\pi a)^4 (m^2 - 1)^2}{2\lambda^3} \left( 1 + \left[ \frac{2 \cos \theta}{m^2 + 1} \right]^2 \right)$$

Where symbols have their usual meanings and  $\lambda$  and  $\theta$  represent the photon wavelength and the scattering angle respectively,  $n_g$  is the refractive index of the ground substance,  $a$  is the fibril radius, and  $m$  is the refractive index contrast between fibril and extrafibrillar substance.

When the interfibrillar spacing is increased, it follows that the fibril number density  $\rho$  decreases. Mathematically, this is evidenced by the equation relating density to interplanar separation, which may be derived from equations 4.2 and 4.3 above:

Eq 4.12

$$\rho = (1.06d_h^2)^{-1}$$

By using Eqn 4.12 on the ultrastructural data presented in table 4.1, it can be shown that fibril number density decreases by approximately 27% from the centre to the far periphery. Using equation 4.10 it can be shown that the lower fibril number density is sufficient in the peripheral regions to mathematically cancel out much of the effect that the increase in corneal thickness has on light propagation through the stroma.

X-ray diffraction data have suggested that fibril radii increase by a modest amount (Boote et al., 2003) and it is mathematically straightforward to show the impact that this may have on visible light propagation with the aid of equation 4.11. In doing so it is noted from equation 4.11 that fibril radius is expressed by a 4<sup>th</sup> power term. Assuming a 1nm diameter increase, the fourth power radial dependence term in equation 4.11 will cause a 22% increase in the differential scattering cross section per length. The increase in fibril radius thus has a great effect on light propagation through the stroma and under numerical analysis seems to be the source of the

quadratic decrease in transmission as a function of position seen in the peripheral regions.

There is one additional factor that must be accounted for in this formulation, and this is the relative refractive index between the hydrated fibrils and the interfibrillar matrix. In this chapter, a simplified model was developed which assumed that volumetrically the amount of extrafibrillar material remains constant as the unit cell dimensions expand.

It was found experimentally that the transmitted intensity showed only a gradual decrease across the central, prepupillary zone, which is some 3mm in diameter. This was consistent with our theoretical deductions, and by reference to tables 4.2 and 4.3 it can be seen that the experimental and predicted transmitted light fractions are similar. Outside the central zone, as the fibril radii start to increase, scatter increases. Experimentally, an average decrease of approximately 14% in light propagation is observed going from the central optical axis to a displacement of 5mm at the periphery. The 9.7% change predicted by theory is consistent with the standard deviations of the experimental results, as illustrated in figure 4.7.

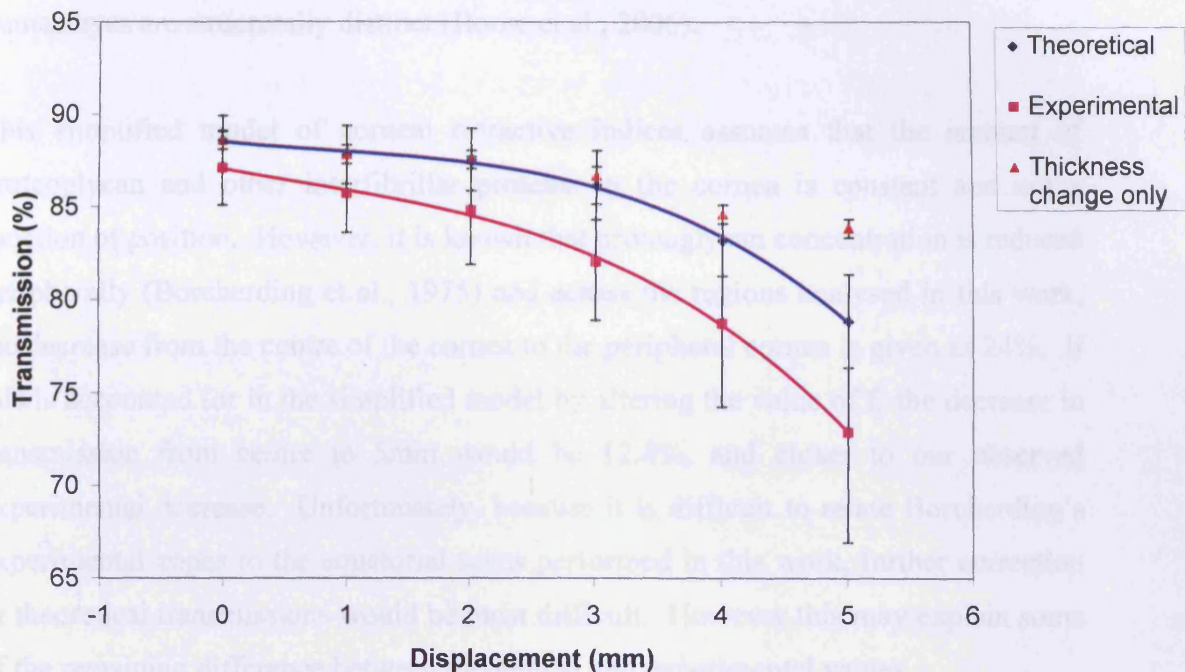


Figure 4.7. Theoretical versus experimental deductions of corneal transparency across the surface at 500nm (scales adjusted for clarity)

Although the theoretical and experimental analyses here are comparable, they do not coincide exactly. There are a number of explanations for this. First it is necessary to apply the caveat that transmission can only be computed for a small segment of one cornea assuming that the spatial ordering is homogeneous throughout the whole path length; this work attempts to account for this by analysing more than one micrograph from several sources. Also, there would appear to be asymmetry in thickness at different meridians across the cornea, coupled with a degree of individual variation; an increase of 100 $\mu$ m in the peripheral thickness at a position of 5mm would reduce the transmission of a given image by some 3%. It must also be noted that theoretical computation is from average parameters; there is some, albeit quite small, variance in structural parameters between different individual corneas. Previously it has been commented on that there is a possible anisotropy of light propagation between any two given meridians of a stroma radiating outwards from the optical centre (Doutch et al., 2007). Since, in the experiments described, it was not possible for human corneas to be placed in the cell with a known orientation, this anisotropy leads to variance in

our results, especially in light of the observation by x-ray diffraction that left and right human eyes are structurally distinct (Boote et al., 2006).

This simplified model of corneal refractive indices assumes that the amount of proteoglycan and other interfibrillar proteins in the cornea is constant and not a function of position. However, it is known that proteoglycan concentration is reduced peripherally (Borcherding et al., 1975) and across the regions analysed in this work, the decrease from the centre of the cornea to the peripheral cornea is given as 24%. If this is accounted for in the simplified model by altering the value of  $f_p$  the decrease in transmission from centre to 5mm would be 12.8%, and closer to our observed experimental decrease. Unfortunately, because it is difficult to relate Borcherding's experimental zones to the equatorial scans performed in this work, further correction of theoretical transmissions would be most difficult. However this may explain some of the remaining difference between theoretical and experimental values.

It is known that keratocyte cell density increases in the peripheral regions of the cornea (Moller-Pedersen and Ehlers, 1995). The human corneas used in this study were likely to contain some dead keratocyte cells which essentially form voids in the stroma, which in turn act as Mie scattering points; this could therefore further contribute to the divergence between experiment and theory.

It is obvious that non-normal incidence effects will occur on the collagen fibrils in the periphery, especially in certain lamellar orientations. The effects this will cause are unclear; adjustment of the direct summation of scattered fields model is beyond the scope of this work. It must be remembered that the algorithms used to predict transparency (Freund et al., 1986) are, in effect utilising two dimensional projections of the fibril distribution and thus the angle of incidence is a parameter which is not implicit (and is difficult to calculate, regardless). Non-normal incidence effects are difficult to avoid even in the central region under normal incidence due to undulations in the lamella (Christens-Barry et al., 1996), and in any spectrometry investigation on the corneal stroma these effects will also occur due to the size of the beam. An examination of the scattering theory for an infinitely long dielectric cylinder (van de Hulst, 1981) shows that in oblique incidence additional components are generated which are dependent on the incident angle. It is crucial to understand that non-normal

incidence angles will only be large for a small number of lamellar orientations even in the far peripheral regions. The total intensity signal of a dielectric cylinder at non-normal incidence as a function of scattering angle is known (Yousif, Mattis and Kozminski, 1994). Specifically, it is known that as the angle of incidence deviates from the perpendicular, the scattered intensity as a function of angle becomes smoother and the distribution of scattered light resembles that from a cylinder of smaller radius (if the total signal from  $0^\circ$  to  $180^\circ$  is analysed). The scattering in the forward direction, however, would appear to be largely unaffected, with high angle components having the greatest degree of perturbation from the form at normal incidence. It would seem that if non-normal incidence effects were significant, the X-ray diffraction method for deriving fibril radii would be unusable on the peripheral cornea; however the determinations by this method (Boote et al., 2003) are known to be consistent with those obtained from electron microscopy (Borcherding et al., 1975).

It would be of particular interest to contrast the off-axis transmission in human corneas with various other species. Data are presently available for the bovine cornea (Doutch et al., 2007), as shown in figure 4.8, and lead to an interesting observation.

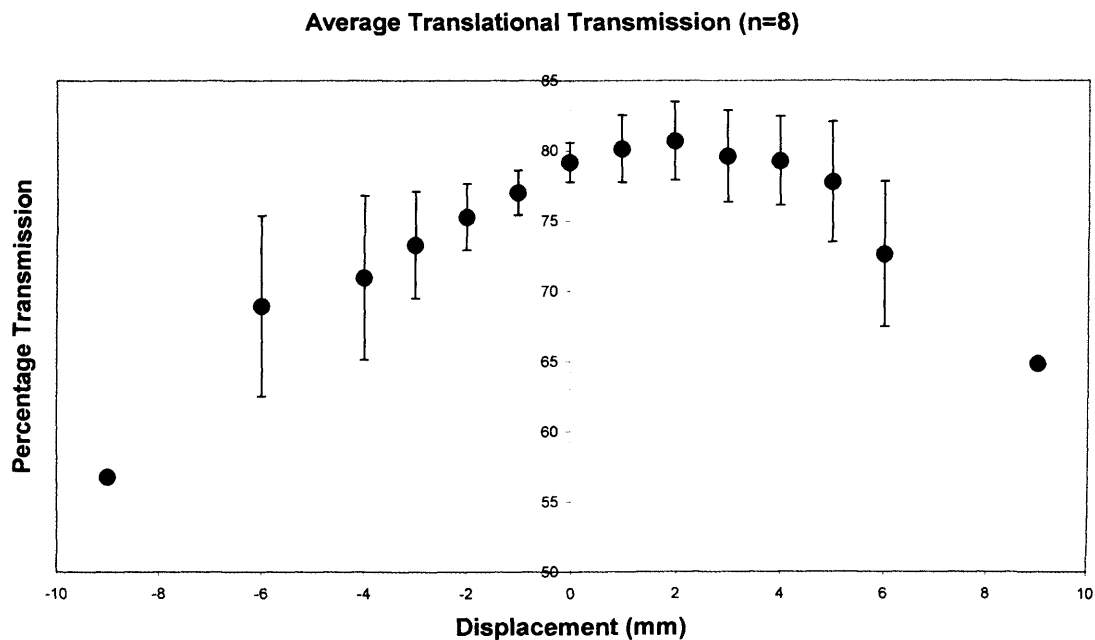


Figure 4.8 Transmission as a function of position for bovine cornea (at 500nm, errors are s.d.)



It is possible to perform a crude alignment when using the bovine cornea due to the shape. Measurements were taken in a meridian through the centre of the cornea along the longer, horizontal transept of the bovine cornea. Here, it can be seen that the point of least optical density does not coincide with the geometric centre of the cornea. Specifically, the most transparent point is displaced by 2mm from this point; figure 4.8 shows the result when every corneal data-set is transposed to the same lateral alignment (Doutch et al., 2007). As it is not known whether the eyes are left or right, it is difficult to comment definitively on this observation. However, the bovine eye is located on the side of the bovine head. This may therefore be an optical adaptation to give an optimum corneal transmission for an eye mounted on the side of the head, in a forward direction. It would be useful to determine whether this effect occurs systematically in similar animals. At the time of writing, initial work on this is underway on sheep and ovine corneas.

In conclusion, this chapter has investigated how corneal transparency changes away from the central axis and has shown that the observed decrease is much greater than would be expected if the transmission decreased purely as a function of thickness. Using the direct summation of scattered fields method it has also shown that the decrease in the peripheral regions is explained by reference to the increase in fibril diameter and the scaling of refractive indices caused by the increase in interfibril spacing. A better fit between experiment and theory is obtained when the changes in the proteoglycan concentration in the peripheral regions are accounted for.

## **Chapter 5. Light transmission and thickness of oedematous corneas: A comparison between central and peripheral zones**

The previous chapter detailed efforts to determine an experimental and theoretical basis for peripheral light transmission in the normal human cornea at physiological hydration. This chapter will investigate experimentally how light scattering changes under oedema in human cornea, with particular reference to peripheral stroma. It is also of interest to determine whether there is a difference in swelling rates between central and peripheral cornea, and the implications this may have for peripheral light scattering.

### **5.1 Introduction**

During the process of corneal swelling, it is well known that the cornea loses transparency and becomes quite opaque (Maurice and Giardini, 1951). This loss of transparency has its basis in several ultrastructural changes which take place as the stroma swells.

At the most basic structural level, the central corneal thickness increases in a linear fashion with hydration (Hedbys and Mishima, 1966). By reference to equation 4.10, it can be seen that thickness increases reduce overall corneal light transmission. Previous calculations have suggested that an increase of 300 $\mu$ m in corneal thickness corresponds to around a 5-10% decrease in corneal transmission (Meek et al., 2003b) at 500nm.

It is also known, from X-ray diffraction studies, that interfibrillar spacing squared increases in a linear fashion with increasing stromal hydration (above  $H=1$ ) (Meek et al., 1991). This has the effect of altering the fibril volume fractions, which in turn alters the relative refractive index ratio between fibril and ground substance. This effect can be seen by reference to equations 4.7 and 4.9 in the previous section. Under the assumption that all of the excess water goes into the extrafibrillar space, it can be shown that refractive index of the ground substance will decrease (i.e. it will become closer to that of liquid water, 1.333). If the refractive index of a fibril,  $n_f$ ,

remains constant, then clearly the value  $m$  will increase. It has been shown previously that at 500nm, an increase in  $m$  value from 1.03 to 1.07 leads to a decrease in light transmission of around 10% (Meek et al., 2003b). It should also be noted that, in the context of Maurice's original (1957) lattice model for corneal transparency, the loss of transmission under oedema was explained by an increase in interfibril spacing disrupting the interference function.

Taking these factors together suggests that they only account for a modest proportion of the increased light loss in the oedematous cornea. They also do not explain the variation in wavelength dependence, under the assumption that there is no dispersion in the refractive index of the cornea, an effect known to occur at shorter wavelengths (Sivak and Mandelman, 1982).

The balance of scattering in the oedematous cornea is believed to be caused by the formation of voids or lakes in the stroma. These are regions which appear on transmission electron micrographs to be devoid of regularly arranged fibrils (Goldman et al., 1968). It is known from the literature that the wavelength dependence of corneas under oedema changes considerably from the physiological condition; specifically the dependence changes from the inverse-cubic relation (see chapter 4) to an inverse-square relation. The scattering is believed, from theoretical considerations, to become particularly significant when the size order of fluctuations in fibril number density approaches 200nm (Benedek, 1971).

In order to understand why this change in wavelength dependence occurs, it will be useful to refer to the formulation of the interference function for X-ray scattering, seen in equation 3.1. Here the term  $S(\mathbf{q})$  is defined in more detail from first principles (Ziman, 1979):

Eq 5.1

$$S(\mathbf{q}) = \frac{1}{N} \sum_{i,j} \exp(-i\mathbf{q} \cdot (\mathbf{r}_i - \mathbf{r}_j))$$

Here,  $N$  is the number density of scattering objects,  $\mathbf{q}$  is the scattering vector and the quantity  $\mathbf{r}_i - \mathbf{r}_j$  is the vector displacement between two scattering elements  $i$  and  $j$ . Since corneal transparency is dependent on the structure factor, it follows that  $S(\mathbf{q})$  can be indirectly probed by carefully measuring the amount of transmitted light through the cornea – this procedure has been utilised in section 3.3.3.

There is to be found here a simple analogy with Bragg diffraction – the spatial coordination between the scattering elements is of course fixed, therefore by varying the incident wavelength, it follows (c.f. Bragg's law) that the scattering vector  $\mathbf{q}$  is altered. When spatial disorder on the same length scale as visible light appears, it therefore follows that scattering will increase markedly, and will affect the long wavelength region ( $>550\text{nm}$ ) much more than the normal fibrillar based scattering mechanism in the stroma; this can be investigated by reference to equation 5.1. If the spacing between the scattering elements becomes larger and approaches that of the illuminating wavelength, equation 5.1 would suggest that the scattering cross-section becomes much larger. This is in essence what leads to the copious reduction in transmission (Farrell et al., 1973; Farrell and McCally, 1976).

Like the normal human cornea, the transmission properties of the peripheral regions in the oedematous cornea do not appear to have been investigated previously. There is clinical evidence to suggest a differential between central and peripheral cornea *in vivo* (Bonanno and Polse, 1985; Holden et al., 1985) during contact lens wear and nitrogen anoxia. Maurice was also able to infer from some of his data that there was uneven topographical swelling in the cornea, but did not investigate it directly (Maurice and Giardini, 1951). A similar effect has been demonstrated in the cat cornea, although some caution should be made in applying this to the human cornea; the human cornea becomes thicker in the peripheral regions but this does not appear to be the case in cat (Ling, 1987). In all cases the swelling differential is thought to be caused by the 'clamping' effect exerted by the limbal region – a cellular contribution would appear to be ruled out (Ling, 1987). There is evidence from X-ray scattering methods that corneal collagen fibrils change direction approaching the limbus and begin to run in a circumferential fashion approaching the corneoscleral interface (Meek and Boote, 2004), possibly implying a change in the tissue biomechanical

properties at the limbal region, lending weight to the hypothesis that it may exert an anchoring effect on corneal swelling.

This chapter will aim to investigate this interesting differential in the context of corneal transparency. This has clinical relevance as there is a curious form of corneal oedema known as Brown-McLean syndrome which only affects the peripheral cornea, many years post-cataract surgery (Brown and McLean, 1969).

### 5.2 Methods

General methods pertaining to tissue handling may be found in section 2. For this study, time expired human corneas ( $n = 6$ ) obtained from UKTS Bristol Unit were used. The corneas were equilibrated by the method of section 2.5 to just below physiological hydration using 2.7% PEG, in order to give a slightly larger range for analysis, with epithelial and endothelial cell layers removed.

After dialysis, the corneas were placed in 0.154M NaCl solution and allowed to freely swell, with the scleral rim in place, for intervals of 30 minutes. At the end of each interval, corneas were removed from the osmotic solution and had the thickness in the centre and peripheral zones measured by ultrasound pachymetry. The central zone was taken to be the geometric centre of the cornea, and the peripheral zone was taken as an average of four equidistant points approximately 2mm from the limbus. The thickness of the central cornea was converted into a hydration value using the relationship derived by Hedbys and Mishima (1966) shown in equation 5.2:

Eq 5.2.

$$\Delta = (H + 0.64)/7$$

Here, H is corneal hydration,  $\Delta$  is corneal thickness (in mm).

After several hours a point would be reached where corneal thickness would not appreciably increase further; for these corneas this point was generally reached after

3-5 hours. At this point, the swelling experiment was terminated and corneal transmission in the central and peripheral regions was evaluated using the methods of section 4.2.2.

### 5.3 Results

#### 5.3.1 Ultrasound pachymetry of central and peripheral zones

Central and peripheral corneal thickness for any given central corneal hydration is shown in figure 5.1 below. For each hydration point analysed, there are two experimental points; a blue point which indicates the central thickness, and a red point which indicates average peripheral thickness.

Since the hydration was derived from the central corneal thickness, the fit line between thickness and hydration is linear. It is, however, much more difficult to make an accurate fit line to the averaged peripheral thickness which seem to demonstrate quite large variations. Generally, peripheral thickness also appears to increase in a very approximate fashion in concert with central corneal hydration. Overall, as a general trend, it would appear that there is greatest difference between central and peripheral thickness at low hydration values, below the physiologically normal range  $H=3.0-3.5$ . It would appear that, for certain corneas, central and peripheral thicknesses start to converge at a point at which they are only slightly swollen (note in particular the readings at  $H=4.1$ ). Several corneas appear to have central thickness greater than peripheral once hydrations of  $H>5.0$  have been reached, and indeed  $H=5.5$  is the point at which the peripheral trendline crosses over the central one. After this point, peripheral thickness is less than the central thickness, demonstrated quite strikingly by hydration levels of  $H=6$ .

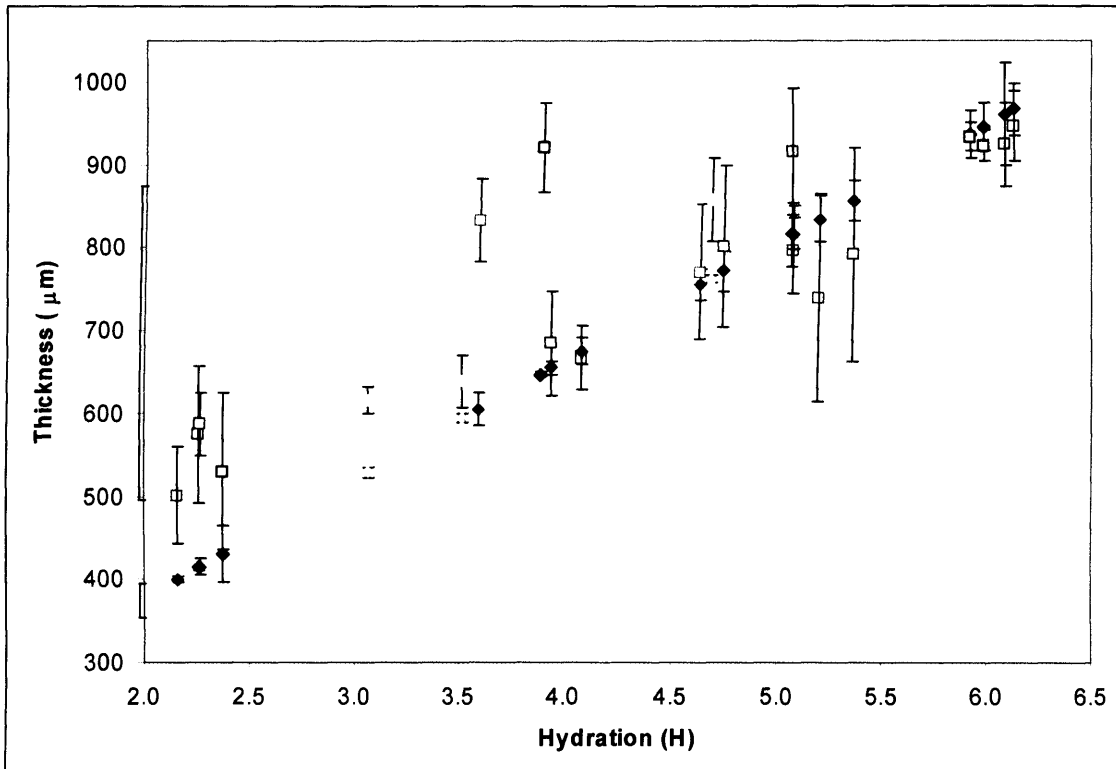


Figure 5.1 Central and peripheral corneal thickness as a function of central corneal hydration (central cornea labelled as solid diamonds, peripheral cornea labelled as hollow squares; different colours denote separate corneas)

Indeed, figure 5.1 would seem to indicate that there is a degree of convergence between central and peripheral thickness at very high hydrations around 6; in the results presented here at these high hydrations the central cornea appears thicker than the average obtained from the peripheral region, but, this does not appear to be statistically significant.

### 5.3.2 Light transmission as a function of position

With this in mind, attention can now be diverted to how this may affect corneal transmission off-axis. This is shown below in figures 5.2 and 5.3 for four corneas, and for a representative individual cornea (88B) in figure 5.4. In keeping with the format presented in chapter 4, here the experimental data in Fig 5.4 are shown at a fixed wavelength of 500nm. Note that, unlike section 4, results here are not laterally corrected in order to account for any shift that may occur. This is because, during the execution of this experiment, more experience had been gained in ensuring that there

was no lateral shifting of the cornea in-situ within the holder; this was achieved by moderating the amount of clamping holding the cornea in place, whilst ensuring that it could still be pressurised.

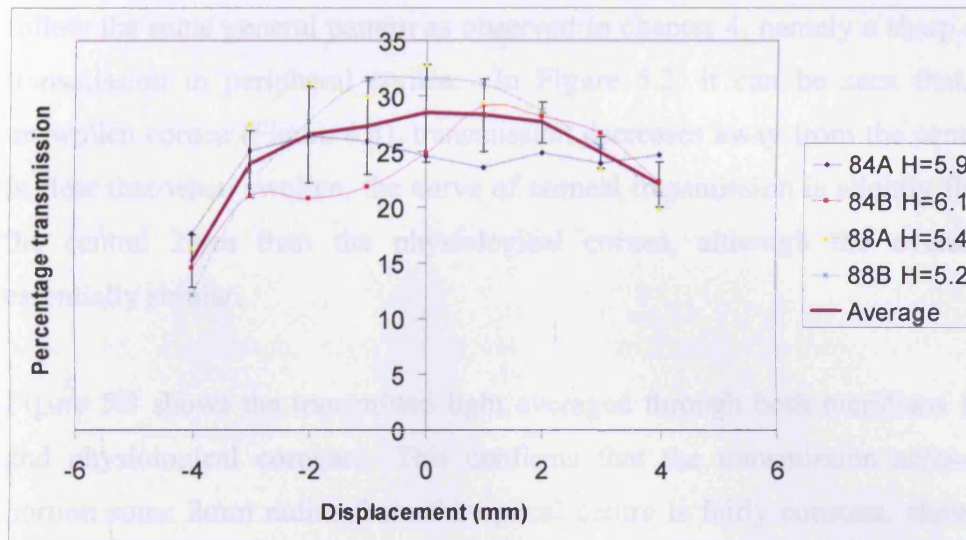


Figure 5.2 Corneal transmission as a function of position in swollen human corneas; taken at 500nm. Error bars are one SD.

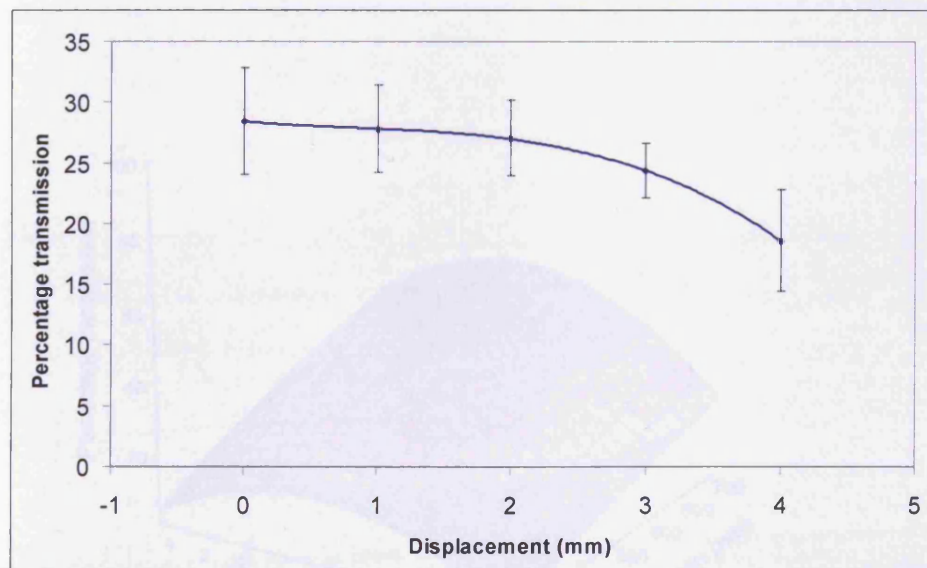


Figure 5.3 Average of transmission at 500nm of both meridians as a function of displacement. Fit line is cubic polynomial function.

The results presented here demonstrate that, as determined from normal human corneas in chapter 4, corneal transmission decreases peripherally. The transmission



values of swollen corneas are much lower than those in normal, physiologically hydrated cornea shown in section 4. Here, however, measurements were not taken at the 5mm position as it was determined that the signal became too low for a satisfactory signal to noise ratio at short wavelengths. Nevertheless they do appear to follow the same general pattern as observed in chapter 4, namely a sharp decrease in transmission in peripheral cornea. In Figure 5.2, it can be seen that, as in the unswollen cornea (Figure 4.4), transmission decreases away from the central axis. It is clear that when swollen, the curve of corneal transmission is slightly flatter across the central 2mm than the physiological cornea, although the overall trend is essentially similar.

Table 5.1 Wavefront aberrance factor  $\times$  calculated for wavelength range 400-

Figure 5.3 shows the transmitted light averaged through both meridians for swollen and physiological corneas. This confirms that the transmission across a central portion some 2mm radius from the optical centre is fairly constant, showing a very gradual decline. This decrease is much less distinct than that seen in normal cornea. There is greater extinction at the 3 and 4mm radial displacement from the centre, here assuming the 'quadratic' form seen from normal cornea in chapter 4.

Wavelength (nm)	1.75	1.87	1.99	2.11	2.23
400	1.38	1.40	1.42	1.44	1.46
450	1.40	1.42	1.44	1.46	1.48
500	1.42	1.44	1.46	1.48	1.50
550	1.44	1.46	1.48	1.50	1.52
600	1.46	1.48	1.50	1.52	1.54
650	1.48	1.50	1.52	1.54	1.56
700	1.50	1.52	1.54	1.56	1.58

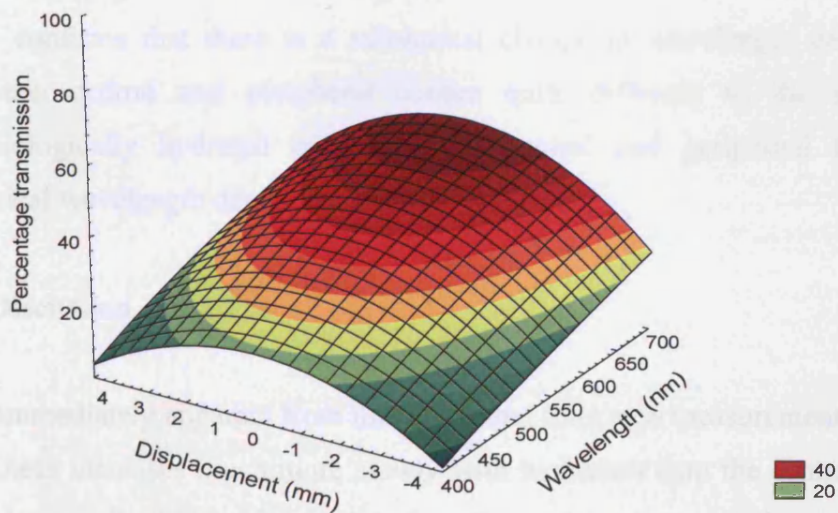


Figure 5.4 Three dimensional plot of corneal transmission as a function of position for a single cornea



Finally, Figure 5.4 shows a three-dimensional plot of wavelength and meridional displacement against transmission for an individual swollen cornea. This plot suggests that there is a change in inverse wavelength dependence from centre to periphery. Specifically, it can be observed that the inverse dependence changes from what appears to be an inverse square in central cornea to being almost linear in the periphery. To quantify this, wavelength dependencies were calculated with the aid of equation 3.7, and are shown below in table 5.1 for central and far periphery (i.e. 4mm).

Table 5.1 Wavelength dependence factor  $n$  calculated for wavelength range 400-700nm.

Cornea	Wavelength dependence factor $n$			
	Central	Peripheral (meridian 1)	Peripheral (meridian 2)	Peripheral (avg)
84A	1.61	1.15	1.20	$1.18 \pm 0.03$
84B	1.62	1.39	0.88	$1.14 \pm 0.26$
88A	1.75	1.67	1.30	$1.49 \pm 0.19$
88B	1.58	1.62	1.23	$1.43 \pm 0.20$

This confirms that there is a substantial change in wavelength dependence factor between central and peripheral cornea quite different to the situation in the physiologically hydrated cornea, where central and peripheral have essentially identical wavelength dependence.

#### 5.4 Discussion

It is immediately apparent from the ultrasound thickness measurements that peripheral thickness increases much more slowly with hydration than the central portion. This correlates well with previous, clinical studies and suggests that the swelling properties of the cornea *in-vitro* and *in-vivo* are, at the very least, broadly similar (Ling, 1987).

It is likely that this effect is due to changes in the distribution of collagen fibrils in the peripheral and limbal regions. There are a number of well known changes in matrix architecture in the peripheral cornea. It is well known from electron microscopy and X-ray scattering that interfibril spacing and diameter increase (Borcherding et al., 1975; Boote et al., 2003), although it is likely that the bulk of the effect has its origins in the known interweaving of layers of lamellae, particularly in the anterior tissue portion (Radner et al., 1998); X-ray diffraction has also suggested that fibrils begin to run preferentially in an approximately circumferential pattern around a distinct annulus in the limbal region (Newton and Meek, 1998) and this is hypothesised to affect the biomechanical properties of the cornea, particularly with regards to maintaining corneal curvature.

The change in wavelength dependence between central and peripheral portions was rather unexpected. This would seem to imply some manner of change in spatial ordering between central and peripheral cornea. The transmission properties as a function of position are much more irregular than those from human cornea at physiological hydration described in chapter 4. Transmission across the central region of 4mm is fairly constant, in some cases, very nearly equal at all points (Figure 5.2). As might be expected from the analysis of chapter 4, transmission begins to decrease much more rapidly approaching the limbus itself; this correlates to the point at which fibril radii start to increase as determined in normal cornea (Boote (2003)) although X-ray scattering measurements will need to be taken to confirm this is significant in the swollen cornea.

Taking into account the low differential between central and peripheral thickness at high hydrations, a hypothesis for the fairly constant transmission in the central zone suggests itself. The theoretical results of chapter 4 suggested that the geometric centre of the human cornea has the highest transmission as it possesses the shortest optical path length; the packing of collagen fibrils was also shown to produce the lowest refractive index contrast in the centre. With the knowledge that central corneal thickness increases at a faster rate than the peripheral segments, it would appear that this causes a non uniform decrease in transparency across the cornea, with the centre reducing its light propagation at a faster rate than the more peripheral parts.

The change in wavelength dependence factor is worthy of further investigation. Overall, the factors,  $n$ , are somewhat lower than the rather arbitrary ‘inverse square’ i.e.  $n$  value of 2. Fibril number density will not directly affect the wavelength dependence. Generally, the interfibrillar spacing increases as the cornea undergoes oedema. Although at first glance this may appear to increase corneal transmission (cf equation 4.1), in fact, as seen in chapter 4, this induces a change in relative volume fractions of the stromal components, ergo causing a change in refractive index. Put simply, as the extrafibrillar matrix becomes more hydrated, its refractive index ( $n_g$ ) approaches that of water and thus the contrast value,  $m$ , increases. However, this only explains a moderate fraction of the scattering, certainly in the centre of the cornea; a contrast value of  $m=1.07$  modifies the scattering cross section such that transmission would decrease by about 15% at most (Meek et al., 2003b). At this time it is not known from the literature whether interfibrillar spacing in the peripheral regions increases linearly with hydration, as it does in the central portion. However, using the methodology of chapter 4 suggests that this would make very little material difference to the light loss; there it was found that a decrease in fibril number density had remarkably little impact on light transmission.

To explain the balance of scattering and the change in wavelength dependence, attention must be directed to the concept of ‘lakes’. As outlined in section 5.1 ‘lakes’ can be thought of as being discontinuities in fibril distribution (or refractive index). Therefore, the concept of wavelength dependence is intimately related to changes in spatial ordering in the system under test; the mechanism by which this occurs was outlined in section 5.1. The wavelength dependence will vary with the size of the objects being illuminated (Farrell et al., 1973; Farrell and McCally, 1976) – on the assumption that they occur with random spatial distribution within the sample. It is likely that the lowered wavelength dependence peripherally is indicative of larger fibril-free voids existing at this point. There is a corollary for this from the study of light scattering mechanisms within skin, where the size of collagen/elastin bundles affects the wavelength dependence in differing portions of the spectrum (Bashkatov et al., 2005). This wavelength dependence also agrees with that theoretically calculated for mixtures of large spherical particles.

Modelling this light scattering using the direct summation of fields method is, unfortunately, not straightforward. It has been shown previously that modelling random voids within a given normal distribution of fibrils has the effect of lowering transmission, and that this effect becomes more pronounced when larger voids are used. However, the predicted decrease is not as severe as that observed experimentally. It is likely that a correction must be applied to model the amount of Mie light scattering from these inhomogeneous regions of the stroma when they become quite large in relation to the wavelength of light. Examination of basic light scattering theory suggests that the absolute magnitude of transmission is most strongly affected by the number density of voids, whereas the wavelength dependence is mostly affected by changes in the geometry and size of the voids.

It is likely that the peripheral cornea is particularly affected by this as the interfibrillar spacings here are greater to begin with (Boote et al., 2003). Therefore any voids which form may have increased size versus those in the central portion due to the greater initial spacing between fibrils. This will affect the structure factor and therefore have an effect on wavelength dependence.

This can be crudely tested using the sunflower system outlined in chapter 3. By placing a circular void of diameter 150nm in the centre of the system, transmission was determined, using the direct sum method, to be 48% at 500nm, with dependence,  $n$ , of 2.3. If the size of the void is doubled to 300nm, then transmission is decreased to 14%. However, dependence,  $n$ , only decreases very slightly to 2.1. A certain degree of caution must be applied to these calculations; in particular the inverse wavelength dependence is likely to be overestimated due the employment of ensemble averages by which light transmission is computed in the direct summation of scattered fields procedure; this method would appear to reduce the apparent impact of the lakes on the structure factor. Additionally the model may not provide the correct structure factor for particularly large inhomogenities in fibril distribution. However, it does elucidate the general principle. It has been shown previously that the direct summation of scattered fields model does not appear to predict the transmission of pathological or swollen corneas in a manner which offers good agreement with experimental data (Leonard, 1996).

It will be of interest at this juncture to compare the wavelength dependence of the swollen human corneas in this chapter with that of the developing chick cornea. The developing chick cornea is naturally swollen during gestation, with the hydration decreasing quite rapidly as the chick approaches hatching, with increasing compaction of the matrix and decrease in interfibrillar spacing (Hay and Revel, 1969; Siegler and Quantock, 2002; Connon et al., 2003b). It therefore becomes naturally transparent over a fairly well defined timescale (Linsenmayer et al., 1998). It is well known from photometry measurements that the transmission of the developing chick cornea increases from 40% at day 14 of development to over 90% by day 19 (Coulombre, 1958). Inverse wavelength dependence was calculated from transmission data gathered by Ms. Barbara Palka using the methods outlined previously. The results are shown in table 5.2.

Table 5.2 Wavelength dependence of developing chick cornea

Developmental day (E)	Inverse wavelength dependence (error s.d.)
12	$0.65 \pm 0.12$
13	$0.58 \pm 0.05$
14	$0.76 \pm 0.12$
15	$0.96 \pm 0.13$
16	$1.08 \pm 0.07$
17	$1.21 \pm 0.07$
18	$1.56 \pm 0.14$

It can be seen that the inverse wavelength dependence of the developing chick cornea shows great variation with developmental day, gradually increasing with developmental day. The values determined at earlier developmental days are however markedly different, almost approaching an effective linear dependence at days 12 and 13. By comparison with the swollen human corneas, it can be seen by comparison of tables 5.1 and 5.2 that corneas at developmental stages E16-E17 are similar to the dependence of peripheral cornea. Stage E18 most closely matches that of the central corneal portions. During the developmental period investigated in table 5.2, interfibrillar spacing decreases as the fibrils subsume into an orderly array, from an

## **Chapter 5**

arrangement consisting of bundles of collagen, essentially analogous to the lakes present in swollen corneas (Hay and Revel, 1969; Connon et al., 2004). This reinforces the hypothesis suggested earlier that this very low inverse wavelength dependence is caused by scattering from large voids and distinct bundles of collagen, and that the wavelength dependence is in turn dictated by the geometry of these complexes.

In conclusion, the results of this chapter show that corneal thickness in the peripheral regions increases at a slower rate when the cornea undergoes oedema, in comparison with the central cornea. This leads to a slightly more uniform transmission across the central zone of swollen human cornea than is found in the physiologically hydrated cornea. A change in wavelength dependence occurs in the peripheral regions, which can be explained qualitatively by larger fibril free voids forming in this region.

## Chapter 6. Infrared absorption in the cornea

In previous chapters, this work has investigated various aspects of visible light (400 - 800nm) propagation through corneal stroma. In this wavelength region, light scattering is the principle cause of attenuation of the incident beam. In the infrared portion of the spectrum (0.8 – 1000 $\mu$ m), attenuation is caused primarily by absorption, i.e. the removal of certain incident wavelengths and the conversion of the energy into some other form. This chapter seeks to determine whether absorption in the infrared can be correlated with the corneal hydration state in a straightforward way, by exploiting the infrared absorption properties of liquid water.

### 6.1 Introduction

Up to this point this work has focused primarily on the influence of nanoscale protein structure on electromagnetic propagation. At this juncture, it is worth repeating that the cornea, is primarily composed of water which constitutes some 78% of the corneal mass in the physiological condition (Scott and Bosworth, 1990). It is this hydrated fraction, and how it can be investigated using infrared absorption, that will figure most prominently in this chapter.

Despite there being very little data available on the infrared transmission of the corneal stroma (Kenshalo, 1960; Boettner, 1962; van den Berg and Spekrijse, 1997), infrared transmission is of interest for several reasons. It is interesting to those who investigate light losses in the cornea as an example of an absorptive loss mechanism rather than a scattering mechanism. It is also pertinent to those who wish to evaluate thermal damage pathways, particularly with reference to the use of infrared lasers in eye surgery.

Most investigators of transmission properties of ocular media in the infrared have generally concluded that it may be best modelled by the spectrum of a layer of liquid water of uniform thickness. The infrared transmission of all the ocular media are generally dominated by strong water absorption bands in the near infrared. Transmission in the infrared appears to be independent of age (Boettner, 1962). Some



authors have suggested that data on water absorbance in the infrared is actually more accurate for modelling the interaction of infrared wavelengths with cornea than much of the extant data on ocular media (van den Berg and Spekreijse, 1997). Data obtained from the absorbance of liquid water may be useful to roughly determine the magnitude of transmission at a given wavelength, but will be insufficient to those seeking to elucidate damage mechanisms, for example through the effects of infrared lasers. Analysis of past work has suggested that there is a contribution from non-water components detectable in the measured spectra (van den Berg and Spekreijse, 1997).

In general it is shown that the cornea is highly transparent in much of the red/near infrared portion of the spectrum. The first absorption occurs at 1400nm, which represents an OH stretch overtone. There are deviations present in the spectrum of the cornea from that which would be found in the equivalent layer of liquid water. These cannot be explained purely on the basis of a small reduction in water path length to account for the finite water content (van den Berg and Spekreijse, 1997).

Since the non-stromal layers of the cornea are vanishingly thin it is reasonable to assume that this extra contributory term has its origin in the infrared active features of the collagen molecule, which have been deduced and theoretically analysed previously (Doyle, Bendit and Blout, 1975). The collagen molecule possesses the usual absorption bands that would be expected from a protein molecule. The spectrum of thin sections of corneal stroma (~20 $\mu$ m) have shown that it is compatible with that of collagen (Jayasuriya et al., 2003). Bulk tissue will be the focus of this work.

The question asked in this chapter is whether there is any correlation between corneal hydration state and infrared transmittivity. In the visible wavelength region, light propagation is dependent on hydration state, with an optimum being achieved at the physiological hydration. However, this change in transmitted flux is the result of modification of various ultrastructural parameters, such as fibril ordering and refractive index ratio between the ground substance and the collagen fibrils (Meek et al., 2003b). In the infrared region it is reasonable to suggest that changes in transmission with hydration will occur primarily due to changes in the amount of primary absorbent (i.e. water) present. It is well known that an increase in hydration

level as the cornea experiences oedema is accompanied by an increase in thickness, and that this relationship is linear (Hedbys and Mishima, 1966). This suggests that a reproducible correlation should be found between hydration and transmitted intensity. It is of note that there is already a well known correlation between the infrared spectra of skin and its hydration state (Sowa, Payette and Mantsch, 1999).

### 6.2 Methods

General methods may be found in chapter 2.

#### 6.2.1 Tissue Preparation and swelling experiment

Four bovine corneas were obtained fresh from a local abattoir within hours of death. Upon receipt at the laboratory, the epithelial cell layer was removed with an appropriate blade, taking care not to damage the stromal surface. The corneas were then excised by scalpel at the limbus. The endothelial cell layer was removed with the aid of laboratory blotting paper.

Post-mortem corneas are subject to oedema. These experiments used a physiological hydration as a starting point. It was therefore necessary to de-swell the corneas. This was achieved by the use of dialysis in a 4.45% solution of polyethylene glycol, in 0.154M NaCl and Hepes buffer solution. The exact methodology is outlined elsewhere (Kostyuk et al., 2002). The corneas were equilibrated in these solutions for approximately 24 hours. For use in the FTIR spectrometer, corneal biopsy buttons of 12mm diameter were used. These were mounted between two mylar substrates (0.9 $\mu$ m thickness) to secure the cornea and to prevent desiccation during the course of our experiments.

Initial readings were taken through the centre of the cornea, at a physiological hydration. The corneas were then permitted to swell in 0.154M NaCl solution for 15 minute intervals, at the end of which FTIR measurements were again taken. A 1 hour swelling interval was permitted. Wet weights were taken prior to all readings.

At the end of each experimental set, the corneal biopsies were placed in an oven and heated at 60°C for at least 48 hours. The dry weight was then measured and hydration is calculated from by calculating the quantity (wet weight – dry weight) / dry weight), as in previous chapters.

### 6.2.2 Fourier Transform Infrared Spectroscopy

Fourier transform infrared (FTIR) spectroscopy was performed on bovine cornea prepared as described in 2.1. The FTIR spectrometer used was a commercial *Bomem DA8*, configured with a KBr beamsplitter, cooled MCT (mercury cadmium telluride) or pyroelectric detector, and Globar source. Broad-band spectra were therefore taken from 4000-6000 $\text{cm}^{-1}$ , with medium resolution (4.7 $\text{cm}^{-1}$ ) and good signal to noise ratio.

Corneal samples in their Mylar holders were placed within the evacuated sample chamber of the FTIR spectrometer and these spectra were ratioed against 'backgrounds' of the Mylar alone.

### 6.2.3 Analysis of experimental measurements

Experimental results were analysed in Excel 2003 (Microsoft). After examination of the results, a wavenumber of 4500 $\text{cm}^{-1}$  (2.22 $\mu\text{m}$ ) was chosen as a point for the analysis. The intensity at this point was recorded and compared with the calculated hydration level. This point was chosen for favourable signal to noise ratio.

## 6.3 Results

### 6.3.1 Theoretical considerations

Prior to reviewing our experimental results, it is pertinent to investigate the spectrum of an equivalent layer of liquid water, and compare this with that of a bovine cornea. We do this by reference to equation 6.1.

Eq 6.1

$$I = \exp(-\alpha l)$$

To calculate the transmittivity of a layer of liquid water we need to know the absorption coefficient ( $\alpha$ ) for appropriate sampling frequencies within our range of interest. Here, we take the optical path length as  $800\mu\text{m}$ , equivalent to a bovine cornea near to physiological hydration. The appropriate data is obtained from the literature (Wieliczka, 1989; Kou, 1993).

By reference to equation 6.1, the spectrum is computed for the wavenumber range  $3500\text{-}6600\text{cm}^{-1}$ , shown in fig. 6.2.

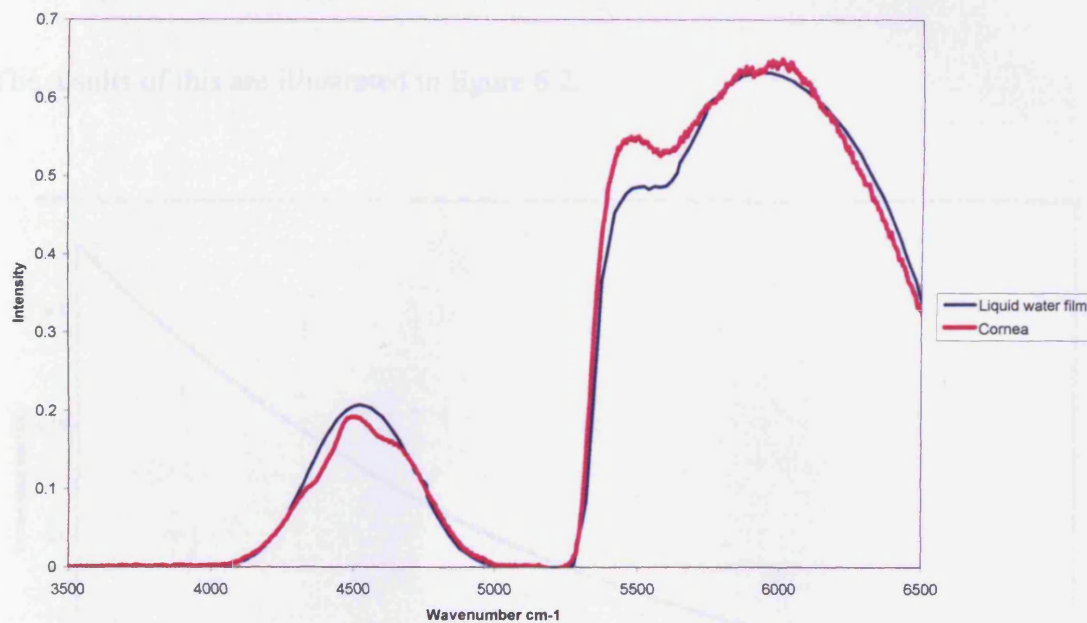


Figure 6.1. Infrared transmission of the cornea versus that of an equivalent path length of pure liquid water

It can be seen from fig. 6.1 that the water model is satisfactory, with certain perturbations from the expected form. It must be remembered that the absorption coefficients used in this work have been calculated for pure water films, whereas the water molecules present in the cornea are affected by the ionic content of the stroma and by hydrogen bonding to the collagenous matrix (Jayasuriya et al., 2003). It is

reasonable to suggest that the region around  $4500\text{cm}^{-1}$  may be affected by overtones from the protein vibrational features in the  $2200\text{cm}^{-1}$  region.

It is also informative to model the relationship between hydration state and intensity with the aid of equation 6.1. From the cornea readings (pink line) shown in fig. 6.1, an absorption coefficient of  $2.21\text{mm}^{-1}$  is calculated at  $4500\text{cm}^{-1}$ . Using the formulae of Hedbys (Hedbys and Mishima, 1966) relating corneal thickness and hydration in the bovine cornea (equation 6.2) we can calculate the theoretical thickness for certain hydration levels, and thence use eq. 6.1 to calculate theoretical transmission.

Eq 6.2

$$\Delta = \frac{H + 0.67}{5.3}$$

The results of this are illustrated in figure 6.2.

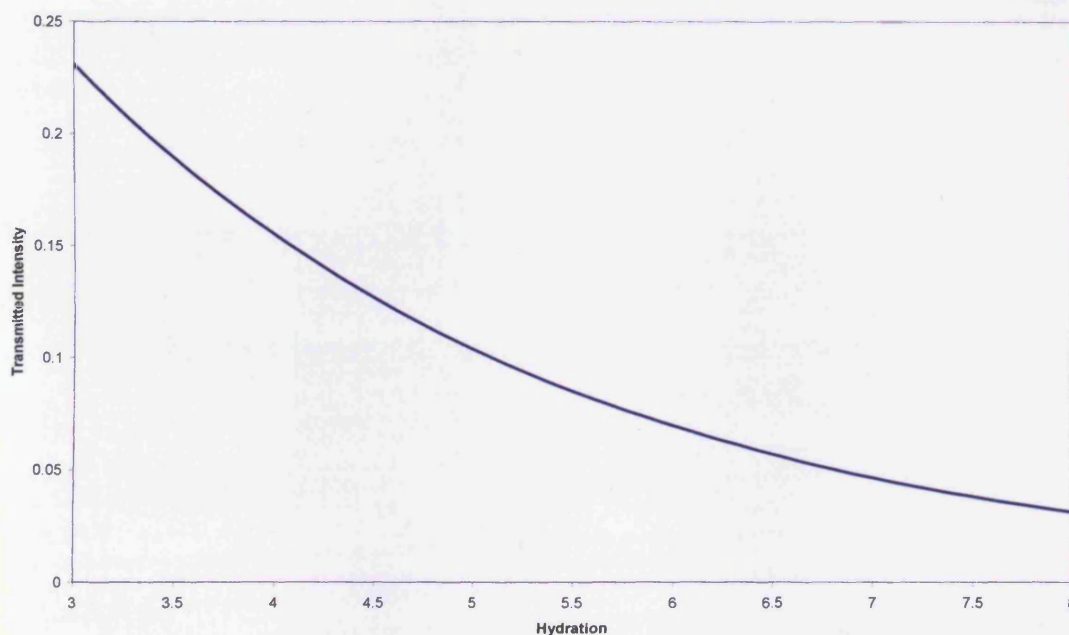


Figure 6.2 Theoretical decreases in transmission (at  $4500\text{cm}^{-1}$ ) with increase in corneal hydration values (exponential fit line)

Using this methodology, we obtain an exponential relationship between corneal hydration and transmitted flux, as should be expected from first principles. The actual transmission values obtained by experiment can now be investigated.

### 6.3.2 Corneal transmittance

The results of the swelling experiment outlined in section 2.1 are presented in table 6.1, and in figures 6.3 and 6.4. Intensity was measured from the IR peak near  $4500\text{cm}^{-1}$  (Figure 6.3). Due to individual variation in collagen mass between animals, there is variation in the hydration start point. Machine failure prevented five readings being obtained from one animal (purple squares fig 6.4). Corneal thickness is calculated from the hydration value using Eq 6.2. It is important to note that these calculated thicknesses do not account for any dry weight mass variations between samples.

Table 6.1 Experimental dry/wet weights and intensities

	Time (minutes)	Wet weight (g)	Calculated thickness (mm)	H	Intensity
<b>Cornea 1</b>	0	0.157	0.785	3.49	0.190
	15	0.215	1.096	5.14	0.143
	30	0.252	1.298	6.21	0.082
	45	0.285	1.474	7.14	0.057
	60	0.312	1.619	7.91	0.037
<i>Dry weight</i>	<i>0.0350g</i>				
<b>Cornea 2</b>	30	0.1870	1.162	5.49	0.117
	45	0.2098	1.311	6.28	0.103
	60	0.2296	1.442	6.97	0.062
<i>Dry weight</i>	<i>0.0288g</i>				
<b>Cornea 3</b>	0	0.1263	0.468	3.15	0.210
	15	0.1585	0.921	4.21	0.139
	30	0.1910	1.123	5.28	0.111
	45	0.2127	1.258	6.00	0.101
	60	0.2554	1.523	7.40	0.060
<i>Dry weight</i>	<i>0.0304g</i>				
<b>Cornea 4</b>	0	0.1762	0.983	4.54	0.159
	15	0.1908	1.070	5.00	0.147
	30	0.2115	1.192	5.65	0.122
	45	0.2194	1.240	5.90	0.111
	60	0.2353	1.334	6.40	0.098
<i>Dry weight</i>	<i>0.0318g</i>				



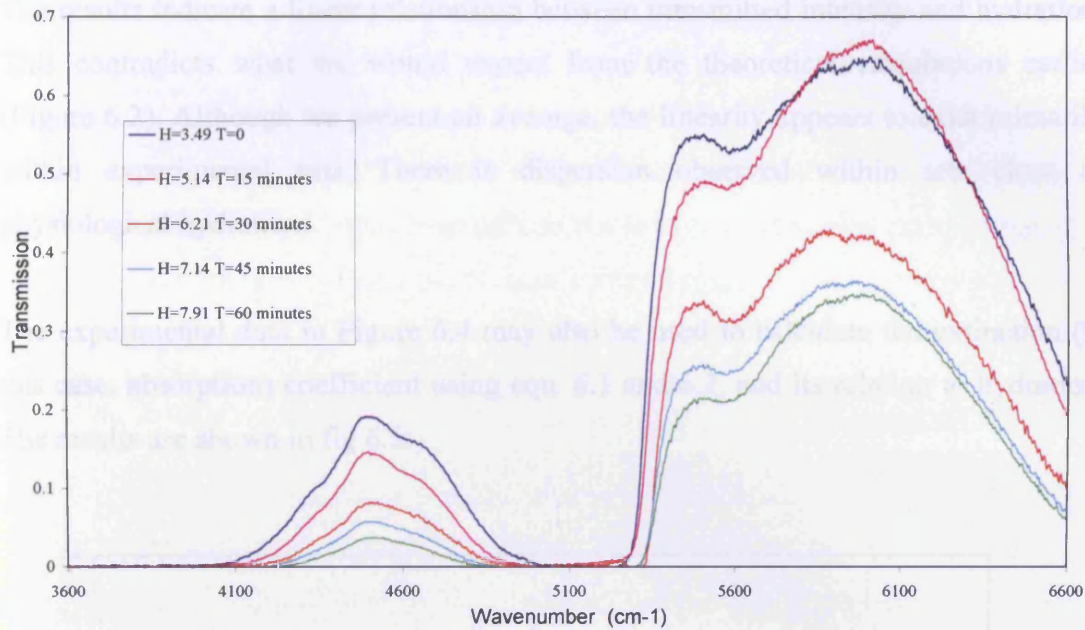


Figure 6.3 Transmitted Intensity in the Mid Infrared with increasing hydration (H) for one cornea (shown as blue diamonds in figure 6.4)

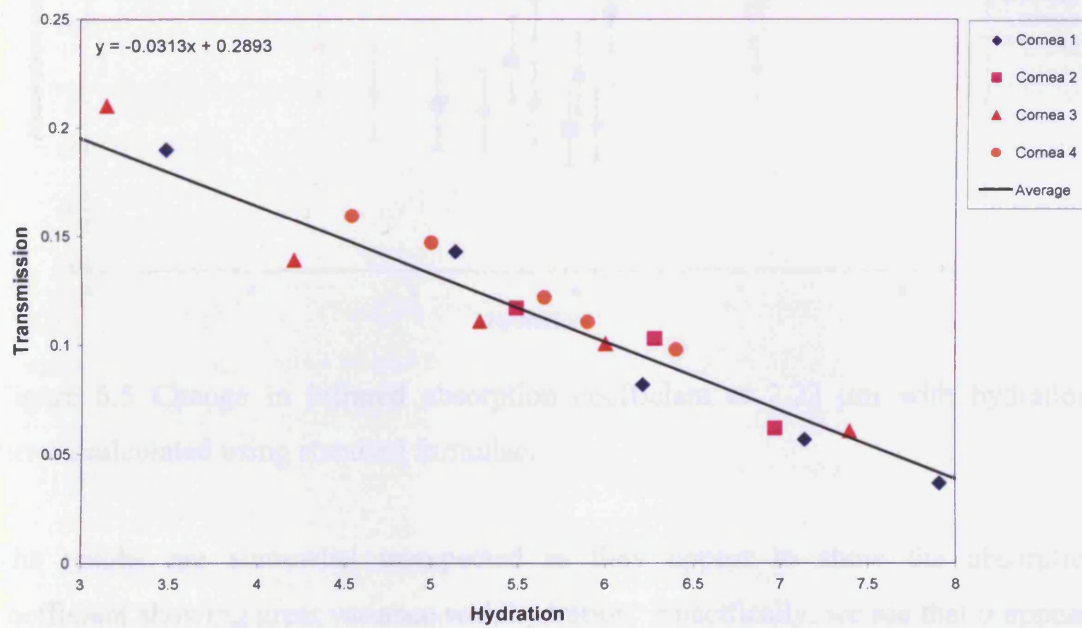


Fig. 6.4 Transmitted intensity at  $4500\text{cm}^{-1}$  ( $2.22\mu\text{m}$ ) against hydration, with average (bold line). Average  $R^2$  value is 0.914, equation of average fit line shown.



The results indicate a linear relationship between transmitted intensity and hydration. This contradicts what we would expect from the theoretical calculations earlier (Figure 6.2). Although we present an average, the linearity appears to exist primarily within experimental sets. There is dispersion observed within sets close to physiological hydration.

The experimental data in Figure 6.4 may also be used to calculate the extinction (in this case, absorption) coefficient using eqn. 6.1 and 6.2, and its relation to hydration. The results are shown in fig 6.5.

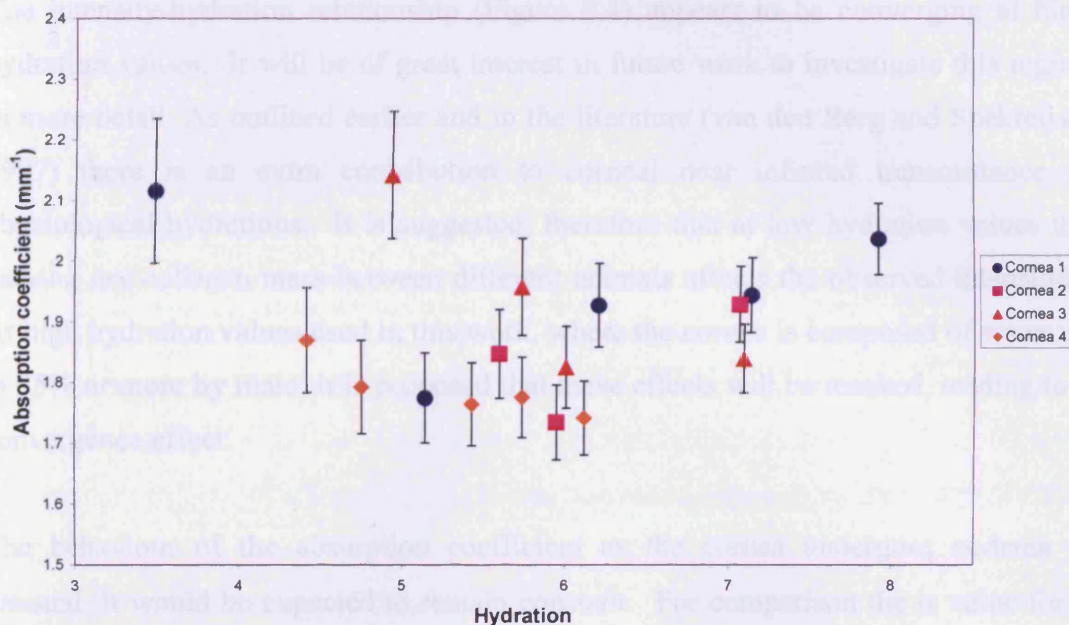


Figure 6.5 Change in infrared absorption coefficient at 2.22  $\mu\text{m}$  with hydration. Errors calculated using standard formulae.

The results are somewhat unexpected as they appear to show the absorption coefficient showing great variance with hydration. Specifically, we see that  $\alpha$  appears to decrease under small increases in hydration, gradually increasing back towards the value we see at physiological hydrations. Analysis suggests that the relation between absorption coefficient and hydration can be approximated to a quadratic fit line when an average of all the data sets is taken (a squared fit line gives an  $R^2$  value of 0.64).

## 6.4 Discussion

This investigation set out to determine whether there was a straightforward relationship between corneal hydration and transmission in the infrared portion of the spectrum. Specifically, it was observed that the Intensity-Hydration relationship of at least the  $4000\text{-}5000\text{cm}^{-1}$  region of the near infrared spectrum of the cornea is linear. This does not fit the theoretical deductions outlined in section 6.3.1, which based on the assumption that the absorption coefficient has a constant value of  $2.21\text{mm}^{-1}$  at  $4500\text{ cm}^{-1}$  regardless of hydration.

The intensity-hydration relationship (Figure 6.4) appears to be converging at high hydration values. It will be of great interest in future work to investigate this region in more detail. As outlined earlier and in the literature (van den Berg and Spekreijse, 1997) there is an extra contribution to corneal near infrared transmittance at physiological hydrations. It is suggested; therefore that at low hydration values the varying dry collagen mass between different animals affects the observed intensities. At high hydration values used in this work, where the cornea is composed of water up to 85% or more by mass, it is proposed that these effects will be masked, leading to a convergence effect.

The behaviour of the absorption coefficient as the cornea undergoes oedema is unusual. It would be expected to remain constant. For comparison the  $\alpha$  value for a film of pure liquid water at  $4500\text{cm}^{-1}$  is  $2.013\text{mm}^{-1}$  (Kou, 1993). If the absorption coefficient for cornea does vary, intuitively, as the hydration increases, it should continuously increase and approach that of liquid water (compare this with the situation where the refractive index of the corneal ground substance approaches that of liquid water under oedema). There are a number of possible explanations why this does not appear to occur:

1. The formulae of Hedbys used to derive thickness from hydration for the central cornea is incorrect
2. There may be some change in the properties of water molecules in the cornea at certain hydration states

It must be noted that this effect has been observed in all data-sets and in intensities obtained from two separate detectors. If the formula of Hedbys is not correctly predicting thickness of the central cornea in relation to its hydration, the absorption coefficient we calculate will be shown to vary as an incorrect thickness value will be used in its calculation. However, it is necessary to note that the work of Hedbys utilised a large sample set with excellent statistical correlation in all species analysed (human, cow and rabbit). There are also theoretical considerations which point towards a linear relation between hydration and thickness based on arguments on the unidirectional action of swelling and the relation of this to stromal volume. It was also noted by linear regression that the point at which the corneal thickness is shown to converge occurs at approximately the same H value for all species tested (Hedbys and Mishima, 1966).

It is known from the literature that the infrared absorption coefficient of cornea and cartilage shows variance with temperature. Specifically, it is shown that the absorption coefficient decreases above 50°C (Sobol et al., 2003). There is no evidence of abnormal behaviour below this point. The samples are not able to heat to this temperature within the spectrometer. Of course, in the visible spectrum scattering increases drastically due to the presence of lakes, as fluctuations in fibril number density approach similar length scales to that of visible light. Whether a similar effect could be occurring here is difficult to evaluate; the wavelength dependence cannot be reliably estimated at the wavelengths used here due to absorption. It is likely here that the wavelength used is sufficiently long to avoid the effects of Mie scattering from lakes except at very high hydrations.

From a molecular perspective, there are certain observations from chemical studies (mainly conducted with the aid of magnetic resonance) of collagen water interactions which may prove useful in suggesting potential explanations for changes in absorption coefficient. It has been determined that in tendon (a tissue containing collagen and proteoglycans) there are three distinct populations of water molecules present; a fraction tightly bound to the collagen triple helix; a second fraction which can be regarded as being present within fibrils, and a third fraction contained within the ground substance (Peto, Gillis and Henri, 1990). There is known to be a change in molecular dynamics of proteoglycans and collagen as their hydration is varied, in the

sense that the returned NMR signals suggest that the proteins gain mobility as they are surrounded by more water molecules (Huster, Schiller and Arnold, 2002; Reichert et al., 2004).

In order for the linear relation between transmission and hydration to be exploited it would first be necessary to apply some form of normalisation to negate variance between sets. It is possible to achieve this by applying a methodology similar to that used by Kostyuk et al (2003) to normalise visible light transmission through cornea for small inter-sample variations in stromal thickness (i.e. mass variations).

Firstly it is necessary to reassert the observation that hydration and thickness have a linear relationship. Unfortunately the apparent variance in absorption coefficient would appear to exclude directly using thickness as a means of normalisation. However, as stated earlier there is a known interplay between the dry mass of the cornea and the overall size of the animal; this therefore begs the question as to whether it is possible to correct the infrared measurements obtained earlier to some standard dry mass.

First, the well known relationship between hydration ( $H$ ), wet weight ( $w_w$ ) and dry weight ( $w_d$ ) is restated. Here overbars are used to signify that these values are relative to averages derived from corneas used in this chapter.

Eq. 6.3

$$\overline{H} = \frac{\overline{w_w} - \overline{w_d}}{\overline{w_d}}$$

This can be easily rearranged to give

Eq 6.4

$$\overline{w_w} = \overline{H} \overline{w_d} + \overline{w_d}$$

Equation 6.4 can be immediately recognised as an equation of a straight line. The result is intuitive since it reveals that the corneal weight will equal the corneal dry weight at a hydration of zero. The average dry weight for the ensemble of corneas is 0.0318g.

Since we have shown there is a relationship between transmission and hydration, equation 6.4 would indicate a relationship between wet weight and transmission, shown below in figure 6.6.

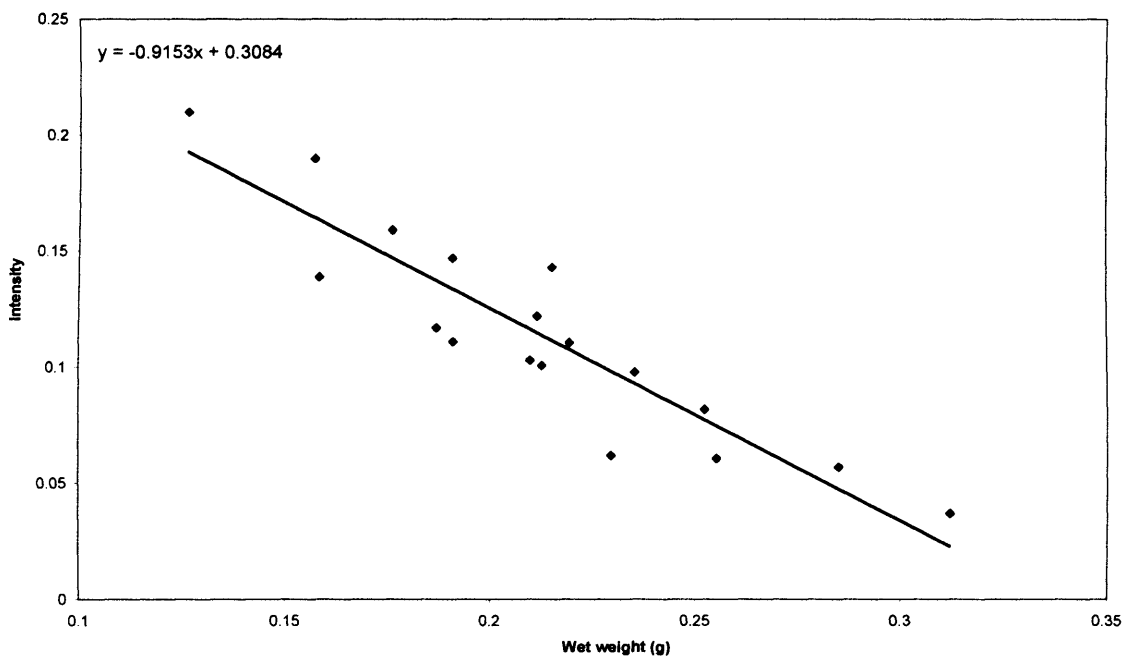


Figure 6.6 Relation between wet weight and infrared transmission (at 4500cm<sup>-1</sup>). Equation of average fit line (black) shown.

As can be seen from figure 6.6, wet weight and transmission are directly proportional. Specifically it is determined that a line of best fit with the following equation can be fitted to the data from an ensemble of 4 corneas:

Eq. 6.5

$$\overline{w_w} = 0.3161 - 0.9102I_\eta$$

Here,  $I_{\eta}$  is the intensity at  $4500\text{cm}^{-1}$ . By substituting equation 6.4 in eqn. 6.5 and rearranging the following result is obtained:

Eq 6.6

$$\bar{H} = \frac{0.2843 - 0.9102I_{\eta}}{0.0318}$$

This equation can be used to normalise the intensities obtained at  $4500\text{cm}^{-1}$  to an average hydration value based on the size of the calibration ensemble used. Figure 6.7 is produced by using all values of intensity obtained in this chapter to give the normalised hydration value.

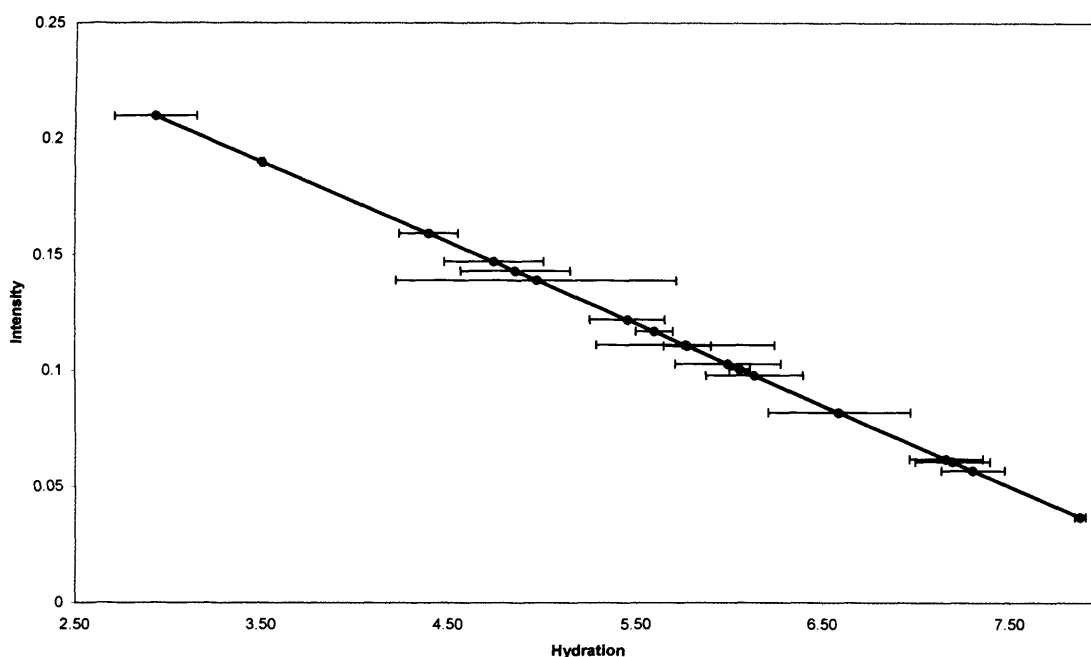


Figure 6.7 Normalised hydration values

The error bars in figure 6.7 show the difference between the actual hydration obtained by the desiccation method and using normalising equation 6.6. The average degree of variance from the 'true' (weight measured) hydration is  $0.23 \pm 0.18$ . This certainly gives a reasonable tolerance. Dispersion of normalised results from the true value appears to be higher in a central range, which appears to correspond with the range

across which the absorption coefficient shows most variation (compare figure 6.7 with 6.6).

This method could be easily utilised as a hydration monitoring system for corneas; it could easily be used for analysing research tissue and in eye banking systems. One common clinical method of determining hydration is to use ultrasound pachymetry to analyse tissue thickness and then use the known formulae to convert this into hydration (Hedbys and Mishima, 1966). The method here has the advantage that it requires no tissue contact, a factor clearly desirable for eye bank operations where corneas are required to be handled under aseptic technique. It is possible this method could be integrated into microscopy, for example.

Raman spectroscopy has also been suggested as a method for determining corneal hydration. This method would be most useful for determining the axial distribution of corneal hydration through the thickness of the tissue and analysing molecular level changes; it would be less useful to gauge the gross hydration through the tissue. Dielectric spectroscopy is also somewhat sensitive to corneal hydration (Oltrup et al., 1999) although it is more sensitive to changes at hydrations far below the physiological. Plasma emission spectra also appear to correlate with corneal water content. It is notable that laser based techniques such as Raman spectroscopy and plasma emission have safety restrictions which may be incompatible with obtaining effective signal to noise ratio in use outside research settings.

## **Chapter 7. Spectroscopic and swelling studies of corneas cross-linked with Riboflavin-Ultraviolet A (UVA)**

This chapter will focus on the use of spectrophotometry to study riboflavin Ultraviolet-A mediated collagen cross-linking. This is a novel and relatively new technique used to retard the progress of keratoconus, a structural disorder of the cornea which causes substantial distortion to vision and is one of the leading causes for keratoplasty (corneal transplant). This chapter investigates two themes; can the degree of riboflavin penetration be subjectively measured using visible spectroscopy, and can any conclusions be drawn as to the cross-linking mechanism by investigating the swelling properties of treated corneas in free solution.

### **7.1 Introduction**

Keratoconus is a degenerative disorder of the corneal stroma in which the cornea becomes much thinner due to changes at the ultrastructural level. The disease is typically first diagnosed when sufferers reach their late teenage years and results in progressive increases in optical aberrations as the cornea ‘bulges’ centrally (ectasia) as a result of the pressure exerted from within the eye, as shown below in figure 7.1. The keratoconic cornea lacks the mechanical strength of the normal cornea. There are a number of treatments available, including specialised contact lenses, intracorneal rings and keratoplasty, which is ultimately indicated in roughly a quarter of all keratoconus cases. Recently, a promising new technique, which aims to tackle the underlying nanostructural causes of keratoconus head on has been piloted which has met with considerable success and is apparently sustainable over the long-term.





Figure 7.1 Human eye affected by keratoconus

(<http://en.wikivisual.com/index.php/Image:Keratoconus1-800.jpg>; accessed October 2008)

It has been noted that keratoconic corneas have significantly different elastic modulus from that found in normal corneas (Andreassen, Simonsen and Oxlund, 1980; Nash, Greene and Foster, 1982). From a structural perspective, it has been observed that although interfibrillar spacings are invariant between normal and keratoconic corneas, there is a significant change in collagen molecular spacing (Fullwood et al., 1992); there are also variations in fibril orientations and mass distribution of collagen (Hayes et. al. 2007). This therefore begs the question of whether the progression of keratoconus can be arrested by modifying the mechanical properties of the tissue. One way of achieving this in collagenous tissue is the induction of structural cross-links. The concept of cross-linking is well known in the field of polymer chemistry. They can take the form of ionic or covalent molecular links between the chains which make up such a structure. Liquid polymers for example can be reconstituted as solids or gels. This has the effect of reducing molecular mobility within the structure. Cross-links are induced by chemical reaction. There are a number of mechanisms for initiating these reactions. One example would be through exposure to aldehydes such as glutaraldehyde and formaldehyde; glutaraldehyde is particularly efficient due to its ability to form cross-links of varying length between different parts of the protein chains, although it has a somewhat slow penetration into tissues. Cross-linking reactions can also be induced using high energy radiation, for example exposure to ultraviolet wavelengths or electron beams. It has previously been determined that UV

light alone, operated at a wavelength of 254nm, is not sufficient to induce statistically significant cross-linking measured as a function of corneal stiffness (Spoerl, Huhle and Seiler, 1998), possibly due to extensive scattering at this wavelength range causing a low penetration depth into the tissue.

It is worth noting that the number of cross-links in corneal tissue is thought, in general to naturally increase during the aging process; additionally extra collagen cross-links are known to be associated with diabetes (Malik et al., 1992; Hadley, Meek and Malik, 1998).

There are three principal methods by which collagens have been cross-linked:

1. Exposure to ultraviolet/blue wavelengths, with and without photosensitisers
2. Using conventional fixative agents
3. Non-enzymatic glycation, the process by which sugar molecules are bonded to a protein (Malik et al., 1992)

The use of a photosensitiser permits a wider range of wavelengths to be used to induce the cross-linkage effect; the photosensitiser compound acts as an intermediary, converting some of the energy from the incident wavelengths into a form which can be utilised by the reaction. Such molecules should induce little or no immunological or toxic response in tissue, and be pharmacologically stable. Generally, agents possessing absorptions in the red end of the visible spectrum are preferred for many uses since these wavelengths have a greater penetration into tissue (as discussed in previous chapters). This issue is not as pressing in the cornea which is obviously, by design, transparent.

One such molecule is riboflavin, a compound which has an absorption spectrum such that it contains absorptions in the visible (blue) and near ultraviolet spectral portions (Moffatt et al., 1980). Specifically, riboflavin is found to possess strong absorption bands at 450nm, 370nm, 265nm and 220nm. This compound is thought to induce cross-linking in collagen by participating in a photo-oxidation reaction; under the influence of UV/blue light, a free radical of oxygen is generated, which then acts to induce molecular cross-links between collagen molecules. This reaction has been

induced in cornea using UV-A (370nm) and blue (450nm) wavelengths; presumably the effects of scattering would be more significant at the shorter wavelengths. Cross-linking of lens crystallin proteins is thought to occur using the same mechanism (Krishna et al., 1991) and leads to the yellowing discoloration observed in the ageing lens.

### **7.1.2 Clinical effects of Riboflavin/UV-A cross-linking on corneal stroma**

The Riboflavin/UV-A procedure is always performed with a local anaesthetic (e.g. lidocaine), prior to removal of the epithelial cell layer. After epithelial debridement a solution of riboflavin and dextran is applied to the corneal surface. The dextran component is used to prevent swelling of the corneal tissue during application of the riboflavin solution. UV-A irradiation is then applied at 370nm and the whole procedure takes about 35 minutes. The initial clinical study was pioneered by Wollensak (2003) who determined that all treated eyes showed no further keratoconic progression, and that certain corneas even showed a certain amount of regression (Wollensak, Spoerl and Seiler, 2003a).

The effects of the treatment are found to vary quite substantially with depth through the corneal tissue. Specifically, the treatment is found to have greatest effect on the anterior segment of the cornea. Biomechanical testing of corneal stress-strain has demonstrated that there is a maximal increase in corneal rigidity only in the first 300µm of the corneal stroma (Wollensak, Spoerl and Seiler, 2003b). This is also supported by the observation that collagen fibril diameter appears to be significantly increased in the corneas treated using this method, particularly in the anterior segment (Wollensak et al., 2004). There are case reports in the literature of stromal hazing resulting from riboflavin-UVA cross-linking. This is seemingly associated, by confocal microscopy, with a stromal scar component. This effect did not appear to alter visual acuity, however (Mazzotta et al., 2007). This effect appears to occur in cross-linked corneas which were previously in an advanced state of keratoconus.

The long-term efficacy of this treatment is somewhat unknown at present. Clinical trials are at this time still in progress; bearing in mind that collagen turnover in the

cornea takes place on timescales of the order of 3 years, it is considered possible that repeat treatments may have to be provided at future time points (Wollensak et al., 2003a). However, some recent research has suggested that the mechanical strength of rabbit corneas subjected to cross-linking does in fact increase with time post-treatment (Wollensak and Iomdina, 2008). Studies on human corneas cross-linked over three years previously also suggest that the procedure results in long-term stabilisation (Raiskup-Wolf et al., 2008).

The ultraviolet wavelength used (370nm) does have the potential to induce deleterious effects on keratocytes, corneal endothelial cells, the lens, and the retina. The riboflavin does however act to absorb a good deal of the energy. However, the procedure has been shown to induce apoptosis in keratocyte cells in the anterior segment of the cornea; these effects occur up to a depth of about 350µm from the front surface of the cornea. These segments of the cornea appear to be repopulated from the posterior, untreated, segment, with near-complete repopulation after about six months (Mazzotta et al., 2007b). Some have, however, suggested that the apoptosis induced may be a useful effect for those seeking to minimise or eliminate immunological reactions from donor corneas in keratoplasty, and that endothelial UV damage may be reduced by altering beam flux (Wang, 2008). Ultraviolet-A exposures are below the known damage thresholds for corneal tissue, although to ensure safety it is recommended that a corneal thickness of below 400µm be regarded as a contraindication (Spoerl et al., 2007).

In addition, it has been suggested that cross-linking treatment can, indirectly, lead to errors in intraocular pressure measurement. Conventional tonometry equipment is operated using standard values for rigidity or elasticity. These values are fundamentally altered by the nature of collagen cross-linking which changes the biomechanical properties of cornea. This appears to cause an overestimation in the value of intraocular pressure (Romppainen et al., 2007).

The use of the cross-linking technique is not limited to the control of keratoconus; it has also been utilised in corneal melting processes, where such processes fail to

respond to more conventional treatment methodologies (Iseli et al., 2008). It has also been indicated in keratectasia as result of LASIK (Hafezi et al., 2007).

At this juncture, it should be noted that in spite of the clinical literature on the subject demonstrating changes in corneal biomechanics, there is little written on the biochemical or biophysical aspects of the treatment. It is known by electron microscopy that the collagen fibrils appear to undergo a modest (12%) increase in diameter, presumably as the collagen molecules increase their cross-section under cross-linking (Wollensak et al., 2004), particularly in the anterior segment. Biochemical analysis by gel electrophoresis has shown that cross-linked corneas by the riboflavin-UVA method have an intense polymer band of molecular weight of 1000 kDa resistant to most denaturation methods (Wollensak and Redl, 2008).

There are two factors affecting the clinical outcome of this treatment that this chapter will address:

1. Can the diffusion of the riboflavin molecule through the tissue, from anterior to posterior, be determined with the aid of visible spectrophotometry?
2. Is there a significant difference in the rate of swelling between treated and untreated corneas?

With regards to the first point, it is known from the literature that the cross-linking effect occurs in the anterior segment, as discussed earlier. In light of the known changes in fibrillar packing between anterior and posterior segments (Freund et al., 1995) it will be of interest to determine whether riboflavin molecules do in fact reach the posterior segment.

The swelling properties of cross-linked corneas have been sparsely studied. It is known from the literature that swelling properties can be a good indicator of the type and degree of cross-linking present within a collagenous sample (Charulatha and Rajaram, 2003). Previous studies on cross-linked porcine cornea have suggested that the procedure reduces the swelling ability of the anterior segment of the cornea (Wollensak et al., 2007).

## **7.2 Methods**

### **7.2.1 Preparation of corneas**

Porcine corneas were obtained from the abattoir and transported on ice within 24 hours of death. The cornea of each eye was examined and any with visible corneal defect were not used for this experiment. After this was done, ultrasound pachymetry (Pachette 2, DGH) was performed on the central cornea – post mortem it is inevitable that there will be a degree of swelling present in the tissue. The standard thickness of the porcine cornea has been shown to be approximately 900 $\mu\text{m}$  (Scott and Bosworth, 1990). Although all corneas had swollen above this level, a random sample of eight corneas in which central thickness did not exceed 1050 $\mu\text{m}$  was selected.

Twelve human corneas were obtained from the UK Transplant Service Bristol and Manchester eye banks and stored under organ culture in DMEM (Dulbecco's Modified Eagle Medium) medium until needed.

Porcine and human tissue were dissected according to protocols outlined in the general methods section 2.1.

### **7.2.2 Cross-linking of corneas**

Four porcine corneas and three human corneas were selected for UVA-riboflavin cross-linking. The corneal epithelium was removed with the aid of a scalpel blade and riboflavin drops were added. After 5 minutes the corneas were exposed to a 3mW cm<sup>-2</sup> dose of Ultraviolet-A at a wavelength of 370nm using a laser diode source (UV-X, IROC AG, Zurich) aimed at the anterior surface of the cornea. Dosage was checked with an ultraviolet photometer. Riboflavin drops were then applied to the cornea at 5 minute intervals for a period of 30 minutes. Riboflavin drops were composed of 10mg riboflavin-5-phosphate in 10mL of 20% dextran T-500. The basic experimental set up is shown in figure 7.2.



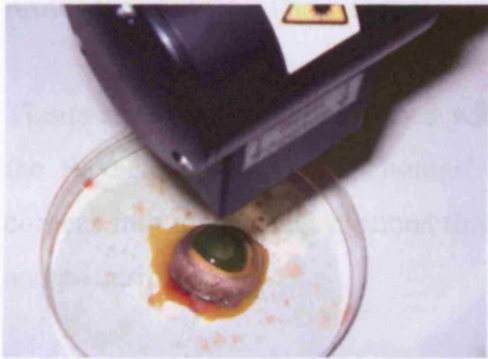


Figure 7.2 Experimental set up for riboflavin-UVA cross-linking of porcine cornea, showing whole porcine eye in Petri dish with UVA diode source placed above.

### 7.2.3 Swelling studies of cross-linked corneas

The swelling study was performed on porcine corneas. Corneal buttons were excised using an 8.5mm trephine. Treated and untreated (n=4 in each group) corneas were placed in 0.9% sodium chloride solution and permitted to undergo swelling. An initial wet weight was taken of each sample prior to immersion in the saline solution; wet weights were then taken at 10 minute intervals for 1 hour. Time intervals were lengthened after this point, with the final reading being taken at 360 minutes. Samples were then dried at 60°C for 48 hours at which point the dry weight was taken. Hydration was then calculated by noting that it can be calculated from the ratio of the difference between wet and dry weights to dry weight.

### 7.2.4 Spectrophotometric studies of riboflavin penetration

The purpose of this study was to investigate the amount of riboflavin diffusion through different portions of the corneal stroma under a standard clinical protocol. The corneas in the riboflavin cross-linked group (n=6) were treated using the protocol outlined above in section 6.2.2. Of this group, three were treated and then sectioned. The corneas were debrided of the epithelial cell layer and placed in Barron artificial anterior chambers (Katena products, Denville, NJ). These were then pressurised using the culture medium in which the samples had been stored. The other three were

## **Chapter 7.**

sectioned first and then treated as individual layers in Petri dishes using the same protocol as before. Three corneas were then used as a control.

Tissue sectioning was performed with an Intralase femtosecond laser (AMO, CA) at the Rayne Institute in St Thomas' Hospital (London). This was used to section corneas into three equal portions through the thickness of the tissue; anterior, middle and posterior.

Sections were then transported in labelled containers under dry ice back to the Cardiff laboratory and stored at  $-70^{\circ}\text{C}$  until they could be analysed by spectrophotometry. This was performed by placing the tissue sections within standard quartz cuvettes in the optical path length of the spectrophotometer (Pye Unicam SP8-100) used for the studies in chapters 4 and 5. As in chapter 4, silicon oil was used as a bathing medium to minimise reflections.

Porcine corneas were studied by utilising the techniques of chapter 4. Porcine corneas were prepared by Dr. K. Samaras of the Rayne Institute. Porcine corneas were placed in the human spectrophotometer cell. A visible light transmission spectrum was then determined through the centre of the cornea.

### **7.3 Results**

#### **7.3.1 Swelling studies on cross-linked corneas**

The results of the swelling experiment conducted on untreated and treated porcine corneas are outlined in table 7.1. This gives the weights recorded as a function of time immersed in the saline swelling solution.



Table 7.1 Wet weights of control and riboflavin-UVA treated corneas as a function of time in swelling solution

Time (minutes)	Control cornea wet weight (g)				Treated cornea wet weight (g)			
	A	B	C	D	E	F	G	H
<b>0</b>	0.0693	0.0735	0.0821	0.0607	0.0688	0.0681	0.0619	0.0615
<b>10</b>	0.083	0.0815	0.0891	0.0725	0.0742	0.0926	0.0700	0.0722
<b>20</b>	0.0862	0.0879	0.093	0.0843	0.0780	0.0846	0.0777	0.0823
<b>30</b>	0.0905	0.0931	0.0965	0.0858	0.0883	0.0877	0.0807	0.0828
<b>40</b>	0.0901	0.1072	0.1027	0.0857	0.0983	0.0930	0.0860	0.0806
<b>50</b>	0.0943	0.1002	0.1028	0.0907	0.0923	0.0923	0.0874	0.0862
<b>60</b>	0.0966	0.1125	0.1111	0.0932	0.0946	0.0939	0.0881	0.0903
<b>75</b>	0.0999	0.1098	0.1144	0.0977	0.1021	0.0985	0.0951	0.0912
<b>100</b>	0.1098	0.1083	0.1174	0.1036	0.1095	0.1052	0.0966	0.098
<b>130</b>	0.1189	0.1144	0.1198	0.1100	0.1210	0.1092	0.1026	0.1045
<b>200</b>	0.1195	0.1280	0.1323	0.1184	0.1208	0.1207	0.1117	0.112
<b>360</b>	0.1372	0.1445	0.1491	0.1339	0.1408	0.1422	0.1308	0.1298
<i>Dry weight (g)</i>	<i>0.0093</i>	<i>0.0087</i>	<i>0.0117</i>	<i>0.0108</i>	<i>0.0116</i>	<i>0.0099</i>	<i>0.0104</i>	<i>0.0085</i>

From this data, the actual hydration can be calculated as a function of swelling time as outlined in section 7.2.4. This is shown in table 7.2.

**Table 7.2** Hydration values of control and riboflavin-UVA treated corneas as a function of time

Time (minutes)	Control corneas hydration (H)				Treated corneas hydration (H)			
	<b>A</b>	<b>B</b>	<b>C</b>	<b>D</b>	<b>E</b>	<b>F</b>	<b>G</b>	<b>H</b>
<b>0</b>	6.5	7.4	6.0	4.6	4.9	5.9	5.0	6.2
<b>10</b>	7.9	8.4	6.6	5.7	5.4	8.4	5.7	7.5
<b>20</b>	8.3	9.1	6.9	6.8	5.7	7.5	6.5	8.7
<b>30</b>	8.7	9.7	7.2	6.9	6.6	7.9	6.8	8.7
<b>40</b>	8.7	11.3	7.8	6.9	7.5	8.4	7.3	8.5
<b>50</b>	9.1	10.5	7.8	7.4	7.0	8.3	7.4	9.1
<b>60</b>	9.4	11.9	8.5	7.6	7.2	8.5	7.5	9.6
<b>75</b>	9.7	11.6	8.8	8.0	7.8	8.9	8.1	9.7
<b>100</b>	10.8	11.4	9.0	8.6	8.4	9.6	8.3	10.5
<b>130</b>	11.8	12.1	9.2	9.2	9.4	10.0	8.9	11.3
<b>200</b>	11.8	13.7	10.3	10.0	9.4	11.2	9.7	12.2
<b>360</b>	13.8	15.6	11.7	11.4	11.1	13.4	11.6	14.3

The average hydration as a function of time for the control and treated corneas is shown in table 7.3.

Table 7.3 Average hydration of treated and untreated corneas (errors are s.d.)

Time (minutes)	Average hydration (H)	
	Control corneas	Treated corneas
0	6.1 ±1.2	5.5 ±0.7
10	7.2 ±1.2	6.7 ±1.4
20	7.8 ±1.1	7.1 ±1.3
30	8.2 ±1.3	7.5 ±1.0
40	8.7 ±1.9	7.9 ±0.6
50	8.7 ±1.4	8.0 ±1.0
60	9.4 ±1.9	8.2 ±1.1
75	9.5 ±1.5	8.7 ±0.9
100	10.0 ±1.4	9.2 ±1.1
130	10.6 ±1.6	9.9 ±1.0
200	11.5 ±1.7	10.6 ±1.3
360	13.1 ±2.0	12.6 ±1.5

The data shown in table 7.3 indicate that hydration increases as a function of time spent in the saline solution, as should be expected. There is however little identifiable difference between hydrations at various time points between control and riboflavin-UVA treated corneas. Although the treated corneas generally have slightly lower average hydration at each time point, the two data sets do fall within the standard deviations of each other. The data can be analysed for statistical significance by utilising the Student t-test. When this is done for both sets of data the t value given by a t-test assuming equal variances is 0.36. This is far above the general threshold limit of 0.05 at which results are generally assumed to be statistically different. The data are represented graphically in figure 7.3.

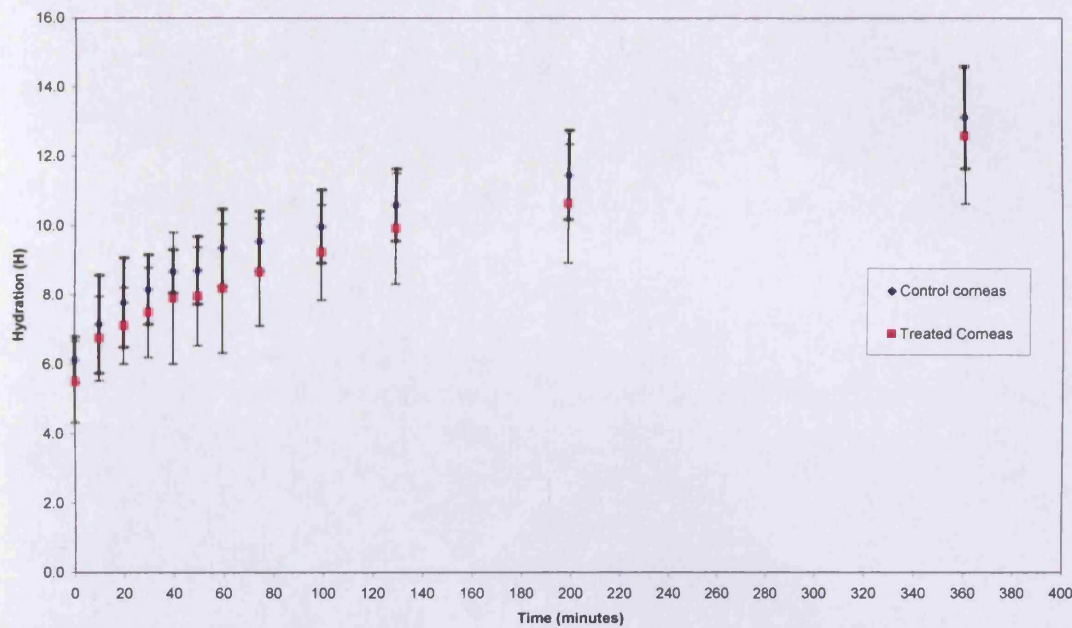


Figure 7.3 Graph of hydration versus time spent in saline solution for untreated (control) corneas and treated (UVA-riboflavin) treatment (errors are s.d.)

By reference to figure 7.3 it can be seen that hydration increases quite rapidly during an initial 80 minutes of immersion within the saline solution. After this, the rate of swelling decreases somewhat. However, the results suggest that samples are still swelling after six hours in solution. Figure 7.3 reinforces the conclusion that although the treated corneas have slightly lower hydration, the data-sets are well within each others dispersion.

There is an unusual discontinuity observed at the 50 minute time point. Here, both of the sets –treated and untreated – appear to stop swelling, relative to the previous time sampling point at 40 minutes. After this time point, swelling appears to continue as before.

### 7.3.2 Analysis of cross-linking agent penetration by means of spectrophotometry.

For each human cornea analysed, three sections were obtained (anterior, middle and posterior) with the aid of the laser using the method outlined in section 7.2.4. The average results are shown in figures 7.4-7.6 for each experimental group.

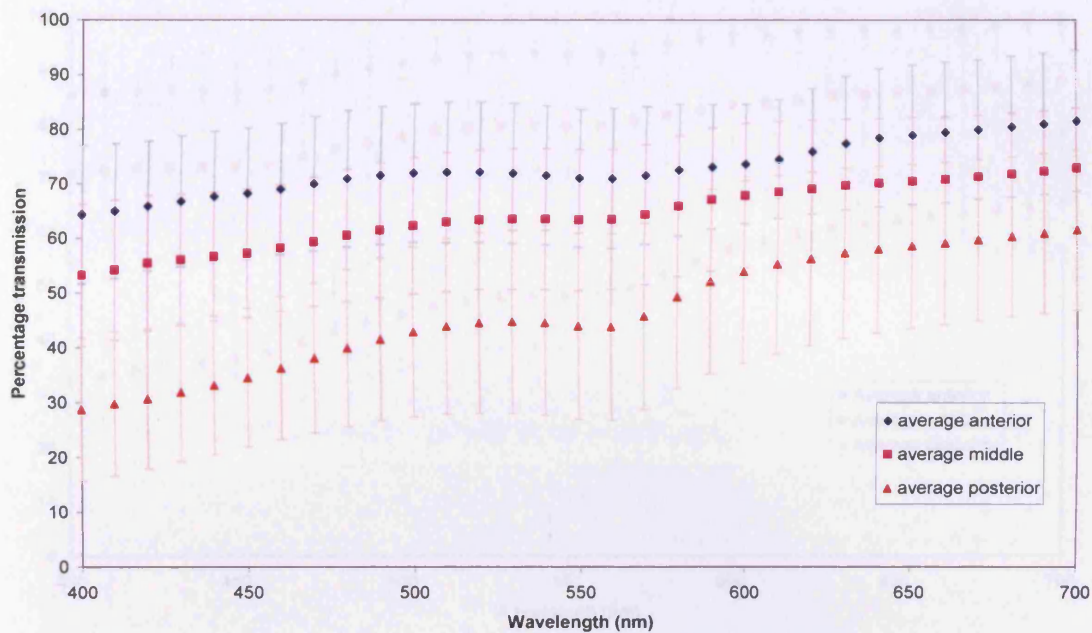


Figure 7.4 Light transmission for sections of untreated human cornea (n=3, error bars are s.d.)

The thin layers of cornea (untreated) appear to have the expected wavelength dependence, i.e. greater light scattering in the short wavelength limit. The scattering is lowest in the anterior region and highest in the posterior segment of the tissue. There is absorption present at 560nm. This is noticeable in the anterior and posterior segments; less so in the middle of the stroma. It is almost certain that this is indicative of the penetration, into the stroma, of phenol red, a component of the culture medium in which the corneas were bathed. This particular chemical is known to possess absorption at this wavelength (Mukai et al., 2004). Although unavoidably present in the corneas used in the present study, phenol red appears to be removed from the corneal stroma when the dialysis procedure outlined in section 2.3.



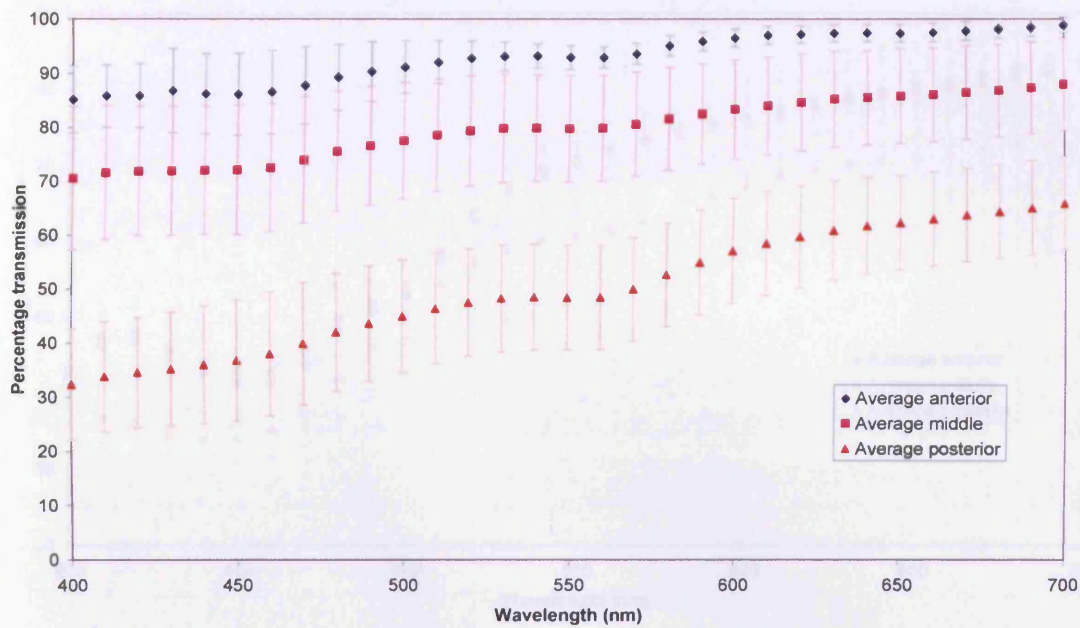


Figure 7.5 Light transmission for treated and sectioned human corneas (n=3 in each group, error s.d.)

The thin layers shown in figure 7.5, treated before sectioning, show the same absorption at 560nm as the control corneas, indicating the presence within the matrix of phenol red. There is an additional absorption at 450-460nm noticeable in the anterior and middle tissue segments, consistent with small concentrations of riboflavin within these segments. This still appears to be present in the posterior segments of tissue, albeit at a much reduced value. Overall light scattering in the posterior segment again appears to be much increased. The corneas used in this study had undergone oedema. It seems likely that dextran, a component of the riboflavin mixture used in the present study, acted to reduce the level of oedema in the anterior and middle tissue sections. This would then increase transmission in these sections.

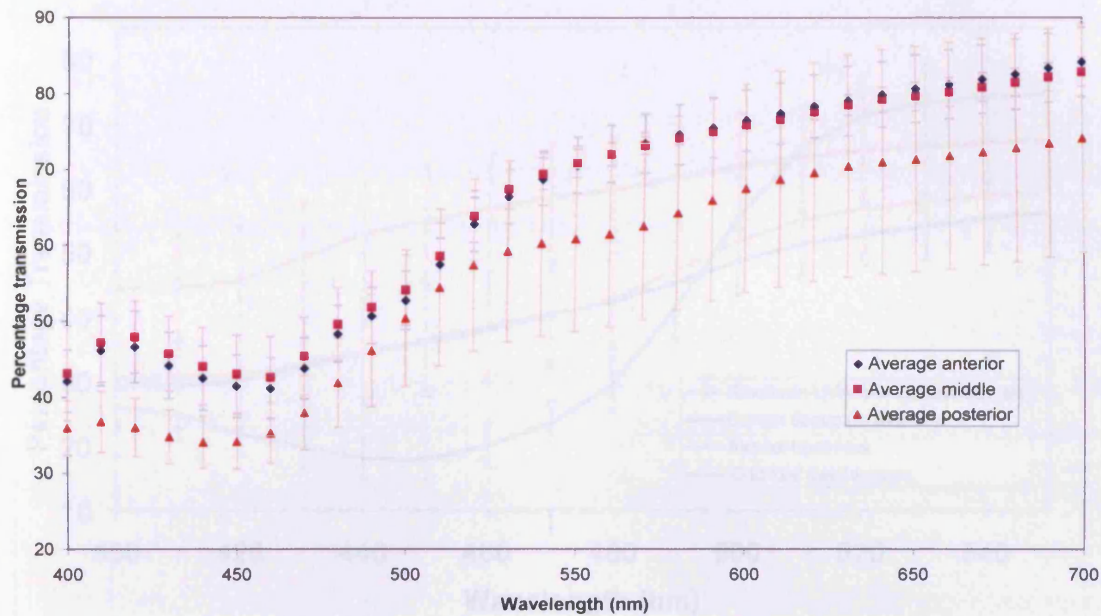


Figure 7.6 Light transmission for layers treated after tissue sectioning

When the treatment protocol is performed on individual layers, as shown in figure 7.6, it can be seen that there is an obvious absorption band which appears to extend from approximately 420-510nm, with a minimum seeming to fall between 450-460nm. After 550nm the wavelength dependence returns to what we would normally expect from corneal stroma. There is a much diminished difference between the various layers in these tissue segments. There is also an apparent shift in wavelength of the riboflavin absorption feature in the posterior segment. Specifically it appears to move towards shorter wavelength.

A further extension to this project was carried out in association with Drs Kostas Samaras and D.P. O'Brart from St Thomas' Hospital. We had previously shown that it was necessary for the epithelial cell layer to be fully removed to ensure optimum penetration of riboflavin (Hayes et al., 2008). However, epithelial removal represents a non-optimal experience for the patient. Therefore, it was decided to repeat the studies of Hayes et al. (2008) using partial debridement. This was achieved using alcohol solution to loosen the epithelial cells, and by using a 'patterned' debridement whereby epithelial cells were removed in a grid-like pattern across the corneal surface.



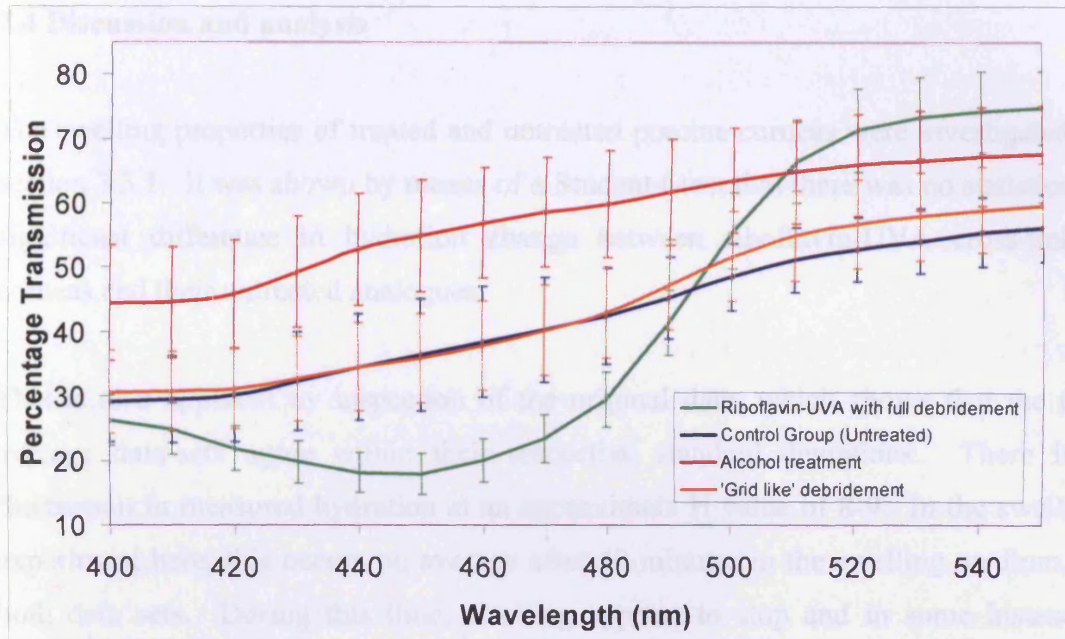


Figure 7.7 Transmission spectra for porcine corneas subjected to various methods of epithelial debridement ( $n=6$  for each set, errors are s.d.)

As can be seen from figure 7.7, the control corneas do not show any evidence of absorption in the riboflavin chromophore region around 450nm. The transmission is fairly low and appears to possess inverse square wavelength dependence, consistent with that of a swollen cornea, as was expected. The normal treatment protocol, with full epithelial debridement, shows a very obvious absorption feature due to riboflavin centred on 450nm. The alcohol treated corneas show no evidence of any riboflavin absorption; however the overall transmission is increased. This is due to the dehydrating effects of both the alcohol solution and, presumably, dextran used in the treatment procedure. The grid-like debridement leads to a broad region of absorption in the 450nm region, with a modest overall increase in corneal light transmission, again, due to dehydration effects. The penetration is however very modest. It should be noted that physical examination of the corneas subjected to the grid treatment showed some evidence of highly non-uniform riboflavin uptake outside of the central treatment zone examined by spectrophotometry.



#### **7.4 Discussion and analysis**

The swelling properties of treated and untreated porcine corneas were investigated in section 7.3.1. It was shown by means of a Student t-test that there was no statistically significant difference in hydration change between riboflavin-UVA cross-linked corneas and their untreated analogues.

This is also apparent by inspection of the original data, which shows that the two average data-sets agree within their respective standard deviations. There is a fluctuation in measured hydration at an approximate H value of 8-9. In the swelling experiment here, this occurs on average after 40 minutes in the swelling medium, in both data sets. During this time, swelling appears to stop and in some instances reverse the degree of swelling. After this point, hydration continues to increase in both data-sets as before. The origin of this is unclear however inspection of the data suggests it is not an artefact. It may represent the point at which either the extrafibrillar or fibrillar matrices undergo a change in their hydration properties. As pointed out in previous sections, water molecules will occur in a number of states in the cornea, and the GAG molecules vary in their ability to bind to water molecules. It therefore seems likely that at these hydration values the relative dynamics of this system are in some way altered. The point is relatively immaterial to the present discussion as it appears to occur in both treated and untreated corneas. However it is worthy of future investigation. It would be interesting to determine how the infrared transmission spectrum varied with hydration, in accordance with the methods presented in chapter 6, in the light of the strange variance in absorption coefficient which seems to occur in the bovine cornea.

The primary purpose of the swelling experiment was to attempt to uncover whether the cross-linking mechanism is primarily inter- or intra-fibrillar. The hypothesis underlying these investigations was that if the cross-links were intrafibrillar, this may have an effect on the tissue swelling properties. In this case, the cornea would swell at a much slower rate, or even cease swelling as the fibrils would be constrained and unable to increase their relative spacing to enable extra water molecules to penetrate. This experiment appears to demonstrate that cross-linking does not occur between fibrils as there is no statistically significant change in the rate of swelling between the

two sample sets, although it must be noted that in terms of averages the cross-linked material appears to swell at a slightly reduced rate. One factor which may affect this observation is the dextran component within the riboflavin solution used here. This will have the effect of deswelling the treated corneas so that in general the starting hydration point will be slightly lower than the untreated groups.

The results presented here would therefore seem to suggest that cross-linking occurs either in an intrafibrillar fashion or perhaps due to interaction with the extrafibrillar matrix. It would be of great interest to repeat this experiment with the posterior surface of the cornea subjected to cross-linking rather than the anterior surface. There are known differences in composition between anterior and posterior cornea (Freund et al., 1995) and since, as outlined in the introductory section, the cross-linking effect appears to occur in the first 300um of stroma, performing the treatment procedure on this segment of tissue may act to further confirm the findings here that cross-links do not occur between fibrils. At the time of writing, a project is under way to utilise Fourier Transform Infrared Spectroscopy to attempt to further define the chemical properties of this cross-linking mechanism.

An earlier study by Wollensak et al. (2007) showed, by a combination of optical coherence tomography (OCT) and light microscopy, that riboflavin-UVA treated corneas did not reach the same hydration point when subjected to tissue swelling. However the swelling study used by Wollensak is not directly comparable to the one used in this study. Wollensak caused the corneas to become oedematous using a 'moist chamber' into which the corneas were placed for a period of 24 hours. The corneas used in the Wollensak study would have been severely swollen (Wollensak et al., 2007). This was performed on whole porcine eyes. It could be postulated that since the corneas were still integrated with the eye, the more rigid cross-linked corneas would fail to swell to such a degree, constrained by both the limbus and sclera, regardless of whether the cross-linking mechanism occurs in an intra or inter fibrillar fashion. In this work, the corneal buttons were used and as such there was no constraint on corneal swelling. It is felt that this is advantageous since, if the cross-linking were interfibrillar, this effect would be best observed with the cornea effectively as a gel free of any constraining effects due to the limbus, as has been observed in section 5.

The visible light transmission spectra reveal intriguing data, which assist in monitoring the rate of diffusion of the riboflavin molecule into the stromal matrix. Here, the primary interest is in the riboflavin absorption which occurs at approximately 440-450nm. The data in figures 7.2, 7.3 and 7.4 show the total visible light transmission for human corneas. This includes the effects of absorption and scattering. To ease comparison between data-sets it is possible to factor out much of the scattering contribution using the method outlined in section 3.3.3 in which the wavelength dependence is evaluated. Using this method, the scattering contribution is found to take the form of a straight line when the function  $\ln(-\ln(T(\lambda)))$  is plotted against the natural logarithm of transmission. Absorptions appear as regions of anomalous scattering, with the greatest perturbation from the linear form of scattering observed at the wavelength of maximal absorbance. This may be seen below in figure 7.8 which shows the above procedure as applied to light transmission data from the anterior segment shown in figure 7.4.

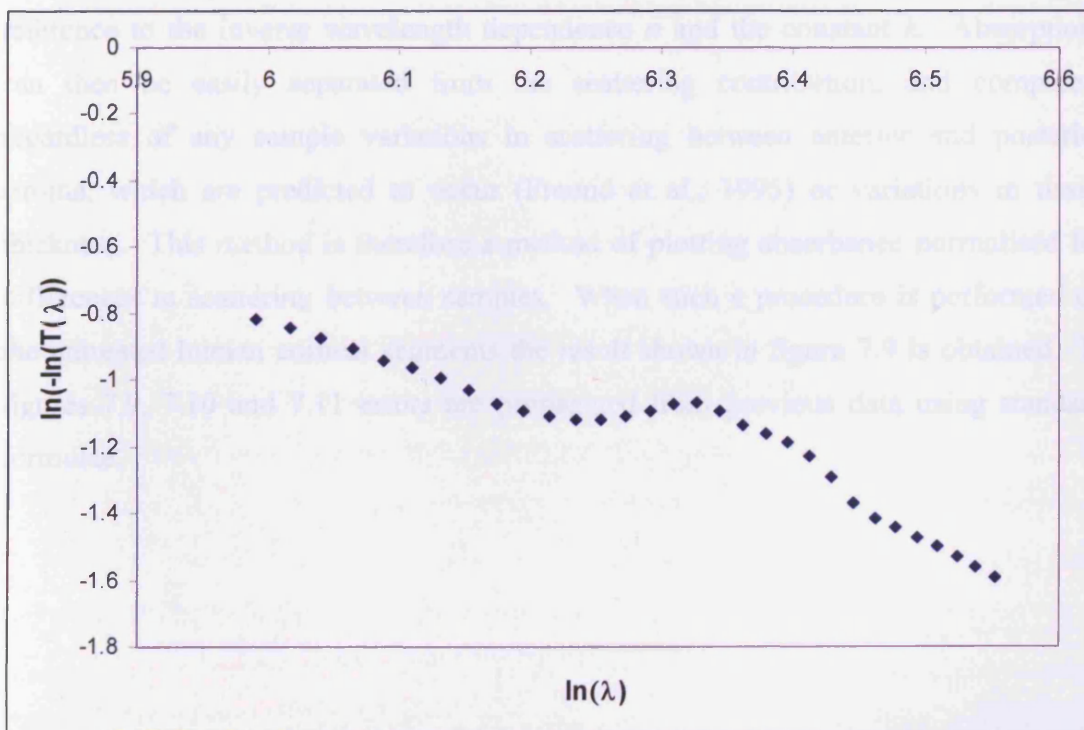


Figure 7.8. Transformed transmission data from anterior segment of untreated cornea

By reference to figure 7.8, it can be seen that when transmission data from an untreated cornea are transformed using the methodology of section 3.3.3, the data

points mainly lie on a straight line, with the exception of a region that lies between 6.19 and 6.46 (a region which correlates to  $\ln(490\text{nm})$  and  $\ln(640\text{nm})$ ). If this anomalous region is eliminated from this analysis, then a straight line can be fitted to the data as per section 3.3.3. It will be useful at this point to restate the equation for this straight line, slightly modified here:

Eq. 7.1

$$\ln \alpha(\lambda) = -n \ln \lambda + \ln k$$

Here,  $\alpha(\lambda)$  denotes the total absorption and scattering coefficient. This includes the total scattering and absorption cross-section. In this section by necessity it will be assumed that effects due to the variable optical depth of the samples are contained within the term  $k$ , which as before is a constant of proportionality. The scattering part of  $\alpha(\lambda)$  can be normalised to oscillate around 1 when plotted against wavelength by reference to the inverse wavelength dependence  $n$  and the constant  $k$ . Absorptions can then be easily separated from the scattering contribution, and compared, regardless of any sample variations in scattering between anterior and posterior stroma, which are predicted to occur (Freund et al., 1995) or variations in tissue thickness. This method is therefore a method of plotting absorbance normalised for differences in scattering between samples. When such a procedure is performed on the untreated human corneal segments the result shown in figure 7.9 is obtained. In figures 7.9, 7.10 and 7.11 errors are propagated from previous data using standard formulae.



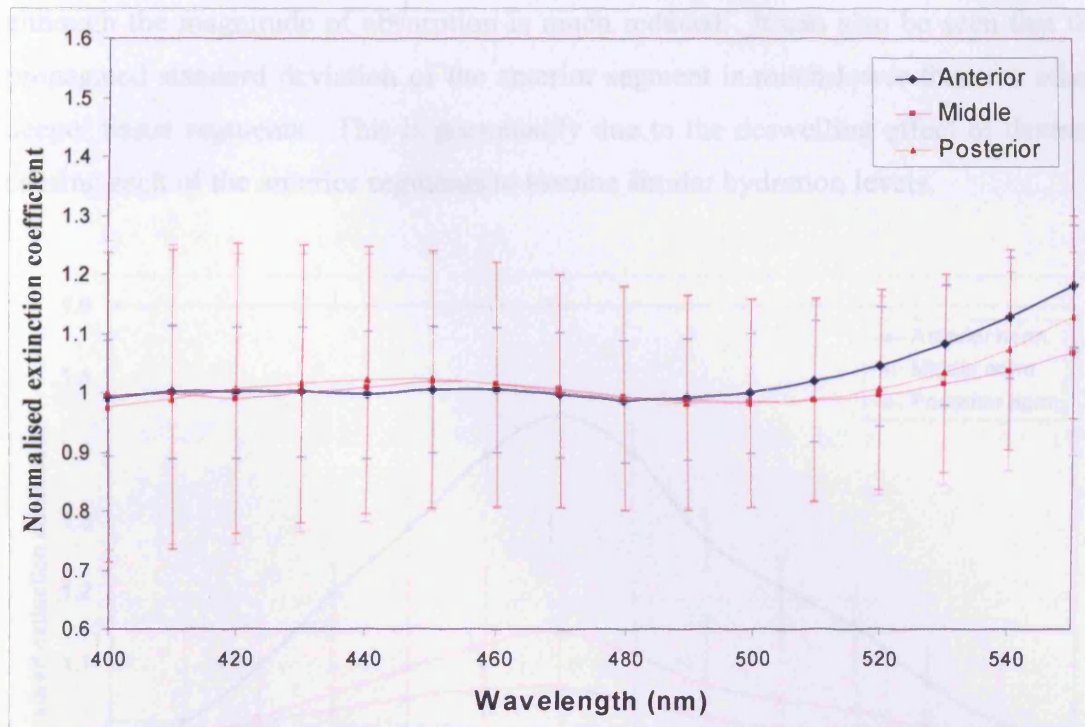


Figure 7.9 Normalised extinction coefficient for untreated human stromal sections (n=3 each set).

Figure 7.9 shows no evidence of any absorptive loss due to the presence of riboflavin. The absorption due to phenol red from the culture medium can however be seen to be present from 500nm. Although not the focus of this work, it is interesting to note that it appears to have penetrated more into the anterior segment of the tissue, but is present in all sections of the tissue, presumably due to the time available for diffusion whilst the samples are under organ culture. There is a considerable amount of dispersion within each data-set when errors are propagated. This is presumably due to variation in hydration state between samples. For this experiment, it was not possible to measure hydration by taking relative wet and dry weights as the corneas were required for X-ray diffraction. Therefore the distribution of hydrations is not known.

Figure 7.10 shows the normalised extinction coefficient for corneas treated with riboflavin-UVA and then sectioned by laser. Here it can be seen that, as expected, the bulk of absorption occurs in the anterior tissue segment. The absorbance due to riboflavin decreases quite rapidly away from this region, however. It is of note that a small concentration of riboflavin does appear to have reached the posterior region,

although the magnitude of absorption is much reduced. It can also be seen that the propagated standard deviation of the anterior segment is much lower than the other, deeper tissue segments. This is presumably due to the deswelling effect of dextran, causing each of the anterior segments to assume similar hydration levels.

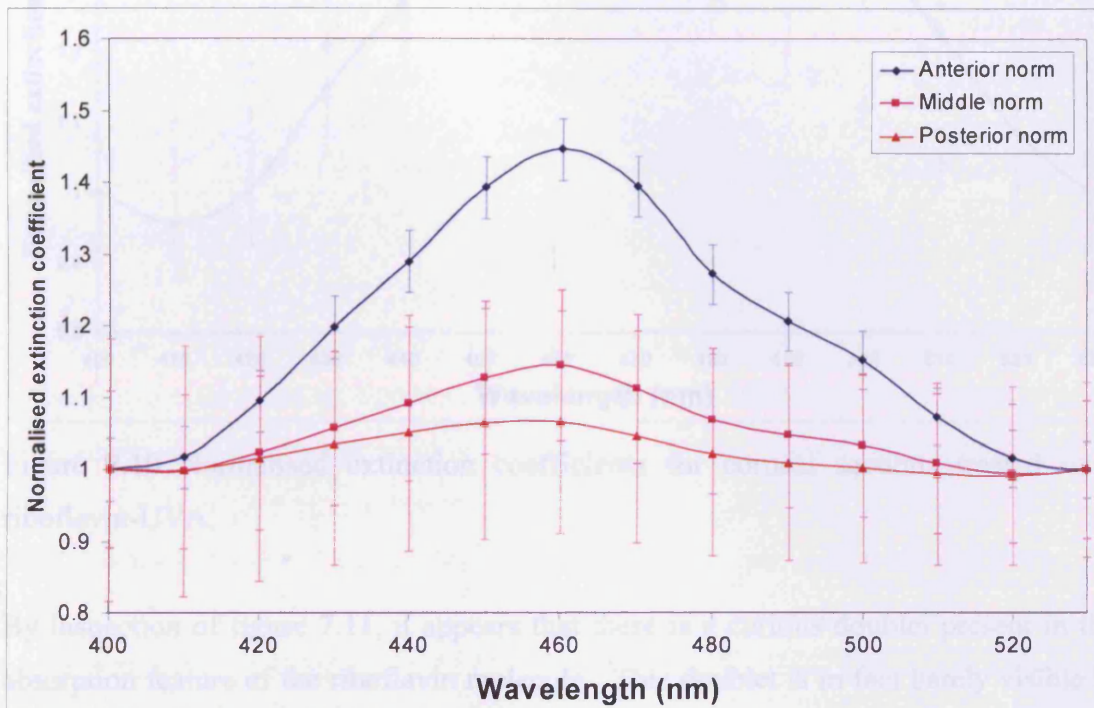


Figure 7.10 Normalised extinction coefficients for riboflavin-UVA treated corneal sections (treatment performed prior to sectioning)

The results of performing this analysis on sections of cornea which have been individually treated using the riboflavin-UVA protocol are shown in figure 7.11. Here it can be seen that the anterior and posterior tissue segments appear to have a nearly equal amount of riboflavin present within the tissue.



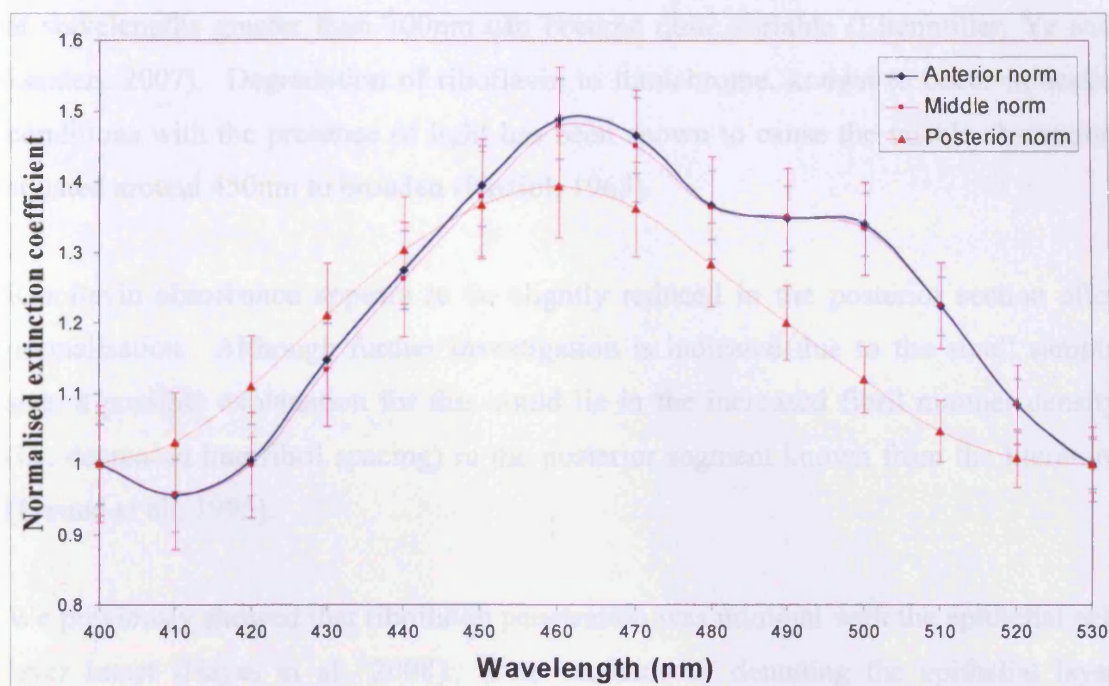


Figure 7.10 Normalised extinction coefficients for corneal sections treated with riboflavin-UVA.

By inspection of figure 7.11, it appears that there is a curious doublet present in the absorption feature of the riboflavin molecule. This doublet is in fact barely visible in figure 7.10 and occurs at 500nm. The spectroscopic origin of this feature is not clear from a search of the extant literature on the spectral properties of the riboflavin molecule. It does not appear to be present in known spectra obtained from riboflavin in simple solvents. However, it is not known how the polar environment within the corneal stroma may interact with riboflavin or its degradation products to affect the detected spectra. Notably, this effect is not present in the posterior samples. It must be noted that the posterior sections, due to the nature of the tissue sectioning procedure were slightly thicker than the anterior and posterior sections. Anterior and posterior segments were sectioned to approximately 100 $\mu$ m. The remainder was thus the posterior segment. Even after normalisation, therefore, more discrete detail in the absorption feature may be diffused due to the greater optical path.

Furthermore, in the posterior samples there appears to be a slight shift in riboflavin absorbance towards shorter wavelengths. The reason for this is unclear. However, it is known that when flavins are subjected to reduction reactions spectroscopic features

## **Chapter 7.**

at wavelengths greater than 300nm can become quite variable (Eitenmiller, Ye and Landen, 2007). Degradation of riboflavin to lumichrome, known to occur in acidic conditions with the presence of light has been shown to cause the visible absorption situated around 450nm to broaden (Koziol, 1965).

Riboflavin absorbance appears to be slightly reduced in the posterior section after normalisation. Although further investigation is indicated due to the small sample size, a possible explanation for this could lie in the increased fibril number density (i.e. decreased interfibril spacing) in the posterior segment known from the literature (Freund et al., 1995).

We previously showed that riboflavin penetration was minimal with the epithelial cell layer intact (Hayes et al., 2008). Two methods of denuding the epithelial layer without its wholesale destruction were attempted in this chapter. It was determined that neither was particularly effective. Alcohol treatment does not appear to allow any riboflavin to penetrate the stroma, although it does appear to dehydrate the cornea. The grid debridement did not appear, by spectrophotometry, to produce significant levels of riboflavin diffusion into the cornea. However, it was noted that there were 'patches' of riboflavin absorption into the stroma. This was however, non-uniformly distributed across the treatment area and is unlikely to be effective for this reason. The overall results of this chapter would appear to suggest that, if epithelial removal is to be avoided, perhaps a LASIK (laser-assisted in situ keratomileusis) flap style system should be used.

To conclude this section, it would appear that, as expected, during the conventional protocol whereby the epithelial cell layer is removed and the treatment applied to the anterior surface, the riboflavin, or its degradation products, are present in greatest concentration within the anterior portion of the stroma, even after allowing over 30 minutes diffusion time during the protocol. When the protocol is performed on thin sections of tissue, it is found that the anterior and middle sections appear to absorb similar concentrations of riboflavin. The posterior is found to have somewhat unusual properties with regards to the riboflavin absorption feature, although the concentration absorbed would appear to be broadly similar. It is likely that decreased uptake of



## ***Chapter 7.***

riboflavin towards the posterior surface of corneas in all treatment protocols is due to increases in fibril number density in the posterior segments of the corneal stroma.

## Chapter 8. Epilogue

### 8.1 Summary of Results and Conclusions

#### 8.1.1 Spatial ordering of collagen fibrils within the corneal stroma

Chapter 3 focused on the spatial arrangement of collagen fibrils within corneal stroma. Here, three possible arrangements were investigated:

1. A distorted hexagonal lattice
2. A random, amorphous arrangement
3. Novel aperiodic arrays termed 'round quasicrystals'

It was determined that distorting a hexagonal lattice basis did not produce a structure factor compatible with that of corneal stroma. Specifically it was determined that even when a hexagonal lattice is distorted in real space, the power spectrum of the Fourier transform still shows evidence of the initial hexagonal unit cell.

An amorphous system generated under the condition that fibrils cannot approach closer than touching produces as its structure factor a diffuse halo, the maximum of which gives the frequency space value for the real space average interfibrillar spacing. The pattern is much more diffuse than that seen from corneal stroma, as is its radial distribution function.

A round quasicrystal system with a plausible structure, the sunflower seed head, was also tested as an analogue of corneal ultrastructure. It was determined that the structure factor consisted of a series of rings, similar to those found in the corneal structure factor, but with less diffusion. Adding a small degree of thermal disorder to this structure had the effect of diffusing the rings slightly. The radial distribution function was also analogous to that found in stroma.

Analysis of the optical properties of these types of spatial order suggested that the round quasicrystal best simulates the optical properties in terms of corneal wavelength

dependence. These results therefore suggest that the unique properties of the arrangement of corneal collagen fibrils can be modelled by reference to the novel mathematical system, the round quasicrystal, and in particular the sunflower seed head model.

### 8.1.2 Light transmission through cornea as a function of position

As related in chapter 4 the light transmission through human corneas equilibrated to physiological hydration was determined as a function of position across the corneal surface. Recent X-ray diffraction measurements had confirmed the observation from electron microscopy that interfibril spacing and fibril diameter varied considerably going from central to peripheral cornea. The cornea is also well known to increase its thickness peripherally. In spite of this, light transmission in the peripheral cornea has not been investigated previously.

Visible light transmission was analysed across the corneal surface at 1mm intervals radiating out in a single meridian from the corneal centre up to a distance of 5mm from the centre. This study indicated that human corneal transmission in the central, pre-pupillary region decreases gradually from the optical centre in a linear fashion. Beyond this central section, at a distance of 4mm or more from the centre of the cornea, light transmission begins to decrease more substantially. The total average decrease from central to far peripheral cornea (0-5mm) is found to be 14%.

The change in light transmission was computed theoretically using the direct summation of scattered fields theory, using three electron micrographs from the literature to supply spatial ordering information. Using parameters from X-ray diffraction to vary fibril diameter, spacing and refractive index contrast between fibril and extrafibrillar substance, it is found that there is a theoretical 10% decrease from central to far peripheral cornea. Taking into account the standard deviation of experimental and theoretical sets the two are found to be in agreement. Analysis suggests that the excess balance of light scattering in peripheral cornea, in comparison with central cornea, is caused by an increase in refractive index contrast between fibril and extrafibrillar substance and the slight increase in fibril diameter. Interestingly, it appears that the optical effects of the well known peripheral increase in corneal

thickness are largely cancelled out by the decrease in collagen fibril density as the fibrils move further apart peripherally. Better agreement between experiment and theory can be produced if the known decrease in proteoglycan concentration peripherally is accounted for.

### **8.1.3 Light transmission and thickness of oedematous corneas: A comparison between central and peripheral zones**

Chapter 5 aimed to investigate the optical and swelling properties of oedematous corneas in the central and peripheral regions of the corneal stroma.

It is known clinically that there is a degree of differential in swelling between central and peripheral cornea. Therefore, it was decided to investigate how thickness and visible light transmission vary off axis in oedematous corneas.

It was found that when corneas were swollen with scleral ring attached, the central portion of the cornea increased its thickness much more rapidly than the peripheral segment. This lessened the differential in thickness between central and peripheral cornea to the point at which, for severely swollen corneas the central corneal thickness was actually greater than the average peripheral thickness. This would appear to confirm the clinical observation and suggests that the limbus, the region in which cornea merges into sclera, is able to exert a clamping effect on the peripheral stroma preventing excessive swelling.

In terms of visible central and peripheral transmission in oedematous corneas, in two of the four corneas analysed, the transmission appears to be roughly equal across a meridian extending 4mm from the corneal centre. In the other two samples there appears to be a greater degree of variation.

There is an interesting change in wavelength dependence in the oedematous peripheral cornea. The exact reasons for this are unclear and will require further study. However, it obviously implies a change in spatial ordering in the far periphery (5mm). A search of the literature suggests that variation is probably due to variation

in the geometry and number of lakes, although further work will be required using X-ray diffraction and electron microscopy to quantify this further.

#### **8.1.4 Infrared absorption in the cornea (Chapter 6)**

In the visible portion of the electromagnetic spectrum the cornea acts primarily as a light scatterer. In general, it can be assumed that the molecular complexes which make up the corneal stroma do not have any chromophores in the visible portion of the spectrum, certainly in the human cornea. In the infrared portion of the spectrum however, scattering power decreases considerably, as the wavelengths are much larger than the ultrastructural components of the corneal stroma. The primary extinction mechanism is therefore absorption. Although as complex organic molecules, collagen and proteoglycans are themselves prolific absorbers, certainly in the mid-infrared, the vast majority of absorption is due to the presence of liquid water in the stroma, a powerful absorber across all wavelength regions of the infrared spectrum, from the terahertz to the near-infrared.

It is well known that when the cornea is permitted to swell, the central thickness increases in a linear fashion in cow, human and rabbit, in relation to hydration or relative water content. Since the absorption spectrum of the cornea in the mid and near infrared is known to be almost identical to that of a layer of liquid water of equivalent thickness this begs the question of whether there is a correlation between corneal infrared transmission and corneal hydration state.

From a theoretical perspective, using known the absorption coefficient for liquid water at a wavenumber of  $4500\text{cm}^{-1}$ , it can be shown that there should be an exponential decrease in corneal transmission at this wavenumber, in relation to hydration level. Experimentally, when bovine corneas are swollen in saline solution, however, this does not seem to occur. The experimental data indicate a linear dependence between transmission and corneal hydration. The discrepancy seems to be due to the fact that the absorption coefficient varies as a function of hydration. The relationship was shown to be linear within experimental sets, with variation between individual corneas. This probably relates to the dry mass of collagen present within each given sample.

A normalisation protocol was therefore developed by correcting all results to an average corneal dry weight. This was found to produce low dispersion from actual experimental measurements. An unusual change in absorption coefficient was found to occur as the hydration was increased. The effect proved somewhat difficult to quantify, but it is likely that it indicates some form of change in the way water molecules interact with protein or ionic components of the stroma. Further study will be required.

This observation may be useful both for clinical and research purposes. It would allow the hydration of a cornea to be measured non-destructively and non-invasively during the course of an experiment or during tissue culture for transplant. If adapted for in-vivo use, utilising perhaps FTIR reflection spectroscopy or combined with Optical Coherence Tomography; this would prove useful for example, during the course of refractive surgery.

### **8.1.5 Spectroscopic and swelling studies of corneas cross-linked with Riboflavin/Ultraviolet-A (Chapter 7)**

Keratoconus is a degenerative disorder of the corneal stroma. It leads to corneal thinning in the central cornea, with deleterious changes in the biomechanical and optical properties of the cornea. In the most severe cases, it is necessary to proceed to keratoplasty, or corneal transplant, with concomitant problems such as graft rejection and constrained tissue supply, for example.

It has therefore been seen as desirable to develop a treatment methodology which reduces or eliminates the need for keratoplasty. One way of achieving this is to increase the tensile strength of corneal tissue through the use of collagen cross-linking, whereby collagen molecules are linked together by molecular bridges, or cross-links. This is typically achieved through the use of compounds such as aldehydes. However, it has been determined that exposing corneal stromas to ultraviolet-A radiation in the presence of riboflavin has the effect of inducing a cross-linking effect in the corneal stroma. This acts to stop and in some cases reverse the degenerative progress of keratoconus, so drastically does it alter the biomechanical

properties of the cornea. However, the cross-linking mechanism is poorly understood, as are the diffusion properties of riboflavin within the stroma.

Porcine corneas treated with riboflavin-UVA were allowed to swell freely in a saline solution. The rate of swelling was then contrasted with untreated porcine corneas. It was immediately obvious that there was no statistically significant difference in swelling between the treated and untreated samples. When the cornea swells, the extra water moves in between the fibrils. If the fibrils were cross-linked the fibrils would not be able to move so far apart and the swelling properties of the cornea would be constrained. This would appear to suggest that the cross-linking does not occur between fibrils, although it does not conclusively prove that the cross-linking must be intrafibrillar. It could be in some way affecting the extrafibrillar substance. There is interesting scope for further studies utilising, for example, FTIR or X-ray scattering to further elucidate the cross-linkage mechanism.

Thin sections of treated and untreated human tissue were obtained using a Laser cutting system. This allowed the diffusion of riboflavin to be determined spectrophotometrically in anterior, middle and posterior cornea. Here, it was determined that in full thickness corneas, the majority of the riboflavin appears to remain in the anterior tissue segment, with relatively little diffusing through to the middle and posterior segments. When individual sections were treated, the riboflavin penetrated almost equally into the anterior and middle segments. There appears to be a change in the riboflavin absorption properties of the posterior segment. This is possibly related to changes in the composition of the extrafibrillar substance and the way it interacts either with riboflavin or its degradation product. This will require further research.

### **8.2 Future work**

The results presented in this thesis contribute to our biophysical understanding of the optical properties of corneal stroma. There are additionally several potentially productive avenues for future theoretical and experimental research.



The results presented here suggest that an aperiodic model of the corneal stroma provides the best synthetic template for the distribution of fibrils within a lamella. Further refinement is possible. There are numerous other so called 'rotation invariant' systems which can be tested for compatibility with corneal stroma. There are for example, numerous variants of the pinwheel tiling. A further area of interest would be to apply the photonic band theory to the quasicrystal system with the best compatibility with cornea, and then model how this may vary when discontinuities, such as lakes, are added to the stroma. This is a drawback of the direct summation of scattered fields model; it has been shown previously (Leonard, 1996) that predicted light transmission from swollen and pathological corneas does often correlate with actual transmission. It would also be of great interest to determine the radial distribution function from X-ray diffraction data, in order to obtain this from material in the native state, unaffected by the fixation and embedding required for electron microscopy. In particular, the new microfocus X-ray diffraction techniques available at synchrotrons will allow spatial ordering to be determined in small sections of tissue, for example as a function of depth.

In order to further optimise models of corneal transmission, it will be necessary to accurately determine the refractive index of the stromal keratocytes. It may be possible to use phase contrast microscopy to determine this, and with this in mind collaboration has commenced (at the time of writing) with Dr Brendan Allman of Iatia Imaging Systems (Melbourne, Australia).

The nature of the molecular cross-links in the riboflavin-UVA treatment needs to be better understood in order to optimise the efficacy of the treatment. With this in mind, it is intended to perform Fourier Transform Infrared Spectroscopy on thin segments of treated tissue. It is hoped that this may yield evidence at the molecular level of the cross-linking effect and help elucidate which molecular complex is affected by the process.

## References

- Ameen B, McMullen (1998) A lattice model for computing the transmittivity of the cornea and sclera. *Biophysical Journal* 75: 2520-2531.
- Baldock C, Gilpin C J, Koster A J, Ziese U, Kadler K E, Kielty C M, and Holmes D F (2002) Three-dimensional reconstructions of extracellular matrix polymers using automated electron tomography. *Journal of Structural Biology* 138: 130-136.
- Banwell C N (1983) *Fundamentals of molecular spectroscopy*. 3 ed. London: McGraw-Hill Book Company.
- Bashkatov A N, Genina E A, Kochubey V I, and Tuchin V V (2005) Optical properties of human skin, subcutaneous and mucous tissues in the wavelength range from 400 to 2000nm. *Journal of Physics D: Applied Physics* 38: 2543-2555.
- Beecher N, Carlson C, Allen B R, Kipchumba R, Conrad G W, Meek K M, and Quantock A J (2005) An x-ray diffraction study of corneal structure in mimecan-deficient mice. *Investigative Ophthalmology and Visual Science* 46: 4046-4049.
- Beems E, and Best J V (1990) Light transmission of the cornea in whole human eyes. *Experimental Eye Research* 50: 393-395.
- Benedek G B (1971) Theory of Transparency of the Eye. *Applied Optics* 10: 459-473.
- Berend D, and Radin C (1993) Are there Chaotic Tilings? *Communications in Mathematical Physics* 152: 215-219.
- Best J A V (1988) Corneal transmission in whole human eyes. *Experimental Eye Research* 46: 765-768.
- Bettelheim F A, and Plessy B (1975) The hydration of proteoglycans of bovine cornea. *Biochimica et Biophysica Acta* 381: 203-214.
- Birk D E (2001) Type V collagen: heterotypic type I/V collagen interactions in the regulation of fibril assembly. *Micron* 32: 223-237.
- Boettner E A, Wolter, J.R. (1962) Transmission of the ocular media. *Investigative Ophthalmology* 1: 776-783.
- Bohren C F, and Huffman D R (1983) *Absorption and Scattering of Light by Small Particles*. John Wiley & Sons.
- Boote C, Dennis S, Newton R H, Puri H, and Meek K M (2003) Collagen fibrils appear more closely packed in the prepupillary cornea: optical and biomechanical implications. *Investigative Ophthalmology and Visual Science* 44: 2941-2948.

- Boote C, Hayes S, Abahussin M, and Meek K M (2006) Mapping collagen organization in the human cornea: left and right eyes are structurally distinct. *Investigative Ophthalmology and Visual Science* 47: 901-908.
- Borcherding M S, Blacik L J, Sittig R A, Bizzell J W, Breen M, and Weinstein H G (1975) Proteoglycans and collagen fibre organization in human corneoscleral tissue. *Experimental Eye Research* 21: 59-70.
- Brown S I, and McLean J M (1969) Peripheral corneal edema after cataract extraction. A new clinical entity. *Transactions of the American Academy of Ophthalmology and Otolaryngology* 73: 465-470.
- Chakravarti S, Petroll W M, Hassell J R, Jester J V, Lass J H, Paul J, and Birk D E (2000) Corneal opacity in lumican-null mice: defects in collagen fibril structure and packing in the posterior stroma. *Investigative Ophthalmology and Visual Science* 41: 3365-3373.
- Charulatha V, and Rajaram A (2003) Influence of different crosslinking treatments on the physical properties of collagen membranes. *Biomaterials* 24: 759-767.
- Christens-Barry W A, Green W J, Connolly P J, Farrell R A, and McCally R L (1996) Spatial mapping of polarized light transmission in the central rabbit cornea. *Experimental Eye Research* 62: 651-662.
- Cintron C, Hong B, Covington H I, and Macarak E J (1988) Heterogeneity of Collagens in Rabbit Cornea: Type III Collagen. *Investigative Ophthalmology and Visual Science* 29: 767-775.
- Connon C J, Marshall J, Patmore A L, Brahma A, and Meek K M (2003) Persistent haze and disorganization of anterior stromal collagen appear unrelated following phototherapeutic keratectomy. *Journal of Refractive Surgery* 19: 323-332.
- Connon C J, Meek K M, Kinoshita S, and Quantock A J (2004) Spatial and temporal alterations in the collagen fibrillar array during the onset of transparency in the avian cornea. *Experimental Eye Research* 78: 909-915.
- Connon C J, Nakamura T, Hopkinson A, Quantock A, Yagi N, Dutch J, and Meek K M (2007) The biomechanics of amnion rupture: an x-ray diffraction study. *PLoS ONE* 2: e1147.
- Cooper L J, Bentley A J, Nieduszynski I A, Talabani S, Thomson A, Utani A, Shinkai H et al. (2006) The role of dermatopontin in the stromal organization of the cornea. *Investigative Ophthalmology and Visual Science* 47: 3303-3310.
- Corpuz L M, Funderburgh J L, Funderburgh M L, Bottomley G S, Prakash S, and Conrad G W (1996) Molecular cloning and tissue distribution of keratocan. Bovine corneal keratan sulfate proteoglycan 37A. *Journal of Biological Chemistry* 271: 9759-9763.

- Coulombre A J, Coulombre, J.L (1958) Corneal Development. I Corneal Transparency. *Journal of Cell Physiology* 51: 1-11.
- Cox J L, Farrell R A, Hart R W, and Langham M E (1970) The transparency of the mammalian cornea. *Journal of physiology* 210: 601-616.
- Doutch J, Quantock A J, and Meek K (2007) Changes in visible light transmission across the corneal stroma. *Proceedings of SPIE* 65350V.
- Doyle B B, Bendit E G, and Blout E R (1975) Infrared spectroscopy of collagen and collagen-like polypeptides. *Biopolymers* 14: 937-957.
- Eitenmiller R R, Ye L, and Landen W O, Jr (2007) *Vitamin Analysis for the Health and Food Sciences*. CRC Press.
- Emmertson J, Schwemer J, Muth I, and Schlecht P (1980) Spectral transmission of the ocular media of the pegeion (*Columba livia*). *Investigative Ophthalmology and Visual Science* 19: 1382-1387.
- Farrell R A, and McCally R L (2000) Corneal transparency. In: Albert D M, and Jakobiec F A [eds.] *Principles and Practice of Ophthalmology*. Philadelphia, PA: WB Saunders, pp. 629-643.
- Farrell R A, McCally R L, and Tatham P E (1973) Wave-length dependencies of light scattering in normal and cold swollen rabbit corneas and their structural implications. *Journal of physiology* 233: 589-612.
- Feuk T (1970) On the transparency of the stroma in the mammalian cornea. *IEEE Transactions on Biomedical Engineering* 17: 186-190.
- Feuk T (1971) The wavelength dependence of scattered light intensity in rabbit corneas. *IEEE Transactions on Biomedical Engineering* 18: 92-96.
- Feuk T, and McQueen D (1971) The angular dependence of light scattered from rabbit corneas. *Investigative Ophthalmology* 10: 294-299.
- Fratzl P, and Daxer A (1993) Structural transformation of collagen fibrils in corneal stroma during drying. An x-ray scattering study. *Biophysical Journal* 64: 1210-1214.
- Freegard T (1997) The physical basis of transparency of the normal cornea. *Eye* 11: 465-471.
- Frettlow D (2006) *Golden Pinwheel* [Online]. Available at: [http://tilings.math.uni-bielefeld.de/substitution\\_rules/golden\\_pinwheel](http://tilings.math.uni-bielefeld.de/substitution_rules/golden_pinwheel) [Accessed: 01/12/2007].
- Freund D E, McCally R L, and Farrell R A (1986) Direct summation of fields for light scattering by fibrils with application to normal corneas. *Applied Optics* 25: 2739-2746.

Freund D E, McCally R L, Farrell R A, Cristol S M, L'Hernault N L, and Edelhauser H F (1995) Ultrastructure in anterior and posterior stroma of perfused human and rabbit corneas. Relation to transparency. *Investigative Ophthalmology and Visual Science* 36: 1508-1523.

Fullwood N J, Tuft S J, Malik N S, Meek K M, Ridgway A E, and Harrison R J (1992) Synchrotron x-ray diffraction studies of keratoconus corneal stroma. *Investigative Ophthalmology and Visual Science* 33: 1734-1741.

Funderburgh J L, Cintron C, Covington H I, and Conrad G W (1988) Immunoanalysis of keratan sulfate proteoglycan from corneal scars. *Investigative Ophthalmology and Visual Science* 29: 1116-1124.

Funderburgh J L, and Conrad G W (1990) Isoforms of corneal keratan sulfate proteoglycan. *Journal of Biological Chemistry* 265: 8297-8303.

Funderburgh J L, Funderburgh M L, Mann M M, and Conrad G W (1991) Unique glycosylation of three keratan sulfate proteoglycan isoforms. *Journal of Biological Chemistry* 266: 14226-14231.

Giraud J P, Pouliquen Y, Offret G, and Payrau P (1975) Statistical morphometric studies in normal human and rabbit corneal stroma. *Experimental Eye Research* 21: 221-229.

Godreche C (1992) Indexing the diffraction spectrum of a non-Pisot self-similar structure. *Physical Review B* 45: 176-185.

Goldman J N, and Benedek G B (1967) The relationship between morphology and transparency in the nonswelling corneal stroma of the shark. *Investigative Ophthalmology* 6: 574-600.

Goldman J N, Benedek G B, Dohlman C H, and Kravitt B (1968) Structural alterations affecting transparency in swollen human corneas. *Investigative Ophthalmology* 7: 501-519.

Guggenheim J A, Armitage W J, Evans A D, Davies H, Rebello G, and Hodson S A (1995) Chloride binding in the stroma of cultured human corneas. *Experimental Eye Research* 61: 109-113.

Hafezi F, Kanellopoulos J, Wiltfang R, and Seiler T (2007) Corneal collagen crosslinking with riboflavin and ultraviolet A to treat induced keratectasia after laser in situ keratomileusis. *Journal of Cataract and Refractive Surgery* 33: 2035-2040.

Hart R W, and Farrell R A (1969) Light scattering in the cornea. *Journal of the Optical Society of America* 59: 766-774.

Hayes S, Boote C, Tuft S J, Quantock A J, and Meek K M (2007) A study of corneal thickness, shape and collagen organisation in keratoconus using videokeratography and X-ray scattering techniques. *Experimental Eye Research* 84: 423-434.

Hayes S, O'Brart D P, Lamdin L S, Douth J, Samaras K, Marshall J, and Meek K M (2008) Effect of complete epithelial debridement before riboflavin-ultraviolet-A corneal collagen crosslinking therapy *Journal of Cataract and Refractive Surgery* 34: 657-661.

Hedbys B O (1961) The role of polysaccharides in corneal swelling. *Experimental Eye Research* 1: 81-91.

Hedbys B O, and Mishima S (1966) The Thickness-Hydration relationship of the cornea. *Experimental Eye Research* 5: 221-228.

Hodson S (1971) Why the cornea swells. *Journal of theoretical biology* 33: 419-427.

Hodson S, Kaila D, Hammond S, Rebello G, and al-Omari Y (1992) Transient chloride binding as a contributory factor to corneal stromal swelling in the ox. *Journal of physiology* 450: 89-103.

Hodson S, and Miller F (1976) The bicarbonate ion pump in the endothelium which regulates the hydration of rabbit cornea. *Journal of physiology* 263: 563-577.

Hrynchak P, and Simpson T (2000) Optical coherence tomography: an introduction to the technique and its use. *Optometry and Vision Science* 77: 347-356.

Huang Y, and Meek K M (1999) Swelling studies on the cornea and sclera: the effects of pH and ionic strength. *Biophysical Journal* 77: 1655-1665.

Ijiri S, Kobayashi A, Yoshita T, Yokogawa H, and Sugiyama K (2007) Measurement of light transmission of human limbal epithelial cells cultured on human amniotic membranes. *Cornea* 26: 348-351.

Iseli H P, Thiel M A, Hafezi F, Kampmeier J, and Seiler T (2008) Ultraviolet A/riboflavin corneal cross-linking for infectious keratitis associated with corneal melts. *Cornea* 27: 590-594.

Jayasuriya A C, Scheinbeim J I, Lubkin V, Bennett G, and Kramer P (2003) Piezoelectric and mechanical properties in bovine cornea. *Journal of Biomedical Materials Research A* 66: 260-265.

Jester J V (2008) Corneal crystallins and the development of cellular transparency. *Seminars in Cell and Developmental Biology* 19: 82-93.

Jester J V, Moller-Pedersen T, Huang J, Sax C M, Kays W T, Cavanagh H D, Petroll W M et al. (1999) The cellular basis of corneal transparency: evidence for 'corneal crystallins'. *Journal of Cell Science* 112 ( Pt 5): 613-622.

Kadler K E, Holmes D F, Trotter J A, and Chapman J A (1996) Collagen fibril formation. *Biochemical Journal* 316: 1-11.

Kenshalo D R (1960) Comparison of thermal sensitivity of the forehead, lip, conjunctiva and cornea. *Journal of Applied Physiology* 15: 987-991.

- Khan S (2003) *The structural basis for the loss of transparency when the cornea swells*. University Wales Cardiff.
- Kostyuk O, Nalovina O, Mubard T M, Regini J W, Meek K M, Quantock A J, Elliott G F et al. (2002) Transparency of the bovine corneal stroma at physiological hydration and its dependence on concentration of the ambient anion. *Journal of physiology* 543: 633-642.
- Kou L, Labrie, D., Chylek, (1993) Refractive indices of water and ice in the 0.65-2.5 $\mu$ m spectral range. *Applied Optics* 32: 3531-3540.
- Koziol J (1965) Absorption spectra of riboflavin, lumiflavin, and lumichrome in organic solvents. *Experientia* 21: 189-190.
- Krishna C M, Uppuluri S, Riesz P, Zigler J S, Jr., and Balasubramanian D (1991) A study of the photodynamic efficiencies of some eye lens constituents. *Photochemistry and Photobiology* 54: 51-58.
- Le Berre M, Ressayre E, and Tallet A (2002) Example of a chaotic crystal: The labyrinth. *Physical Review E* 66: 026203.
- Leonard D (1996) *The ultrastructure of the corneal stroma and its implications for transparency*. Open University.
- Leonard D W, and Meek K M (1997) Refractive indices of the collagen fibrils and extrafibrillar material of the corneal stroma. *Biophysical Journal* 72: 1382-1387.
- Lerman S (1984) Biophysical aspects of corneal and lenticular transparency. *Current Eye Research* 3: 3-14.
- Li Y, Shekhar R, and Huang D (2006) Corneal pachymetry mapping with high-speed optical coherence tomography. *Ophthalmology* 113: 799 e791-792.
- Ling T (1987) Osmotically induced central and peripheral corneal swelling in the cat. *American Journal of Optometry and Physiological Optics* 64: 674-677.
- Linsenmayer T F, Fitch J M, Gordon M K, Cai C X, Igoe F, Marchant J K, and Birk D E (1998) Development and roles of collagenous matrices in the embryonic avian cornea. *Progress in Retinal and Eye Research* 17: 231-265.
- Lu P J, Deffeyes K, Steinhardt P J, and Yao N (2001) Identifying and Indexing Icosahedral Quasicrystals from Powder Diffraction Patterns. *Physical Review Letters* 87: 275507.
- Macia E (2006) The role of aperiodic order in science and technology. *Reports on Progress in Physics* 69: 397-441.
- Maksimova I L (2001) Effects of spatial correlation of optical fields scattered by densely packed systems *Proceedings of SPIE* 4242: 91-99.

Malik N S, Moss S J, Ahmed N, Furth A J, Wall R S, and Meek K M (1992) Ageing of the human corneal stroma: structural and biochemical changes. *Biochimica et Biophysica Acta* 1138: 222-228.

Maurice D (1956) The structure and transparency of the cornea. *Journal of physiology* 136: 263-286.

Maurice D M (1957) The structure and transparency of the cornea. *Journal of physiology* 136: 263-286.

Maurice D M (1962) Clinical physiology of the cornea. *International Ophthalmology Clinics* 2: 561-572.

Maurice D M (1970) The transparency of the corneal stroma. *Vision Research* 10: 107-108.

Maurice D M, and Giardini A A (1951) Swelling of the cornea in-vivo after the destruction of its limiting layers. *British Journal of Ophthalmology* 35: 791-796.

Mazzotta C, Balestrazzi A, Baiocchi S, Traversi C, and Caporossi A (2007) Stromal haze after combined riboflavin-UVA corneal collagen cross-linking in keratoconus: in vivo confocal microscopic evaluation. *Clinical and Experimental Ophthalmology* 35: 580-582.

McCally R L, Freund D E, Zorn A, Bonney-Ray J, Grebe R, de la Cruz Z, and Green W R (2007) Light-scattering and ultrastructure of healed penetrating corneal wounds. *Investigative Ophthalmology and Visual Science* 48: 157-165.

Meek K M (2002) The Cornea. In: Roberts D [ed.] *Signals and Perception*. Basingstoke, New York: Palgrave Macmillan, pp. 104-105.

Meek K M, Blamires T, Elliott G F, Gyi T J, and Nave C (1987) The organisation of collagen fibrils in the human corneal stroma: a synchrotron X-ray diffraction study. *Current Eye Research* 6: 841-846.

Meek K M, and Boote C (2004) The organization of collagen in the corneal stroma. *Experimental Eye Research* 78: 503-512.

Meek K M, Dennis S, and Khan S (2003a) Changes in the Refractive Index of the Stroma and Its Extrafibrillar Matrix When the Cornea Swells. *Biophysical Journal* 85: 2205-2212.

Meek K M, Elliott G F, and Nave C (1986) A synchrotron X-ray diffraction study of bovine cornea stained with cupromeronic blue. *Collagen and Related Research* 6: 203-218.

Meek K M, and Fullwood N J (2001) Corneal and scleral collagens--a microscopist's perspective. *Micron* 32: 261-272.



Meek K M, Fullwood N J, Cooke P H, Elliott G F, Maurice D M, Quantock A J, Wall R S et al. (1991) Synchrotron x-ray diffraction studies of the cornea, with implications for stromal hydration. *Biophysical Journal* 60: 467-474.

Meek K M, and Leonard D W (1993) Ultrastructure of the corneal stroma: a comparative study. *Biophysical Journal* 64: 273-280.

Meek K M, Leonard D W, Connon C J, Dennis S, and Khan S (2003b) Transparency, swelling and scarring in the cornea. *Eye* 17: 927-936.

Michelacci Y M (2003) Collagens and proteoglycans of the corneal extracellular matrix. *Brazilian journal of medical and biological research* 36: 1037-1046.

Miller A (1976) *Molecular packing in collagen fibrils*. 1 ed. New York: Plenum Press.

Moffatt R J, Murray F A, Grifo A P J, Haynes L W, Kinder J E, and Wilson G R (1980) Identification of Riboflavin in Porcine Uterine Secretions. *Biology of Reproduction* 23: 331-335.

Moller-Pedersen T (2004) Keratocyte reflectivity and corneal haze development. *Experimental Eye Research* 78: 553-560.

Moller-Pedersen T, Cavanagh H D, Petroll W M, and Jester J V (1998) Corneal haze development after PRK is regulated by volume of stromal tissue removal. *Cornea* 17: 627-639.

Moller-Pedersen T, and Ehlers N (1995) A three-dimensional study of the human corneal keratocyte density. *Current Eye Research* 14: 459-464.

Mukai T, Mera K, Nishida K, Nakashima M, Sasaki H, and Nakamura J (2004) Pharmacokinetics of phenol red in rat models of liver damage prepared by liver targeting of carbon tetrachloride. *Biological and pharmaceutical bulletin* 27: 595-597.

Muller L J, Pels E, Schurmans L R, and Vrensen G F (2004) A new three-dimensional model of the organization of proteoglycans and collagen fibrils in the human corneal stroma. *Experimental Eye Research* 78: 493-501.

Muller L J, Pels L, and Vrensen G F (1995) Novel aspects of the ultrastructural organization of human corneal keratocytes. *Investigative Ophthalmology and Visual Science* 36: 2557-2567.

Nakamura M, Kimura S, Kobayashi M, Hirano K, Hoshino H, and Awaya S (1997) Type VI collagen bound to collagen fibrils by chondroitin/dermatan sulfate glycosaminoglycan in mouse corneal stroma *Japanese Journal of Ophthalmology* 41: 71-76.

Naylor E J (1953) Polarized light studies of corneal structure. *British Journal of Ophthalmology* 37: 77-85.

Newton R H, and Meek K M (1998) Circumcorneal annulus of collagen fibrils in the human limbus. *Investigative Ophthalmology and Visual Science* 39: 1125-1134.

Olstrup T, Bende T, Kramer K D, and Jean B (1999) [Dielectric spectroscopy for noninvasive examination of corneal tissue]. *Biomedizinische Technik* 44: 78-82.

Parker G J, Charlton M D B, Zoorob M E, Baumberg J J, Netti M C, and Lee T (2006) Highly engineered mesoporous structures for optical processing *Philosophical Transactions of the Royal Society A* 364: 189-199.

Pellegata N S, Dieguez-Lucena J L, Joensuu T, Lau S, Montgomery K T, Krahe R, Kivela T et al. (2000) Mutations in KERA, encoding keratocan, cause cornea plana. *Nature Genetics* 25: 91-95.

Pendry J B (1996) Calculating photonic band structure. *Journal of Physics: Condensed Matter* 8: 1085-1108.

Peto S, Gillis P, and Henri V P (1990) Structure and dynamics of water in tendon from NMR relaxation measurements. *Biophysical Journal* 57: 71-84.

Petruska J A, and Hodge A J (1964) A Subunit Model for the Tropocollagen Macromolecule. *Proceedings of the National Academy of Sciences of the United States of America* 51: 871-876.

Pitts D G (1959) Transmission of the visible spectrum through the ocular medium of the bovine eye. *American Journal of Optometry and Archives of American Academy of Optometry* 36: 289-298.

Prydal J I, Franc F, Dilly P N, Kerr Muir M G, Corbett M C, and Marshall J (1998) Keratocyte density and size in conscious humans by digital image analysis of confocal images. *Eye* 12 ( Pt 3a): 337-342.

Radin C (1994) The Pinwheel tilings of the plane. *Annals of Mathematics* 139: 661-702.

Radin C (1999) Symmetries of Quasicrystals. *Journal of Statistical Physics* 95: 827-833.

Radner W, Zehetmayer M, Aufreiter R, and Mallinger R (1998) Interlacing and cross-angle distribution of collagen lamellae in the human cornea. *Cornea* 17: 537-543.

Raiskup-Wolf F, Hoyer A, Spoerl E, and Pillunat L E (2008) Collagen crosslinking with riboflavin and ultraviolet-A light in keratoconus: long-term results. *Journal of Cataract and Refractive Surgery* 34: 796-801.

Ramachandran G N, Bansal M, and Bhatnagar R S (1973) A hypothesis on the role of hydroxyproline in stabilizing collagen structure. *Biochimica et Biophysica Acta* 322: 166-171.

Regini J W, Elliott G F, and Hodson S A (2004) The ordering of corneal collagen fibrils with increasing ionic strength. *Journal of Molecular Biology* 336: 179-186.

Robert L, and Dische Z (1963) Analysis of a sulfated sialofucoglucosaminogalactomannosidoglycan from corneal stroma. *Biochemical and biophysical research communications* 10: 209-214.

Romppainen T, Bachmann L M, Kaufmann C, Kniestedt C, Mrochen M, and Thiel M A (2007) Effect of riboflavin-UVA-induced collagen cross-linking on intraocular pressure measurement. *Investigative Ophthalmology and Visual Science* 48: 5494-5498.

Sadun L (1998) Some Generalizations of the Pinwheel Tiling. *Discrete and Computational Geometry* 20: 79-110.

Schmut O (1977) The identification of type III collagen in calf and bovine cornea and sclera. *Experimental Eye Research* 25: 505-509.

Scott J E, and Bosworth R (1990) A comparative biochemical and ultrastructural study of proteoglycan-collagen interactions in corneal stroma. *Biochemical Journal* 270: 491-497.

Scott J E, and Haigh M (1988) Identification of specific binding sites for keratan sulphate proteoglycans and chondroitin-dermatan sulphate proteoglycans on collagen fibrils in cornea by the use of cupromeronic blue in critical electrolyte concentration techniques. *Biochemical Journal* 253: 607-610.

Senechal M (1996) *Quasicrystals and geometry*. Cambridge: Cambridge University Press.

Siebeck U E, Collin S P, Ghodducci M, and Marshall N J (2003) Occlusable corneas in toadfishes: light transmission, movement and ultrastructure of pigment during light- and dark-adaptation *Journal of Experimental Biology* 206: 2177-2190.

Siebeck U E, and Marshall N J (2001) Ocular media transmission of coral reef fish--can coral reef fish see ultraviolet light? *Vision Research* 41: 133-149.

Sivak J G, and Mandelman T (1982) Chromatic dispersion of the ocular media. *Vision Research* 22: 997-1003.

Smith J W (1970) The transparency of the corneal stroma. *Vision Research* 10: 109-110.

Smith T B (1988) Multiple scatterine in the cornea. *Journal of Modern Optics* 35: 93-101.

Sobol E N, Sviridov A P, Kitai M S, and Edwards G S (2003) Temperature alterations of infrared light absorption by cartilage and cornea under free-electron laser radiation. *Applied Optics* 42: 2443-2449.

Sowa M G, Payette J R, and Mantsch H H (1999) Near-infrared spectroscopic assessment of tissue hydration following surgery. *Journal of Surgical Research* 86: 62-69.

Spoerl E, Huhle M, and Seiler T (1998) Induction of cross-links in corneal tissue. *Experimental Eye Research* 66: 97-103.

Spoerl E, Mrochen M, Sliney D, Trokel S, and Seiler T (2007) Safety of UVA-riboflavin cross-linking of the cornea. *Cornea* 26: 385-389.

Twersky V (1975) Transparency of pair-correlated, random distributions of small scatterers, with applications to the cornea. *Journal of the Optical Society of America* 65: 524-530.

Vaezy S, and Clark J I (1991) A quantitative analysis of transparency in the human sclera and cornea using Fourier methods. *Journal of Microscopy* 163: 85-94.

Vaezy S, and Clark J I (1994) Quantitative analysis of the microstructure of the human cornea and sclera using 2-D Fourier methods. *Journal of Microscopy* 175 ( Pt 2): 93-99.

van de Hulst H C (1981) *Light Scattering by Small Particles*. New York: Dover Publications Inc.

van den Berg T J, and Spekreijse H (1997) Near infrared light absorption in the human eye media. *Vision Research* 37: 249-253.

van den Berg T J, and Tan K E (1994) Light transmittance of the human cornea from 320 to 700 nm for different ages. *Vision Research* 34: 1453-1456.

Vogel H (1979) A better way to construct the sunflower head. *Mathematical Biosciences* 44: 179-189.

Wang F (2008) UVA/Riboflavin-Induced Apoptosis in Mouse Cornea. *Ophthalmologica* 222: 369-372.

Warren B E (1990) *X-ray Diffraction*. New York: Courier Dover Publications.

Wieliczka D M, Weng, S., Querry, M.R., (1989) Wedge shaped cell for highly absorbant liquids: infrared optical constants of water. *Applied Optics* 28: 1714-1719.

Wollensak G, Aurich H, Pham D T, and Wirbelauer C (2007) Hydration behavior of porcine cornea crosslinked with riboflavin and ultraviolet A. *Journal of Cataract and Refractive Surgery* 33: 516-521.

Wollensak G, and Iomdina E (2008) Long-term biomechanical properties of rabbit cornea after photodynamic collagen crosslinking. *Acta Ophthalmologica*.

Wollensak G, and Redl B (2008) Gel electrophoretic analysis of corneal collagen after photodynamic cross-linking treatment. *Cornea* 27: 353-356.

Wollensak G, Spoerl E, and Seiler T (2003a) Riboflavin/ultraviolet-a-induced collagen crosslinking for the treatment of keratoconus. *American Journal of Ophthalmology* 135: 620-627.

Wollensak G, Spoerl E, and Seiler T (2003b) Stress-strain measurements of human and porcine corneas after riboflavin-ultraviolet-A-induced cross-linking. *Journal of Cataract and Refractive Surgery* 29: 1780-1785.

Wollensak G, Wilsch M, Spoerl E, and Seiler T (2004) Collagen fiber diameter in the rabbit cornea after collagen crosslinking by riboflavin/UVA. *Cornea* 23: 503-507.

Wolny J, Wnel A, and Verger-Gaugry J-L (2000) Fractal Behaviour of Diffraction Pattern of Thue-Morse Sequence. *Journal of Computational Physics* 163: 313-327.

Worthington C R (1984) The structure of cornea. *Quarterly Review of Biophysics* 17: 423-451.

Worthington C R, and Inouye H (1985) X-ray diffraction study of the cornea. *International Journal of Biological Macromolecules* 7: 2-8.

Yousif H A, Mattis R E, and Kozminski K (1994) Light scattering at oblique incidence on two coaxial cylinders. *Applied Optics* 33: 4013-4024.

Ziman J M (1979) *Models of disorder: The theoretical physics of homogeneously disordered systems*. Cambridge: Cambridge University Press.

Zimmermann D R, Trueb B, Winterhalter K H, Witmer R, and Fischer R W (1986) Type VI collagen is a major component of the human cornea. *FEBS Letters* 197: 55-58.

Zuclich J A, Blankenstein M F, Thomas S J, and Harrison R F (1984) Corneal damage induced by pulsed CO<sub>2</sub> laser radiation. *Health Physics* 47: 829-835.

## **Appendix 1: List of publications and abstracts**

\*Doutch J, Quantock A.J, Smith V.A, Meek K.M, (2008) Light transmission in the human cornea as a function of position across the ocular surface: theoretical and experimental aspects *Biophysical Journal* 95:5092-5099

\*Doutch J., Tucker, C., Quantock, A.J., Ade, P.A.R., Meek, K.M., (2007) Propagation of infrared wavelengths through the corneal stroma with reference to hydration changes. *Proceedings of SPIE* 65350Q.

\*Doutch J, Quantock A.J., and Meek K.M. (2007) Changes in visible light transmission across the corneal stroma. *Proceedings of SPIE* 65350V.

Samaras K, O'Brart D.P, Doutch J, Hayes S, Marshall J and Meek KM (2008) Analysis of the light transmission properties of porcine corneas after riboflavin/ultraviolet A (370nm) corneal collagen crosslinkage to assess corneal stromal riboflavin absorption:a comparison of 20% alcohol application and partial and complete epithelial removal.. *Journal of Cataract and Refractive Surgery* In Press

Hayes S, O'Brart D.P, Lamdin L.S, Doutch J, Samaras K, Marshall J, and Meek K.M (2008) Effect of complete epithelial debridement before riboflavin-ultraviolet-A corneal collagen crosslinking therapy *Journal of Cataract and Refractive Surgery* 34: 657-661.

Connon C.J, Nakamura T, Hopkinson A, Quantock A.J, Yagi N, Doutch J, and Meek K.M (2007) The biomechanics of amnion rupture: an X-ray diffraction study. *PLoS ONE* 2: e1147.

### **Published Abstracts**

\*Doutch J, Tucker C, Quantock A.J, Ade P.A.R, Meek K.M, (2007), The Correlation Between Corneal Transmission in the Near/ Mid Infrared and Corneal Hydration, *Investigative Ophthalmology and Vision Science* 48, E-abstract 3508

Meek K.M, Quantock A.J, Douth J (2007) Changes in Visible Light Transmission Across the Cornea, Investigative Ophthalmology and Vision Science 48, E-abstract 3506

Connon C.J, Hopkinson A, Nakamura T, Douth J, Kinoshita S, Meek K.M, (2007) The Variation in Transparency of Amniotic Membrane Used in Ocular Surface Regeneration, Investigative Ophthalmology and Vision Science 48, E-abstract 455

